

Engineering Journal



American Institute of Steel Construction

Fourth Quarter 2015 Volume 52, No. 4

- 221 Crippling of Webs with Partial-Depth Stiffeners under Patch Loading
Raghuvir Salkar, Abhishek Salkar and William Davids
- 233 Double-Tee Members in Axial Compression
Leigh Arber, Meng Wang and Pat McManus
- 259 Weld Effective Lengths for Rectangular HSS Overlapped
K-Connections
Kyle Tousignant and Jeffrey A. Packer
- 283 Steel Structures Research Update: System Behavior and Collapse
Assessment of Braced Frames
Judy Liu

ENGINEERING JOURNAL

AMERICAN INSTITUTE OF STEEL CONSTRUCTION

*Dedicated to the development and improvement of steel construction,
through the interchange of ideas, experiences and data.*

Editorial Staff

Editor: MARGARET A. MATTHEW, P.E.

Managing Editor: KEITH A. GRUBB, S.E., P.E.

Research Editor: JUDY LIU, PH.D.

Production Editor: MEGAN JOHNSTON-SPENCER

Officers

JEFFREY E. DAVE, P.E., *Chairman*

Dave Steel Company, Inc., Asheville, NC

JAMES G. THOMPSON, *Vice Chairman*

Palmer Steel Supplies, Inc., McAllen, TX

ROGER E. FERCH, P.E., *President*

American Institute of Steel Construction, Chicago

DAVID B. RATTERMAN, *Secretary & General Counsel*

American Institute of Steel Construction, Chicago

CHARLES J. CARTER, S.E., P.E., PH.D., *Vice President and*

Chief Structural Engineer

American Institute of Steel Construction, Chicago

JACQUES CATTAN, *Vice President*

American Institute of Steel Construction, Chicago

JOHN P. CROSS, P.E., *Vice President*

American Institute of Steel Construction, Chicago

SCOTT L. MELNICK, *Vice President*

American Institute of Steel Construction, Chicago

The articles contained herein are not intended to represent official attitudes, recommendations or policies of the Institute. The Institute is not responsible for any statements made or opinions expressed by contributors to this Journal.

The opinions of the authors herein do not represent an official position of the Institute, and in every case the officially adopted publications of the Institute will control and supersede any suggestions or modifications contained in any articles herein.

The information presented herein is based on recognized engineering principles and is for general information only. While it is believed to be accurate, this information should not be applied to any specific application without competent professional examination and verification by a licensed professional engineer. Anyone making use of this information assumes all liability arising from such use.

Manuscripts are welcomed, but publication cannot be guaranteed. All manuscripts should be submitted in duplicate. Authors do not receive a remuneration. A "Guide for Authors" is printed on the inside back cover.

ENGINEERING JOURNAL (ISSN 0013-8029) is published quarterly. Subscriptions: Members: one subscription, \$40 per year, included in dues; Additional Member Subscriptions: \$40 per year. Non-Members U.S.: \$160 per year. Foreign (Canada and Mexico): Members \$80 per year. Non-Members \$160 per year. Published by the American Institute of Steel Construction at One East Wacker Drive, Suite 700, Chicago, IL 60601.

Periodicals postage paid at Chicago, IL and additional mailing offices. **Postmaster:** Send address changes to ENGINEERING JOURNAL in care of the American Institute of Steel Construction, One East Wacker Drive, Suite 700, Chicago, IL 60601.

Copyright 2015 by the American Institute of Steel Construction. All rights reserved. No part of this publication may be reproduced without written permission. The AISC logo is a registered trademark of AISC.

Subscribe to *Engineering Journal* by visiting our website www.aisc.org/ej or by calling 312.670.5444.

Copies of current and past *Engineering Journal* articles are available free to members online at www.aisc.org/ej.

Non-members may purchase *Engineering Journal* article downloads at the AISC Bookstore at www.aisc.org/ej for \$10 each.

Letter from the Editor

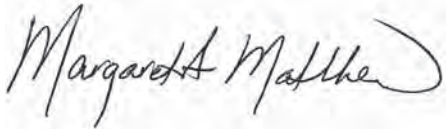
Dear Readers,

Hello from the new editor of *Engineering Journal*! I am very excited to step into this position as we continue to strive to bring you the very best articles and information in the steel construction industry. I am taking over from the very capable hands of Keith Grubb. Keith, who has been at the helm of *EJ* for the past six years, has been promoted to AISC's Director of Publications and is now the *EJ* Managing Editor.

I would also like to take this opportunity to thank our reviewers for all of their hard work, this year and every year. Their contributions are invaluable to the success of the *Journal*. A list of our 2015 reviewers is posted on the AISC website at www.aisc.org/ej.

Is there a steel design topic you would like to see in *EJ*? We are always looking for ideas for papers. Authors interested in submitting papers should visit our website at www.aisc.org/ej for author guidelines and submittal information.

Sincerely,

A handwritten signature in black ink that reads "Margaret A. Matthew". The signature is written in a cursive style with a large, sweeping flourish at the end.

Margaret A. Matthew, P.E.
Editor

Crippling of Webs with Partial-Depth Stiffeners under Patch Loading

RAGHUVIR SALKAR, ABHISHEK SALKAR and WILLIAM DAVIDS

ABSTRACT

Chapter J of the 2010 AISC *Specification* recommends the use of either single- or double-sided minimum half-depth transverse web stiffeners where web crippling strength is less than design concentrated load; use of a doubler plate of minimum half-web depth is also suggested in the *Specification*. Commentary on the *Specification* mentions that because the web crippling phenomenon has been observed to occur in the web adjacent to the loaded flange, a half-depth stiffener (or stiffeners) or a half-depth doubler plate is needed to eliminate web crippling. Research conducted at the University of Maine, however, clearly showed that web crippling can occur even in webs having half-depth stiffeners. Further, the AISC *Specification* does not have a formula to predict crippling strength of webs with partial-depth stiffeners under local compressive loads. This paper presents a formula for evaluating crippling strength of webs with partial-depth stiffeners that considers the effect of depth of stiffener, width of load and eccentricity of loading.

Keywords: web crippling, stiffened webs, transverse stiffeners, nominal resistance or ultimate stiffened web capacity.

INTRODUCTION

Rolled shapes and built-up beams and girders can be subjected to local concentrated compressive loads acting in the plane of the web. Such loads can occur either over supports or between supports of beams and girders. Chapter J of the 2010 AISC *Specification* (AISC, 2010) recommends the use of either single- or double-sided minimum half-depth transverse web stiffeners or web doubler plates where web crippling strength is less than design concentrated load.

Commentary on the AISC *Specification* mentions that because the web crippling phenomenon has been observed to occur in the web adjacent to the loaded flange, a half-depth stiffener (or stiffeners) or a half-depth doubler plate is needed to eliminate web crippling. Research conducted at the University of Maine (Salkar, 1992), however, clearly showed that web crippling can occur in webs having half-depth stiffeners. Therefore, it is important that formulas or procedures are made available for evaluating crippling strength of webs with partial-depth stiffeners.

Although Chapter J of the 2010 AISC *Specification* has formulas for predicting strength of unstiffened webs and stiffened webs with full-depth stiffeners under local compressive loads, it does not have any formula to predict crippling strength of webs with partial-depth stiffeners under local compressive loads. Research on the behavior and design rules of intermediate transverse stiffeners attached on web panels was summarized by Lee et al. (2002, 2003). Research on the requirements of transverse stiffeners in straight and horizontally curved steel I-girders was summarized by Kim et al. (2007). Research on unstiffened webs under compressive edge loads was summarized by Elgaaly (1983). Research on the same topic post-1983 was summarized by Salkar (1992) at the University of Maine.

This paper highlights part of the research at the University of Maine and gives recommendations based on the results of this research. This paper also presents a brief comparison of provisions of the 2010 AISC *Specification*, Canadian codes (CSA, 2006) and Australian (AS, 2012) codes with respect to crippling strength of stiffened webs under local compressive loads.

This paper addresses the strength of stiffened webs of rolled shapes under local compressive patch loads between supports. Three types of local compressive patch loading have been considered:

1. Loading through roller on top flange as shown in Figure 1.
2. Loading through patch plate on top flange as shown in Figure 2.
3. Loading through I-shaped beam on top flange as shown in Figure 3.

Raghuvir Salkar, Ph.D., Consulting Engineer, Kuvelkar Salkar Associates, Goa, India (corresponding). Email: salkar@ksa-india.com

Abhishek Salkar, Undergraduate Student, Department of Civil Engineering, National Institute of Technology, Surathkal, India. Email: salkarabhishek@gmail.com

William Davids, John C. Bridge Professor and Chair, Department of Civil and Environmental Engineering, University of Maine, Orono, ME. Email: william.davids@umit.maine.edu

Paper No. 2014-01R

Various parameters considered are depth of stiffener (d_s), thickness of stiffener (t_s), width of loading (N) and eccentricity of load (e_1) with respect to plane of stiffener. Stiffeners considered in this paper were welded to the web and the loaded flange, but likely transferred part of the load through bearing, similarly to fitted stiffeners with no weld between the stiffener and flange.

RESEARCH AT UNIVERSITY OF MAINE

Research carried out at the University of Maine on the crippling strength of stiffened webs of rolled shapes was sponsored in part by AISC. Salkar (1992) conducted research on intermediate transverse load-bearing stiffeners for rolled shapes, which is summarized in this section. One of the main objectives of the research was to evaluate the then-current 1986 AISC *Specification* (AISC, 1986) design formulas and procedures that predict the strength of stiffened webs and, if necessary, derive new ones. The evaluation was done through experimental investigation as well as analytical work using finite element analysis.

Experimental Investigation

As a part of the experimental work, 27 rolled beams (W16×26 and W12×14) were tested in a Baldwin Testing Machine, and various values of stiffener thickness, t_s , depth of stiffener, d_s , eccentricity of load with respect to the plane of stiffeners, e_1 , and width of patch load, N , were considered as test parameters. Small values of eccentricity up to 0.5 in., which can occur due to fabrication and construction tolerances, were considered. These 27 tests were divided into three groups, of which only group 3 tests were considered for analysis because the yield stress values of the stiffeners were not known for groups 1 and 2.

In all 17 tests of group 3, W16×26 rolled sections were used as test specimens, and the ratio of the length of the beam to its depth (b/d) was 2.3. Three methods of load application on the top flange were considered—namely, loading through a plate, an I-beam and a roller. It was noted that loading through a roller and an I-beam gave similar results. The details of the 17 tests conducted by Salkar (1992) during his experimental work are summarized in Table 1. In this table, P_{tsf} refers to the test failure load and F_{yw} and F_{ys}

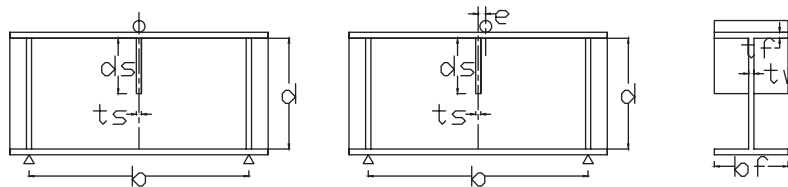


Fig. 1. Loading through roller on top flange.

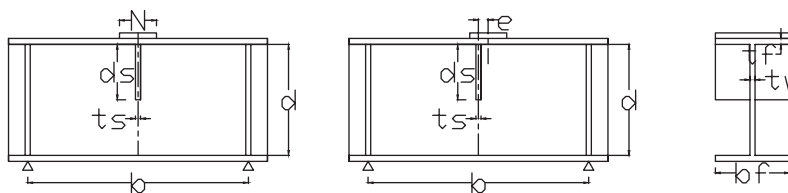


Fig. 2. Loading through patch plate on top flange.

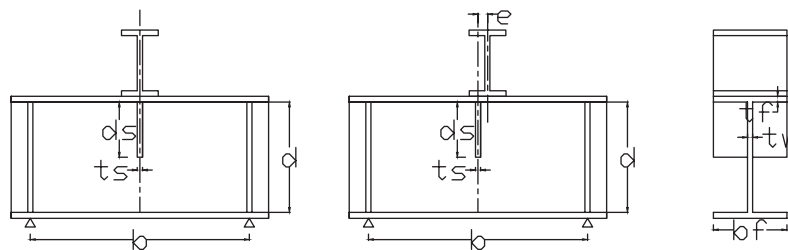


Fig. 3. Loading through I-shaped beam on top flange.

Table 1. Tests on Webs with Intermediate Load-Bearing Stiffeners

Test No.	t_w in.	t_f/t_w	b_f/t_f	d/t_w	t_s/t_w	d_s/d	N/d	e_1 in.	F_{yw} ksi	F_{ys} ksi	P_{fst} kips	Load Application Method	
1	0.262	1.23	17.2	59.9	0.653	0.5	0.303	0	48	55	161.1	Patch plate	
2	0.254	1.24	17.4	61.5	0.673		0	0.5	49	55	107.0	Roller	
3	0.262	1.22	17.2	59.9	0.653		0.303		46	55	161.6	Patch plate	
4	0.249	1.29	17.2	62.8	0.695		0	0	47	53	114.0	Roller	
5	0.253	1.36	16.0	61.8	0.961		0.304		49	48	169.1	Patch plate	
6	0.250	1.26	17.5	62.5	0.972		0	0.5	52	48	120.0	Roller	
7	0.260	1.31	16.2	60.3	0.935		0.304		48	48	161.0	Patch plate	
8	0.255	1.27	17.0	61.3	0.949		0	0	47	48	144.0	Roller	
9	0.256	1.31	16.5	61.0	1.23		0.303		49	47	175.2	Patch plate	
10	0.251	1.29	17.0	62.5	1.25		0	0	0.5	49	47	127.5	Roller
11	0.258	1.27	16.8	60.8	1.22				50	47	148.8	Roller	
12	0.264	1.29	16.1	59.2	1.19				44	49	150.0	Roller	
13	0.253	1.34	16.2	61.8	0.676				47	45	126.0	Roller	
14	0.263	1.29	16.1	59.4	0.932				46	48	153.6	Roller	
15	0.263	1.28	16.3	59.4	1.18				46	48	164.0	Roller	
16	0.262	1.26	16.7	59.6	0.920				0.5	46	48	132.1	Roller
17	0.255	1.29	16.7	61.3	0.945		0.303	0	47	48	145.3	I-section W4×13	

refer to the yield stress of the web and stiffener material, respectively.

Modes of Failure

Three modes of failure were observed in the preceding 17 tests: web crippling below the stiffener, local stiffener crippling and global stiffener crippling. In the following description of the failure modes, the photographs in Figures 4 through 9 were originally published by Elgaaly et al. (1992).

1. *Failure mode 1, web crippling below the stiffener:* Yielding in the web below the bottom of the stiffener with or without excessive yielding in the stiffener led to the web crippling failure mode and was seen in case of all half-depth stiffeners where the load was applied through a plate. It was also seen in the case of specimens with thick half-depth stiffeners subjected to concentric loading through a roller. Figures 4 and 5 show test specimens that failed in this mode.
2. *Failure mode 2, local stiffener crippling:* This occurred in beams with thin to moderately thick half-depth stiffener under concentric loading through a roller. It was also noted in all specimens subjected to eccentric roller loads. In this failure mode, one of the stiffeners crippled with either some or no crippling in adjacent

web. Figures 6 and 7 show test specimens that failed in this mode.

3. *Failure mode 3, global stiffener crippling:* This was found to occur in all specimens with deep stiffeners, subjected to concentric loads through a roller or an I-beam. In this failure mode, a cross-section comprised of both stiffeners and part of the web on each side of the stiffeners crippled together. Figures 8 and 9 show test specimens that failed in this mode.

It is worth noting that web crippling below the stiffeners (failure mode 1) occurred where webs had half-depth stiffeners. This type of failure, however, was not seen in webs with three-quarters-depth stiffeners. This observation led to one of the important conclusions and recommendations of this paper.

Finite Element Analysis (FEA)

A nonlinear finite elemental analysis was carried out using the modified version of the program NONSAP. The original version was developed by Bathe et al. (1974) at the University of California, Berkeley, and modifications were made by Du (1991) at the University of Maine. The main objectives of the analysis were to obtain a better picture of the stiffened web behavior and to conduct a parametric study to

determine the effect of various parameters t_s , d_s , e_1 and N on the stiffened web strength.

A three-dimensional isoparametric shell element was used to discretize the specimens. The eight-node isoparametric doubly curved shell element had six degrees of freedom per node—namely, the displacements along and the rotations about the x , y and z axes. It was the degeneration of the well-known quadratic isoparametric hexahedron. The Updated Lagrangian formulation was employed for considering large displacements. For materially nonlinear analysis, an elastic plastic material model was employed. The nonlinear material model employed the von Mises yield criterion, the Prandtl-Reuss flow rule and isotropic hardening. Hardening

was used because an elastic perfectly plastic material model would have slowed or prevented convergence; the hardening modulus was selected to be 1,000 ksi (about 3.5% of the elastic modulus).

Finite element analyses were conducted to study the web behavior and strength for the following cases. This paper, however, deals only with the fourth case of stiffened stocky webs.

1. Slender and stocky webs under loads in the plane of the web and acting between the supports at the beam mid-span—in-plane interior loading.
2. Slender and stocky webs under interior loads at an



Fig. 4. Failure mode 1—web crippling below stiffeners (test 12).



Fig. 5. Failure mode 1—web crippling below stiffeners (test 9).

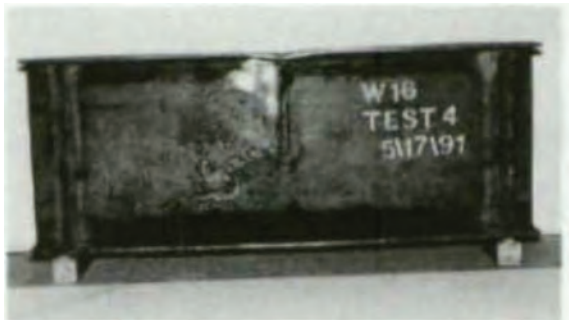


Fig. 6. Failure mode 2—local stiffener crippling (test 4).



Fig. 7. Failure mode 2—local stiffener crippling (test 1).

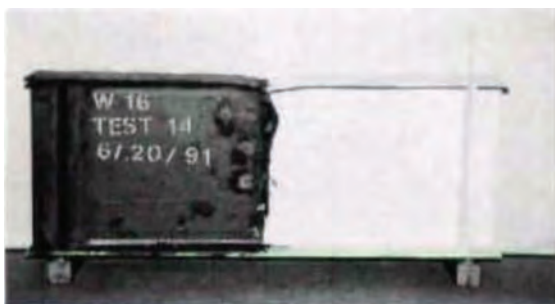


Fig. 8. Failure mode 3—global stiffener crippling (test 14).

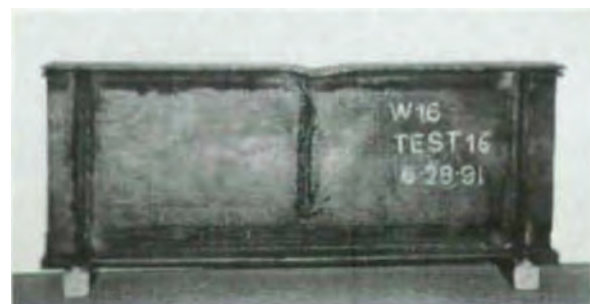


Fig. 9. Failure mode 3—global stiffener crippling (test 16).

Location	Displacements In			Rotations About		
	X	Y	Z	X	Y	Z
Lines ABC and DEF	1	1	1	1	1	0
Lines GHI and JKL	0	1	1	1	1	0
Lines BH and EK, excluding B, H, E, K	0	1	1	1	0	0

1 = degree of freedom is restrained
0 = degree of freedom is not restrained

Test No.	t_s in.	d_s/d	Test Results kips	Test/ Predicted	FEA Predicted Failure Mode	Experimentally Observed Failure Mode
4	0.172	0.5	114.0	1.12	Failure mode 2	Failure mode 2
6	0.243		120.0	0.914	Failure mode 2	Failure mode 2
8	0.243		144.0	1.03	Failure mode 2	Failure mode 2
11	0.313		148.8	1.02	Failure mode 1	Failure mode 1
13	0.172	0.75	126.0	1.06	Failure mode 3	Failure mode 3
14	0.243		153.6	0.96	Failure mode 3	Failure mode 3

eccentricity with respect to the web plane—eccentric interior loading.

- In-plane loads on stocky webs acting at the supports—in-plane exterior loads.
- In-plane interior loads on transversely stiffened stocky webs, acting concentric or eccentric with respect to the vertical axis of the stiffener.

Figure 10 shows a typical finite element mesh that was used to study transversely stiffened webs under in-plane interior loads. The load was either concentric or eccentric with respect to the vertical axis of the stiffener. The mesh was made up of 216 shell elements and 705 nodes. The effect of the end stiffener was considered by imposing certain boundary conditions on the corresponding nodes as shown in Table 2.

The finite element model performed satisfactorily when used to predict failure loads for tests with in-plane interior loading. Table 3 shows a comparison between the test and the predicted failure loads. All six tests listed in the table were conducted on W16×26 rolled sections and were a part of the 17 tests of Table 1. In these tests, the ratio of the stiffener to web depth was 0.5 or 0.75, and the load eccentricity with respect to the vertical axis of the stiffener was 0 or 0.5 in. The values of other parameters, such as t_w , t_f/t_w , b_f/t_f ,

d/t_w , F_{yw} and F_{ys} , were taken as the average values of the 17 tests of Table 1. The average value of the ratio of the test to the finite element analysis failure load was 1.017. Thus, the finite element analysis was able to predict the test results to a very good degree of accuracy.

Note: In all tests, N/d was 0, and the load eccentricity with respect to the stiffener center line (e_1) was 0, except in test 6, where it was 0.5 in. As described earlier, three modes of failure—web crippling below the stiffener, local stiffener crippling and global stiffener crippling—were observed in the FEA results. As may be noted from Table 3 and Figures 11, 12 and 13, the finite element analysis was able to predict these failure modes accurately.

Because the finite element model was found to accurately predict failure loads and failure modes, it was used to conduct a parametric study to determine the effect of parameters t_s , d_s , e_1 and N on the stiffened web strengths. The parametric study was conducted using W16×26 and W12×14 rolled beam sections. The t_s/t_w values varied from 0.625 to 1.22, d_s/d was 0.5 or 0.75, N/d was varied from 0 to 0.4, and e_1 was 0 or 0.5 in.

Results of the parametric study are given in Table 4. One of the important observations of the parametric study is presented in Figure 11. It shows a graph of web crippling strength, P_{fea} , versus ratio of stiffener to web thickness,

(t_s/t_w) , for half-depth and three-quarters-depth stiffeners, indicating that few gains in capacity are observed as stiffener thickness, t_s , is increased beyond t_w .

Summary of Experimental and FEA Investigations

Experimental as well as finite-element based analytical research at the University of Maine led to the following conclusions, which are applicable for rolled beams, and for the

parameters N/d up to 0.3, e_1 up to 0.5 in., and d_s/d value up to 0.75.

1. As may be noted from Figure 14, web strength increases with t_s up to a certain optimum value of t_s , beyond which the increase in strength is not significant. This optimum value was found to be approximately the thickness of the web (valid only for rolled shapes) for all rolled shapes considered in this study.

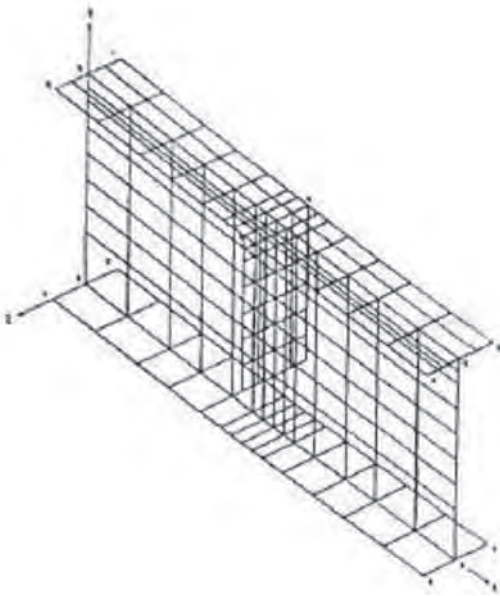


Fig. 10. Finite element mesh for stiffened stocky webs under in-plane (concentric and eccentric) interior loads.

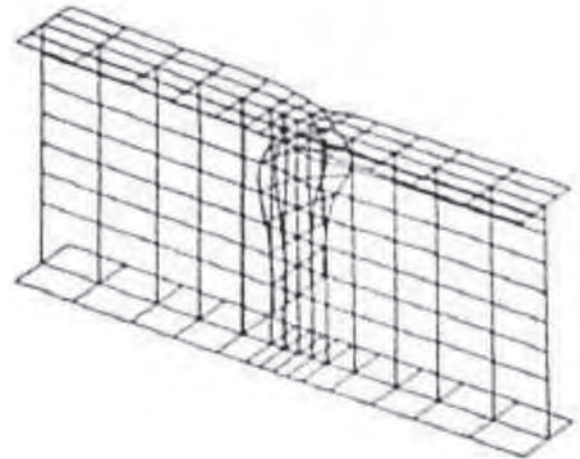


Fig. 11. Three-dimensional view of the deformed beam near failure ($t_s = 1/4$, $d_s/d = 3/4$, $N/d = 0$, $e_1 = 0$). Failure mode 3.

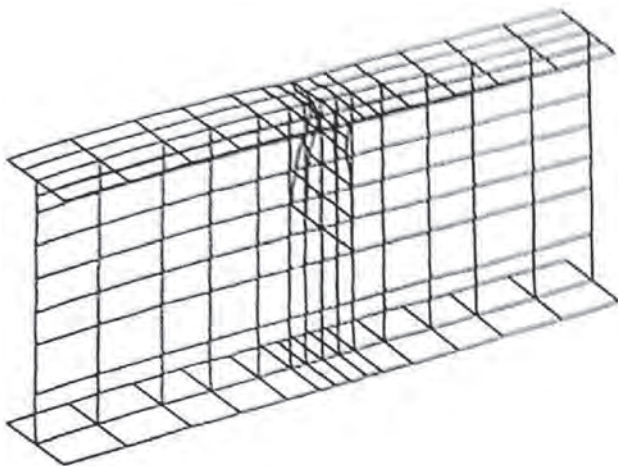


Fig. 12. Three-dimensional view of the deformed beam near failure ($t_s = 3/16$, $d_s/d = 1/2$, $N/d = 0$, $e_1 = 0$). Failure mode 2.

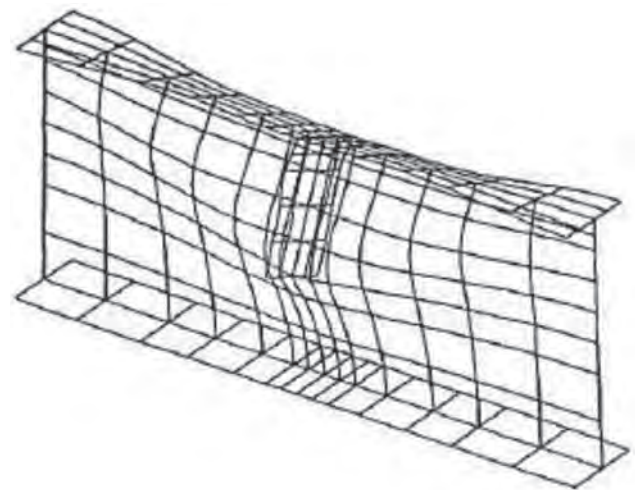


Fig. 13. Three-dimensional view of the deformed beam near failure ($t_s = 3/16$, $d_s/d = 1/2$, $N/d = 0$, $e_1 = 0$). Failure mode 1.

No.	Section	t_s/t_w	d_s/d	N/d	e_1 in.	F_{yw} ksi	F_{ys} ksi	P_{fea} kips
1	W16x26	0.669	0.5	0	0	48	53	102
2		0.944	0.5	0.3	0	48	48	159
3		0.944	0.5	0	0.5	48	48	131
4		0.944	0.5	0	0	48	48	141
5		1.22	0.5	0	0	48	48	147
6		0.699	0.75	0	0	48	53	119
7		0.944	0.75	0	0	48	48	160
8	W12x14	0.625	0.5	0	0	36	36	36
9		0.780	0.5	0	0	36	36	51
10		0.940	0.5	0	0	36	36	63
11		1.00	0.5	0	0	36	36	65
12		1.125	0.5	0	0	36	36	66
13		0.940	0.5	0.2	0	36	36	70
14		0.940	0.5	0.4	0	36	36	77
15		0.940	0.5	0	0.5	36	36	50

- As may be noted from Table 4, increase in d_s from $0.5d$ to $0.75d$ increased stiffened web crippling strength by about 15%. Web strength increased linearly with N . The values of N/d were limited to 0.3, and this is the limit in most practical cases.
- It was noted that eccentric loading through a plate had negligible effect on the stiffened web crippling

strength, while eccentric loading through a roller or an I-beam reduced the stiffened web strength considerably.

- The extent to which the eccentricities of load reduce the stiffened web crippling depends directly upon the magnitude of e_1 , and also factors t_f/t_w and t_f/t_s .

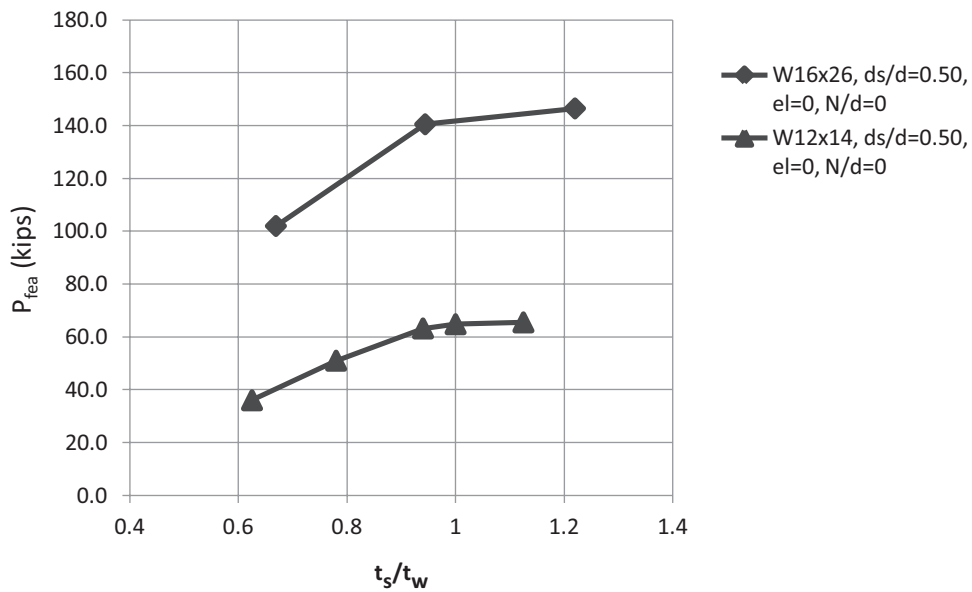


Fig. 14. Effect of stiffener thickness on stiffened web crippling strength.

5. It was noted that relatively thick stiffeners as well as sufficiently wide load patches could cause crippling in the web below the stiffener when it is $0.5d$ deep. This was not found to occur when the stiffener extended $0.75d$. This observation does not support AISC *Specification* recommendation that stiffener of $0.5d$ depth is sufficient to eliminate the limit state of web crippling. This observation also suggests that it is not desirable to have stiffener thickness higher than web thickness, and this led to one of the conclusions and recommendations of this paper.

DEVELOPMENT OF DESIGN EQUATION

The results of the parametric study were used with the test results to develop a formula to predict the stiffened web capacity, P_u , given by:

$$P_u = K + F_{ys}t_s b_s (R)(2d_s/d)^X \quad (1)$$

where K is defined as:

$$K = 0.80t_w^2 \left\{ 1 + 3(N/d)(t_w/t_f)^{1.5} \right\} (EF_{yw}t_f/t_w)^{0.5} \quad (2)$$

$$R = 2e_1 \left\{ (t_f/t_w)^{0.5} (t_f/t_s)^{0.5} / 1.55 - 1 \right\} + 1 \quad (3)$$

$$X = 0.50(d/d_s) \quad (4)$$

b_s = twice the width of the front or back stiffener

Equation 1 is valid only if the stiffener satisfied the width-to-thickness compactness criteria; that is, the ratio of the width of stiffener (front to back) to its thickness should not exceed $0.56(E/F_{ys})^{0.5}$. The effectiveness of this formula is discussed later in this paper when the test results are compared with the predictions of several design codes.

PROVISIONS FOR TRANSVERSE STIFFENERS IN VARIOUS CODES

This section presents design specifications and formulas of various international codes to calculate the strength of webs with full-depth stiffeners under patch compressive loads. The Canadian code (CSA S16-01, 2006), the Australian code (AS, 2012) and the 2010 AISC *Specification for Structural Steel Buildings* (AISC, 2010) have been selected for comparison. None of these codes contains formulas to predict crippling strength of webs with partial-depth stiffeners. In the absence of such a formula for partial-depth stiffeners, strength of webs with full-depth stiffeners as predicted by formulas from these three codes have been compared with the test results conducted at the University of Maine.

Design Specifications of Canadian Code CSA S16-01 2006

Canadian code CSA S16-01 2006 (CSA, 2006) provides formulas to evaluate bearing strength of web with full-depth stiffeners under compressive load on flanges, as given in Equation 5. According to Section 14.4 of CSA S-16-01, the ultimate stiffened web capacity is given by:

$$P_u = AF_y (1 + \lambda^{2n})^{-1/n} \quad (5)$$

where

$$n = 1.34$$

F = yield stress value

A = area of cross-section consisting of the pair of stiffeners and a centrally located strip of the web equal to not more than 25 times its thickness

$$\lambda = (KL/r)(F_y/\pi^2 E)^{0.5} \quad (6)$$

Here, E is the elastic modulus of steel, KL shall be taken as not less than three-fourths of the length of the stiffeners and r is the radius of gyration about the minor axis.

Design Specifications of Australian Code AS 4100 2012

Australian code AS 4100 2012 (AS, 2012) provides formulas to evaluate bearing strength of web with full-depth stiffeners under compressive load on flanges, as given in Equations 8 and 11. Section 5.14 of AS 4100 deals with the design of load-bearing stiffeners. It states that when a load-bearing stiffener is required, the following two conditions should be satisfied:

1. Yield Capacity

$$P_x \leq R_{sy} \quad (7)$$

where

P_x = the design bearing force

R_{sy} = the nominal yield capacity of the stiffened web and

$$R_{sy} = 1.25 b_{bf} t_w f_y + A_s f_y \quad (8)$$

A_s = area of the stiffener in contact with the flange

f_y = maximum yield stress value of steel

$$b_{bf} = N + 5t_f \quad (9)$$

2. Buckling Capacity

This section is applicable for slender webs and not for rolled sections that have stocky webs. For the sake of completeness, however, procedure and formulas for calculating buckling capacity has been given here:

$$P_x \leq R_{sb} \quad (10)$$

where R_{sb} is the nominal buckling capacity of the stiffened web and is determined by the following procedure according to Section 6 of AS 4100:

$$R_{sb} = \alpha_c N_s \leq N_s \quad (11)$$

where

$$\alpha_c = \xi \left\{ 1 - \left[1 - (90/\xi\lambda)^2 \right]^{0.5} \right\} \quad (12)$$

$$\xi = \left\{ (\lambda/90)^2 + 1 + \eta \right\} / 2(\lambda/90)^2 \quad (13)$$

$$\eta = 0.00326(\lambda - 13.5) \geq 0 \quad (14)$$

$$\lambda = \lambda_n + \alpha_a \alpha_b \quad (15)$$

$$\lambda_n = (L_e/r)(k_f)^{0.5} (f_y/250)^{0.5} \quad (16)$$

$$\alpha_a = \left\{ 2100(\lambda_n - 13.5) \right\} / \left(\lambda_n^2 - 15.3 \lambda_n + 2050 \right) \quad (17)$$

$\alpha_b = 0.5$, the appropriate member section constant given in Table 6.3.3 of the Code

$k_f = 1$, as determined in Section 6.2.2 of the Code

$L_e = 0.7d_1$ where d_1 = clear depth between flanges ignoring fillets and welds

r = radius of gyration about the minor axis

$$N_s = k_f A_n f_y \quad (18)$$

A_n = net area of cross-section consisting of the pair of stiffeners and a centrally located strip of the web of width not greater than the lesser of $17.5t_w/\sqrt{(f_y/250)}$ and $s/2$, where s = spacing of stiffeners

AISC Specification for Structural Steel Buildings 2010

Section J10.8 of the AISC *Specification* (AISC, 2010) provides a procedure to evaluate the strength of webs with full-depth stiffeners under compressive load on flanges, as given in Equation 19. As per Section J10.8, transverse full-depth bearing stiffeners for compressive forces applied to a beam or plate girder flange(s) shall be designed as axially compressed members (columns) in accordance with the requirements of Sections E6.2 and J4.4. The member properties shall be determined using an effective length of $0.75h$, a cross-section composed of two stiffeners, and a strip of the web having a width of $25t_w$ at interior stiffeners and $12t_w$ at the ends of members.

As mentioned earlier, Section J10.8 requires that provisions of Section J4.4 be used to evaluate strength of full-length bearing stiffeners under concentrated loads. Section J4.4 states that the available strength of connecting elements in compression for the limit states of yielding and buckling can be determined as follows:

(a) When $KL/r \leq 25$ (yielding)

$$P_n = F_y A_g \quad (19)$$

with

$$\phi = 0.90$$

F_y = specified minimum yield stress

A_g = gross area of a cross-section composed of two stiffeners and a strip of the web having a width of 25 times the thickness of the web

r = radius of gyration about the minor axis

$KL = 0.75h$, where h is the clear distance between the flanges less the fillet or corner radius

(b) When $KL/r > 25$ (buckling), the provisions of Chapter E apply.

Because $KL/r \leq 25$ for all tests reported here, provisions of Section J4.4 (b) are not applicable.

Comparison of Test Results with Nominal Capacity Values and Predictive Equation

A comparison between the test results conducted at the University of Maine and the stiffened web strengths predicted by the AISC, CSA and AS design codes as well as the proposed formula are presented in Table 5.

The average ratios of test results to the predicted failure loads were found to be 1.03 for both AISC and CSA, 1.36 for AS and 0.98 for the proposed formula. The coefficients of variation were found to be 0.13 for both AISC and CSA, 0.22 for AS and 0.05 for the proposed formula. Hence, it may be said that the proposed formula is more consistently able to predict stiffened web strength. Further, the proposed formula is able to evaluate the crippling strength of webs with partial-depth stiffeners and eccentric loading, unlike the design codes.

CONCLUSIONS AND RECOMMENDATIONS

The provisions given in the 2010 AISC *Specification* (AISC, 2010) for calculating the stiffened web strength may be reexamined in the light of the information provided here:

1. Presently, the AISC *Specification* recommends half-depth stiffeners or doubler plates for eliminating web crippling limit state. This, however, is not correct for web crippling under patch loading; failure mode 1, which is web crippling failure below the stiffener, occurs when stiffeners are half depth. Based on the research at the University of Maine, it is recommended that webs shall be provided with minimum three-quarters-depth web stiffeners for eliminating web crippling limit state.
2. Presently, the AISC *Specification* does not recommend any specific optimum thickness for the stiffener. As may be noted from the test results shown in Table 1 and the FEA parametric study (in particular, Table 4 and Figure 14), web strength increased with increase

Table 5: Comparison of Test Results with Design Codes and Proposed Formula

Test No.	Test Results kips	AISC Results (AISC) kips	Canadian Results (CSA) kips	Australian Results (AS) kips	Proposed Formula (Eq. 1) kips	Test/AISC	Test/CSA	Test/AS	Test/Proposed Formula
1	161	135	135	154	169	1.20	1.20	1.05	0.95
2	107	130	130	72	116	0.82	0.82	1.48	0.92
3	162	132	132	150	165	1.23	1.23	1.08	0.98
4	114	123	123	70	114	0.93	0.93	1.62	1.00
5	169	139	139	161	173	1.21	1.21	1.05	0.98
6	120	142	142	89	120	0.84	0.84	1.36	1.00
7	161	142	142	162	171	1.13	1.13	0.99	0.94
8	144	138	138	85	129	1.05	1.05	1.69	1.12
9	175	158	158	178	193	1.11	1.11	0.98	0.91
10	128	154	154	103	126	0.83	0.83	1.23	1.02
11	149	161	161	106	150	0.93	0.93	1.41	0.99
12	150	157	157	102	152	0.96	0.96	1.47	0.99
13	126	115	115	66	122	1.10	1.10	1.92	1.03
14	154	141	141	86	153	1.09	1.09	1.79	1.01
15	164	157	157	102	174	1.04	1.04	1.61	0.94
16	132	140	140	85	139	0.94	0.94	1.56	0.95
17	145	137	137	157	148	1.06	1.06	0.92	0.98

in stiffener thickness and is maximum when stiffener thickness is almost equal to web thickness. Further, it was noted from tests on half-depth stiffeners that when stiffener thickness exceeded web thickness, web crippling occurred under the stiffeners. Therefore, it is recommended that the stiffener thickness be approximately the thickness of the web.

3. Presently, the AISC *Specification* recommends the use of half-depth stiffener to eliminate the web crippling limit state. It, however, does not provide any direct formula to evaluate enhanced web strength due to addition of a half-depth stiffener. Equation 1 provides a means for evaluating stiffened web crippling strength because it considers the effect of all the parameters—namely, depth of stiffener, thickness of stiffener, eccentricity of loading and width of loading—and compares well with the test results, as illustrated in Table 5.
4. Equation 1 could be useful for evaluating the remaining strength of webs with full-depth stiffeners where the bottom portion of the stiffener has been badly corroded. Such an evaluation may be necessary in older structures requiring retrofit and also in structures that are anticipated to be overloaded in specific areas.

REFERENCES

- AISC (1986), *Load and Resistance Factor Design Specification for Structural Steel Buildings*, 1st ed., American Institute of Steel Construction, Chicago, IL.
- AISC (2010), *Specification for Structural Steel Buildings*, ANSI/AISC 360-10, American Institute of Steel Construction, Chicago, IL.
- AS (2012), *Steel Structures*, AS 4100, Australian Standard, Homebush, NSW.
- Bathe, K., Wilson, E. and Iding, R. (1974), “NONSAP, A Structural Analysis Program for Static and Dynamic Response of Nonlinear Systems,” Report No. UCSESM 74-3, Structural Engineering Laboratory, University of California, Berkeley.
- CSA (2006), *Limit States Design of Steel Structures* (update 3, 2006), CAN/CSA S-16-01, The Canadian Standards Association, Mississauga, Ontario.
- Du, C. (1991), “Nonlinear Response of Thin Steel Plate Structures Subjected to Static, Dynamic, and Cyclic Load,” Ph.D. Thesis, Civil Engineering Department, University of Maine.

- Elgaaly, M. (1983), "Web Design Under Compressive Edge Loads," *Engineering Journal*, AISC, 4th Quarter, 1983, pp 153–171.
- Elgaaly, M., Salkar, R. and Eash, M. (1992), "Unstiffened and Stiffened Webs under Compressive Edge Loads," *Proceedings of Annual Technical Session Proceedings*, Structural Stability Research Council, Pittsburgh, Pennsylvania, pp 279–302.
- Kim, Y., Jung, S. and White, D. (2007), "Transverse Stiffener Requirements in Straight and Horizontally Curved Steel I-Girders," *Journal of Bridge Engineering*, ASCE, Vol. 12, No. 2, March–April, pp. 174–183.
- Lee, S., Yoo, C. and Yoon, D. (2002), "Behavior of Intermediate Transverse Stiffeners Attached on Web Panels," *Journal of Structural Engineering*, ASCE, Vol. 128, No. 3, March, pp. 337–345.
- Lee, S., Yoo, C. and Yoon, D. (2003), "New Design Rule for Intermediate Transverse Stiffeners Attached on Web Panels," *Journal of Structural Engineering*, ASCE, Vol. 129, No. 12, December, pp. 1607–1614.
- Salkar, R. (1992), "Strength and Behavior of Webs, With and Without Stiffeners, Under Local Compressive In-plane and Eccentric Loads," University of Maine at Orono, Maine, Vol. 2, Chapter 5, pp 424–522.

Double-Tee Members in Axial Compression

LEIGH ARBER, MENG WANG and PAT MCMANUS

ABSTRACT

This paper presents tabulated compressive strengths of double-tee members, which are comprised of two WT members oriented with their flanges back to back (referred to as “2WTs” or “double WT” hereafter). The benefits and typical use of these members are described, including schematic details of connection designs. All WT members built from the WT7 and WT6 series are included in the table, which gives available strengths in both ASD and LRFD. Slenderness effects and the effects of shear deformations of intermediate connectors are taken into account.

Keywords: compression member, WT section, double WT section, truss.

INTRODUCTION AND DISCUSSION

WT and angle sections, both in single and back-to-back configurations, are commonly used as web members in trusses and as vertical and horizontal bracing members. This is particularly true in industrial construction. While WT and angle sections make for economical tension members, they are generally less economical than wide-flange or HSS sections when utilized as singular members in compression with relatively large unbraced lengths. However, when used in back-to-back built-up configurations, the least radius of gyration is increased, and the sections become more economical. To date, determination of the available compressive strength of built-up back-to-back WT sections involved significant calculation effort on the part of the engineer because compression strength tables had not been made readily available. This paper, however, now provides tables of available strength in axial compression for back-to-back WT sections to assist the engineer in designing with these sections.

WT sections are not rolled directly from the mill but are split from wide-flange sections. Splitting is typically performed by the fabricator or as an additional process by an outside entity before delivery to the fabrication facility. Often, the residual stresses resulting from the mill rolling and splitting processes induce undesirable curvature

of the WT sections such that a straightening process may be required. The costs of splitting and straightening vary depending on the processes used but, together, typically result in a cost increase over unsplit wide-flange material of between approximately 50% for relatively light wide-flange sections (around 35 lb/ft) to approximately 10% for relatively heavy sections (200 lb/ft). The cost of intermediate connectors to create the built-up WT sections is additional to this. While these premium costs may be a reasonably high percentage of the cost of the brace member, they may not be a significant cost to the project in absolute terms. Though costs vary by fabricator and erector, these premium costs can be offset by the savings realized from using inherently more economical end connections.

The greatest advantage of WT connections is that the cross-sectional component of greatest area (the flange) can be directly connected to the support element, typically a gusset plate, using either welds or bolts. An example of such a connection is illustrated in Figure 1. Note that bolted connections at the ends of built-up members require the use of pretensioned bolts with Class A or B faying surfaces in accordance with AISC *Specification* Section E6.1 (AISC, 2010).

Connections for wide-flange braces, on the other hand, require additional connection elements such as plates and angles to transfer forces from the brace to the gusset. As shown in Figure 2, wide-flange member connections typically require fasteners to transfer forces from the brace to the connection elements and then from the connection elements to the gusset plate. The result is twice the total number of fasteners required to connect an equivalent built-up WT section directly to a gusset. Additionally, where large forces are involved, the geometry associated with connection angles attached to the flanges of the brace result in large gusset plates, which are undesirable economically and often aesthetically.

With regard to HSS material, the cold bending and seam

Leigh Arber, P.E., S.E., American Institute of Steel Construction, 1 E. Wacker Dr., Chicago, IL (corresponding). Email: arber@aisc.org

Meng Wang, Stanford University, 6 Comstock Circle, Stanford, CA. Email: mwang15@stanford.edu

Pat McManus, Ph.D., P.E., S.E Martin/Martin Wyoming, 4020 Laramie St., Cheyenne, WY. Email: pmcmanus@martinmartin.com

Paper No. 2014-10

welding processes used to create HSS sections cost approximately 15% more than a wide-flange section of equivalent area. The large radius of gyration in each direction results in a smaller required area to carry compression forces and generally offsets the increased material costs. However, end connections for HSS members are costly. Field-bolted connections can only be achieved by transferring forces through additional connection elements similar to wide-flange sections and are typically only economical under relatively small forces. Consequently, HSS connections are normally slotted and field welded to gusset plates as illustrated in Figure 3. While gusset plates in such a configuration are more compact than large-capacity wide-flange brace connections, HSS connections may require greater connection length than equivalent WT connections to reduce the effects of shear lag. Depending on the fabricator, preparation of the slot can also be costly. Most detrimental to the economy of large-capacity HSS connections is the field welding of the brace to the gusset because field welding is arguably the most expensive process in structural steel construction. As a result, the use of back-to-back WT sections as axial members can prove more economical than wide-flange or HSS sections, particularly where large capacities are required.

DESIGN EXAMPLE AND TABLE

In the table, which appears at the end of this paper, available strengths in axial compression, including the limit states of flexural buckling and torsional buckling, are given for 2WTs. Both ASD and LRFD values are given. The material used is ASTM A992 with $F_y = 50$ ksi, and $\frac{3}{8}$ -in. separation between the flanges is assumed. The values in this table can be used conservatively when a larger separation is provided. The shape slenderness and reduction factor, Q_s , for the 2WT section is calculated in the same manner as for a single WT, and the values of Q_s are taken directly from the AISC Shape Database V14.0 for single WTs. Torsional elastic buckling stress is calculated per *Specification* Equation E4-4, omitting the term with C_w because of its negligible effect. Justification for this omission is illustrated in the design example.

Separate tabulated values are given for the effective lengths with respect to the X-X and Y-Y axes, $(KL)_x$ and $(KL)_y$, respectively, where the lesser of flexural buckling

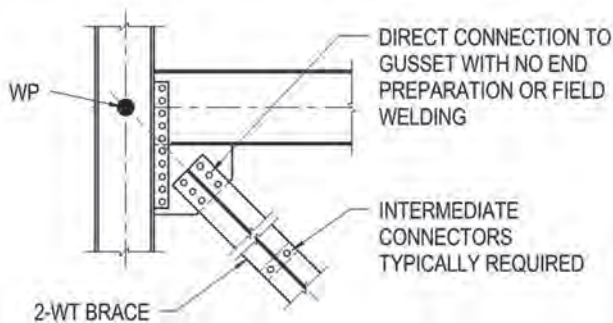


Fig. 1. Example of WT brace connection.

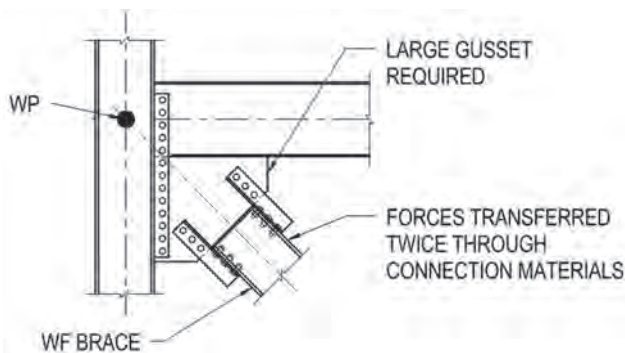


Fig. 2. Example of wide-flange brace connection.

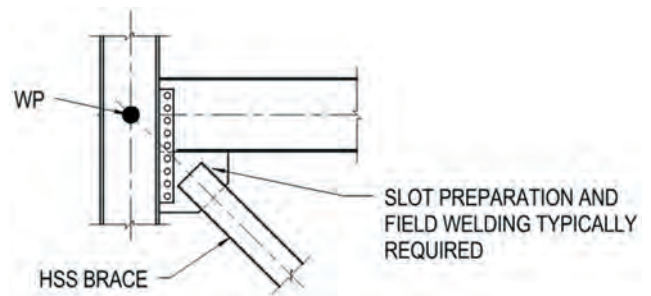


Fig. 3. Example of HSS brace connection.

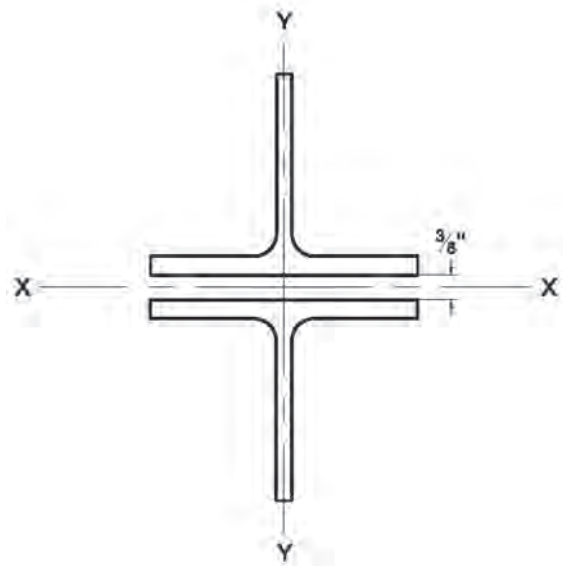


Fig. 4. Orientation of 2WT built-up section.

about the given axis and torsional buckling are reported about each axis. The orientation of the axes is shown in Figure 4.

For buckling about the Y-Y axis, the available strength is not affected by the number of intermediate connectors because slip between the two WT's is not a concern. The slenderness ratio need not be modified by AISC *Specification* Equation E6-1 because the buckling mode does not involve relative deformations that produce shear forces in the connectors between individual shapes. The available compressive strength for buckling about the Y-Y axis for 2WT shapes is twice that of a single WT.

For buckling about the X-X axis, the number of intermediate connectors must be considered. The tabulated values for $(KL)_x$ used to compute the available strength have been adjusted for the shear deformation in accordance with AISC *Specification* Equations E6-2a and E6-2b, which are applicable to welded and pretensioned bolted intermediate shear connectors. The number of intermediate connectors, n , is given in the table and is selected such that the available compression buckling strength about the X-X axis is equal to or greater than 90% of that for compression buckling for the two WT's as a continuously-connected unit. This is the same design choice used for double angles in AISC *Manual*

Tables 4-8, 4-9 and 4-10 (AISC, 2011). If fewer connectors or snug-tightened bolted intermediate connectors are used, the available strength must be recalculated per AISC *Specification* Section E6. According to AISC *Specification* Section E6.2, the slenderness of the individual components of the built-up member based upon the distance between intermediate connectors, a , must not exceed three-quarters of the controlling slenderness of the overall built-up compression member. The connectors are assumed to be equally spaced, and the distance between connectors, a (in.), is calculated as $L/(n + 1)$. K is assumed conservatively to be 1.0 when checking the slenderness of individual components between intermediate connectors.

The following equations are used to calculate geometric properties of 2WT, $\frac{3}{8}$ -in. back to back (symbols without “_2WT” are properties of a single WT):

$$I_{x_2WT} = 2[I_x + A(\bar{y} + \frac{3}{16} \text{ in.})^2]$$

$$r_{x_2WT} = \sqrt{I_{x_2WT}/(2A)}$$

$$I_{y_2WT} = 2I_y$$

$$r_{y_2WT} = r_y$$

$$J_{_2WT} = 2J$$

Design Example

Calculate the available strength of a 2WT7×21.5 section in axial compression with a 14.0-ft unbraced length. As noted in the footnote in AISC *Manual* Table 1-8, this shape is slender for compression. For a single WT7×21.5, from Table 1-8:

$$A = 6.31 \text{ in.}^2$$

$$t_f = 0.530 \text{ in.}$$

$$b_f = 8.00 \text{ in.}$$

$$t_w = 0.305 \text{ in.}$$

$$h = 6.83 \text{ in.}$$

$$I_x = 21.9 \text{ in.}^4$$

$$I_y = 22.6 \text{ in.}^4$$

$$r_x = 1.86 \text{ in.}$$

$$r_y = 1.89 \text{ in.}$$

$$J = 0.522 \text{ in.}^4$$

$$\bar{y} = 1.31 \text{ in.}$$

$$Q_s = 0.773$$

The combined properties, using the preceding equations, are:

$$A_{_2WT} = 12.62 \text{ in.}^2$$

$$I_{x_2WT} = 72.1 \text{ in.}^4$$

$$I_{y_2WT} = 45.2 \text{ in.}^4$$

$$r_{x_2WT} = 2.39 \text{ in.}$$

$$r_{y_2WT} = 1.89 \text{ in.}$$

$$J_{_2WT} = 1.04 \text{ in.}^4$$

Each applicable limit state will be checked separately. AISC *Specification* Section E7 states that slender-element members shall be designed for flexural buckling, torsional buckling and flexural-torsional buckling.

Torsional buckling:

AISC *Specification* Equation E4-4 applies for torsional buckling of 2WT sections. As discussed previously, the term containing C_w is conservatively omitted here.

$$\begin{aligned}
 F_e &= \frac{GJ_{2WT}}{I_{x_{2WT}} + I_{y_{2WT}}} \\
 &= \frac{11,200 \text{ ksi} (1.04 \text{ in.}^4)}{72.1 \text{ in.}^4 + 45.2 \text{ in.}^4} \\
 &= 99.3 \text{ ksi}
 \end{aligned}$$

If the term C_w were used, it would have a negligible effect. Using AISC *Design Guide* 9 Equation 3.35 (Seaburg and Carter, 2003):

$$\begin{aligned}
 C_{w_{2WT}} &= 2 \text{ tees} \left[\frac{t_f^3 b_f^3}{144} + \frac{t_w^3 h^3}{36} \right] \\
 &= 2 \left[\frac{(0.530 \text{ in.})^3 (8.00 \text{ in.})^3}{144} + \frac{(0.305 \text{ in.})^3 (6.83 \text{ in.})^3}{36} \right] \\
 &= 1.56 \text{ in.}^6
 \end{aligned}$$

$$\begin{aligned}
 F_e &= \left[\frac{\pi^2 E C_{w_{2WT}}}{(K_z L)^2} + GJ_{2WT} \right] \left[\frac{1}{I_{x_{2WT}} + I_{y_{2WT}}} \right] \\
 &= \left[\frac{\pi^2 (29,000 \text{ ksi}) (1.56 \text{ in.}^6)}{(14.0 \text{ ft} \times 12 \text{ in./ft})^2} + 11,200 \text{ ksi} (1.04 \text{ in.}^4) \right] \left[\frac{1}{72.1 \text{ in.}^4 + 45.2 \text{ in.}^4} \right] \\
 &= 99.4 \text{ ksi}
 \end{aligned}$$

Including the C_w term results in approximately a 0.1% difference. This would vary with length, but is negligible and will not be included in the strength tables.

As noted in AISC *Specification* Section E7, F_{cr} is determined according to Equation E7-2 or E7-3.

With $QF_y/F_e < 2.25$, Equation E7-2 applies, where $Q = Q_s$.

$$\begin{aligned}
 F_{cr} &= Q \left(0.658 \frac{QF_y}{F_e} \right) F_y \\
 &= 0.773 \left(0.658 \frac{0.773 (50 \text{ ksi})}{99.3 \text{ ksi}} \right) (50 \text{ ksi}) \\
 &= 32.8 \text{ ksi}
 \end{aligned}$$

The available strength in axial compression is:

LRFD	ASD
$\phi P_n = 0.9 (12.62 \text{ in.}^2) (32.8 \text{ ksi})$ $= 373 \text{ kips}$	$\frac{P_n}{\Omega} = \frac{(12.62 \text{ in.}^2) (32.8 \text{ ksi})}{1.67}$ $= 248 \text{ ksi}$

Flexural buckling about the Y-Y axis:

For buckling about the Y-Y axis, there is no issue of slip between the two WT sections and the strength is not dependent on connectors. The slenderness ratio is:

$$\begin{aligned} \frac{KL}{r_{y_2WT}} &= \frac{1.0(14 \text{ ft})(12.0 \text{ in./ft})}{1.89 \text{ in.}} \\ &= 88.9 \end{aligned}$$

The elastic buckling stress, from AISC *Specification* Equation E3-4, is:

$$\begin{aligned} F_e &= \frac{\pi^2 E}{\left(\frac{KL}{r}\right)^2} \\ &= \frac{\pi^2 (29,000 \text{ ksi})}{(88.9)^2} \\ &= 36.2 \text{ ksi} \end{aligned}$$

With $QF_y/F_e < 2.25$, Equation E7-2 applies, where $Q = Q_s$.

$$\begin{aligned} F_{cr} &= Q \left(0.658 \frac{Q_s F_y}{F_e} \right) F_y \\ &= 0.773 \left(0.658 \frac{0.773 (50 \text{ ksi})}{36.2 \text{ ksi}} \right) (50 \text{ ksi}) \\ &= 24.7 \text{ ksi} \end{aligned}$$

The available strength in axial compression is:

LRFD	ASD
$\begin{aligned} \phi P_n &= 0.9 (12.62 \text{ in.}^2) (24.7 \text{ ksi}) \\ &= 281 \text{ kips} \end{aligned}$	$\begin{aligned} \frac{P_n}{\Omega} &= \frac{(12.62 \text{ in.}^2) (24.7 \text{ ksi})}{1.67} \\ &= 187 \text{ ksi} \end{aligned}$

Flexural buckling about the X-X axis:

For buckling about the X-X axis, the number of connectors affects the available strength. Start by determining the strength of the member as though the 2WT member acts as a continuously connected unit:

$$\begin{aligned} \frac{KL}{r_{x_2WT}} &= \frac{1.0(14 \text{ ft})(12.0 \text{ in./ft})}{2.39 \text{ in.}} \\ &= 70.3 \end{aligned}$$

The elastic buckling stress, from AISC *Specification* Equation E3-4, is:

$$F_e = \frac{\pi^2 E}{\left(\frac{KL}{r}\right)^2}$$

$$= \frac{\pi^2 (29,000 \text{ ksi})}{(70.3)^2}$$

$$= 57.9 \text{ ksi}$$

With $QF_y/F_e < 2.25$, Equation E7-2 applies, where $Q = Q_s$.

$$F_{cr} = Q \left(0.658 \frac{QF_y}{F_e} \right) F_y$$

$$= 0.773 \left(0.658 \frac{0.773 (50 \text{ ksi})}{57.9 \text{ ksi}} \right) (50 \text{ ksi})$$

$$= 29.2 \text{ ksi}$$

The available strength in axial compression is:

LRFD	ASD
$\phi P_n = 0.9 (12.62 \text{ in.}^2) (29.2 \text{ ksi})$ $= 332 \text{ kips}$	$\frac{P_n}{\Omega} = \frac{(12.62 \text{ in.}^2) (29.2 \text{ ksi})}{1.67}$ $= 221 \text{ ksi}$

However, this strength is for a continuously connected section. Now consider the effect of connectors on the strength.

Determine the minimum number of intermediate connectors:

As stated earlier, the number of connectors will be chosen so that the strength about the X-X axis is at least 90% of the strength of the member acting as a unit (for any applicable compression limit state). That strength, with flexural buckling about the Y-Y axis as the governing limit state, is:

LRFD	ASD
$\phi P_n = 90\% (281 \text{ kips})$ $= 253 \text{ kips}$	$\frac{P_n}{\Omega} = 90\% (187 \text{ kips})$ $= 168 \text{ ksi}$

Start with one connector following the provisions of AISC *Specification* Section E6. Assume that connectors are welded or connected by pretensioned bolts. One connector at the midspan of the member would result in an unbraced length of 7 ft.

$$\frac{a}{r_i} = \frac{(7.0 \text{ ft})(12.0 \text{ in./ft})}{1.86 \text{ in.}}$$

$$= 45.2$$

where a and r_i are as defined in AISC *Specification* Section E6. Because a/r_i is greater than 40, use Equation E6-2b to determine the modified slenderness ratio of the built-up member:

$$\left(\frac{KL}{r}\right)_m = \sqrt{\left(\frac{14.0 \text{ ft}(12.0 \text{ in./ft})}{2.39 \text{ in.}}\right)^2 + \left(\frac{0.86(7.0 \text{ ft})(12.0 \text{ in./ft})}{1.86 \text{ in.}}\right)^2}$$

$$= 80.3$$

$$F_e = \frac{\pi^2 E}{\left(\frac{KL}{r}\right)^2}$$

$$= \frac{\pi^2(29,000 \text{ ksi})}{(80.3)^2}$$

$$= 44.4 \text{ ksi}$$

With $QF_y/F_e < 2.25$, Equation E7-2 applies, where $Q = Q_s$.

$$F_{cr} = Q \left(0.658 \frac{QF_y}{F_e}\right) F_y$$

$$= 0.773 \left(0.658 \frac{0.773 (50 \text{ ksi})}{44.4 \text{ ksi}}\right) (50 \text{ ksi})$$

$$= 26.85 \text{ ksi}$$

The available strength in axial compression for the limit state of flexural buckling about the X-X axis with one intermediate connector is:

LRFD	ASD
$\phi P_n = 0.9 (12.62 \text{ in.}^2) (26.85 \text{ ksi})$ $= 305 \text{ kips}$	$\frac{P_n}{\Omega} = \frac{(12.62 \text{ in.}^2) (26.85 \text{ ksi})}{1.67}$ $= 203 \text{ kips}$

This is greater than 90% of the governing strength; therefore, one connector is adequate.

Summarize available strengths:

For buckling about the Y-Y axis, flexural buckling governs over torsional buckling, and the available strength is:

LRFD	ASD
$\phi P_n = 281 \text{ kips}$	$\frac{P_n}{\Omega} = 187 \text{ kips}$

For buckling about the X-X axis, one intermediate connector is required. Flexural buckling governs over torsional buckling, and the available strength is:

LRFD	ASD
$\phi P_n = 305 \text{ kips}$	$\frac{P_n}{\Omega} = 203 \text{ kips}$

These results match the available strengths given in the attached tables for a 2WT7×21.5 section in axial compression with a 14.0-ft unbraced length.

In addition, AISC *Specification* Section E6.2 states that the effective slenderness ratio of each of the component shapes between fasteners must not exceed three-fourths of the governing slenderness ratio of the built-up member. As calculated previously, the effective slenderness ratio of the single WT component shape is:

$$\begin{aligned}\frac{a}{r_i} &= \frac{7.0 \text{ ft (12.0 in./ft)}}{1.86 \text{ in.}} \\ &= 45.2\end{aligned}$$

The governing slenderness ratio of the built-up member is about the Y-Y axis:

$$\begin{aligned}\frac{KL}{r_{y_{2WT}}} &= \frac{1.0(14 \text{ ft})(12.0 \text{ in./ft})}{1.89 \text{ in.}} \\ &= 88.9\end{aligned}$$

This requirement is satisfied, because $45.2 \leq 0.75(88.9) = 66.7$.

ACKNOWLEDGMENTS

The authors would like to recognize Puma Steel, Central Texas Iron Works, Prospect Steel Co. and Nucor Yamato Steel for assistance with cost information.

REFERENCES

AISC Shapes Database V14.0 (www.aisc.org/shapes).

AISC (2010), *Specification for Structural Steel Buildings*, ANSI/AISC 360-10, American Institute of Steel Construction, Chicago, IL.

AISC (2011), *Steel Construction Manual*, 14th ed., American Institute of Steel Construction, Chicago, IL.

Seaburg, P.A. and Carter, C.J. (2003), *Torsional Analysis of Structural Steel Members*, AISC Steel Design Guide No. 9, American Institute of Steel Construction, Chicago, IL.

Available Strength in Axial Compression, kips										
Shape		2WT7x365		2WT7x332.5		2WT7x302.5		2WT7x275		
Design		P_n/Ω_c ASD	$\phi_c P_n$ LRFD							
Effective Length, KL (ft), with Respect to Indicated Axis	X-X Axis	0	6330	9520	5780	8690	5250	7900	4770	7170
		10	6080	9140	5530	8310	5000	7510	4510	6780
		12	5950	8940	5390	8100	4860	7300	4370	6570
		14	5790	8700	5230	7860	4700	7060	4210	6330
		16	5610	8430	5050	7590	4520	6790	4030	6060
		18	5420	8140	4850	7300	4330	6500	3840	5770
		20	5210	7820	4650	6980	4120	6190	3640	5470
		22	4980	7490	4420	6650	3900	5870	3420	5150
		24	4750	7140	4190	6300	3680	5530	2930	4400
		26	4510	6780	3610	5430	3120	4700	2980	4490
		28	3860	5810	3720	5590	3220	4840	2760	4150
		30	4020	6040	3480	5230	2990	4490	2540	3820
		32	3770	5660	3240	4860	2760	4150	2120	3190
		34	3520	5280	2740	4120	2300	3460	1910	2870
	36	2980	4480	2500	3760	2320	3480	1910	2880	
	Y-Y Axis	0	6330	9520	5780	8690	5250	7900	4770	7170
		10	6110	9180	5570	8380	5060	7610	4600	6910
		12	5980	8990	5450	8200	4950	7440	4490	6750
		14	5830	8770	5310	7990	4820	7250	4370	6570
		16	5670	8520	5160	7750	4680	7030	4240	6370
		18	5490	8250	4990	7500	4520	6790	4090	6150
		20	5290	7960	4800	7220	4350	6530	3930	5910
		22	5090	7640	4610	6930	4170	6260	3760	5650
		24	4870	7310	4400	6620	3970	5970	3590	5390
		26	4640	6970	4190	6300	3780	5680	3400	5110
		28	4410	6620	3970	5970	3570	5370	3220	4830
		30	4170	6270	3750	5640	3370	5060	3030	4550
		32	3930	5910	3530	5300	3160	4750	2840	4260
34		3690	5550	3300	4970	2960	4450	2650	3980	
36	3450	5190	3080	4630	2750	4140	2460	3700		
Number of Connectors	10	2		2		2		2		
	12	2		2		2		2		
	14	2		2		2		2		
	16	2		2		2		2		
	18	2		2		2		2		
	20	2		2		2		2		
	22	2		2		2		2		
	24	2		2		2		2		
	26	2		2		2		3		
	28	2		3		3		3		
	30	3		3		3		3		
	32	3		3		3		3		
	34	3		3		3		3		
	36	3		3		4		4		

"—" indicates that KL/r is greater than 200.

Available Strength in Axial Compression, kips										
Shape		2WT7x250		2WT7x227.5		2WT7x213		2WT7x199		
Design		P_n/Ω_c ASD	$\phi_c P_n$ LRFD							
Effective Length, KL (ft), with Respect to Indicated Axis	X-X Axis	0	4320	6500	3930	5900	3670	5520	3420	5130
		10	4070	6110	3670	5520	3420	5140	3170	4760
		12	3930	5900	3530	5310	3280	4930	3030	4550
		14	3770	5660	3380	5080	3130	4700	2880	4330
		16	3590	5400	3200	4820	2960	4440	2710	4070
		18	3400	5120	3020	4540	2770	4170	2530	3810
		20	3200	4820	2830	4250	2580	3880	2350	3530
		22	3000	4510	2410	3620	2180	3280	1970	2950
		24	2530	3800	2190	3280	2190	3300	1970	2960
		26	2570	3870	2220	3340	2000	3000	1790	2680
		28	2360	3550	2020	3040	1810	2710	1600	2410
		30	2150	3240	1670	2510	1470	2210	1290	1940
		32	1770	2660	1640	2470	1440	2170	1130	1710
		34	1760	2640	1460	2190	1280	1920	1010	1510
	36	1570	2360	1300	1960	1060	1600	897	1350	
	Y-Y Axis	0	4320	6500	3930	5900	3670	5520	3420	5130
		10	4170	6270	3790	5700	3550	5340	3310	4970
		12	4070	6120	3700	5560	3460	5210	3220	4850
		14	3960	5950	3600	5410	3360	5060	3130	4710
		16	3840	5760	3480	5230	3250	4890	3030	4550
		18	3700	5560	3350	5040	3130	4710	2910	4380
		20	3550	5340	3210	4830	3000	4510	2790	4190
		22	3390	5100	3070	4610	2860	4300	2660	4000
		24	3230	4850	2920	4390	2720	4090	2530	3800
		26	3060	4600	2760	4150	2570	3870	2390	3590
		28	2890	4340	2600	3910	2420	3640	2250	3380
		30	2710	4080	2440	3670	2270	3410	2100	3160
		32	2540	3820	2280	3430	2120	3180	1960	2950
34		2360	3550	2120	3190	1970	2960	1820	2740	
36	2190	3300	1960	2950	1820	2730	1680	2530		
Number of Connectors	10	2		2		2		2		
	12	2		2		2		2		
	14	2		2		2		2		
	16	2		2		2		2		
	18	2		2		2		2		
	20	2		2		2		2		
	22	2		2		2		2		
	24	2		2		3		3		
	26	3		3		3		3		
	28	3		3		3		3		
	30	3		3		3		3		
	32	3		4		4		3		
	34	4		4		4		3		
	36	4		4		4		3		

"—" indicates that KL/r is greater than 200.

Available Strength in Axial Compression, kips										
Shape		2WT7x185		2WT7x171		2WT7x155.5		2WT7x141.5		
Design		P_n/Ω_c ASD	$\phi_c P_n$ LRFD							
Effective Length, KL (ft), with Respect to Indicated Axis	X-X Axis	0	3170	4770	2930	4400	2650	3980	2400	3600
		10	2930	4400	2690	4040	2420	3630	2180	3280
		12	2790	4200	2560	3840	2290	3440	2050	3090
		14	2640	3970	2410	3620	1940	2920	1730	2600
		16	2480	3730	2250	3380	1990	3000	1770	2660
		18	2300	3460	2080	3130	1830	2750	1610	2430
		20	2130	3190	1910	2870	1520	2290	1330	2000
		22	1760	2640	1560	2350	1500	2260	1300	1960
		24	1760	2650	1560	2350	1340	2020	1150	1730
		26	1580	2380	1390	2090	1190	1780	920	1380
		28	1290	1940	1120	1680	939	1410	793	1190
		30	1120	1690	973	1460	818	1230	691	1040
		32	987	1480	855	1290	719	1080	608	913
	34	874	1310	758	1140	637	957	538	809	
	36	780	1170	676	1020	568	854	480	721	
	Y-Y Axis	0	3170	4770	2930	4400	2650	3980	2400	3600
		10	3080	4620	2840	4270	2580	3870	2340	3520
		12	3000	4510	2770	4160	2510	3770	2280	3430
		14	2910	4370	2680	4040	2430	3660	2210	3320
		16	2810	4220	2590	3900	2350	3530	2130	3210
		18	2700	4060	2490	3740	2260	3390	2050	3080
		20	2590	3890	2380	3580	2160	3240	1950	2940
		22	2460	3700	2270	3410	2050	3080	1860	2790
		24	2340	3510	2150	3230	1940	2920	1760	2640
		26	2210	3320	2030	3050	1830	2750	1650	2480
		28	2070	3120	1900	2860	1710	2580	1550	2330
30		1940	2910	1780	2670	1600	2400	1440	2170	
32		1810	2710	1650	2480	1490	2230	1340	2010	
34	1670	2520	1530	2300	1370	2060	1240	1860		
36	1540	2320	1410	2120	1260	1900	1130	1710		
Number of Connectors	10	2		2		1		1		
	12	2		2		1		1		
	14	2		2		1		1		
	16	2		2		2		2		
	18	2		2		2		2		
	20	2		2		2		2		
	22	2		2		3		3		
	24	3		3		3		3		
	26	3		3		3		3		
	28	3		3		3		3		
	30	3		3		3		3		
	32	3		3		3		3		
	34	3		3		3		3		
36	3		3		3		3			

"—" indicates that KL/r is greater than 200.

Available Strength in Axial Compression, kips										
Shape		2WT7×128.5		2WT7×116.5		2WT7×105.5		2WT7×96.5		
Design		P_n/Ω_c ASD	$\phi_c P_n$ LRFD							
Effective Length, KL (ft), with Respect to Indicated Axis	X-X Axis	0	2170	3260	1950	2930	1750	2630	1590	2390
		10	1960	2940	1750	2630	1570	2370	1430	2140
		12	1840	2760	1640	2460	1460	2200	1210	1820
		14	1700	2560	1510	2270	1340	2020	1200	1810
		16	1560	2350	1380	2070	1220	1830	1080	1630
		18	1420	2130	1240	1860	1090	1630	880	1320
		20	1150	1730	992	1490	959	1440	840	1260
		22	1120	1690	965	1450	835	1260	725	1090
		24	983	1480	836	1260	717	1080	566	850
		26	775	1170	654	984	560	842	482	725
		28	668	1000	564	848	483	726	416	625
		30	582	875	491	739	421	632	362	544
		32	512	769	432	649	370	556	318	478
	34	453	681	383	575	328	492	282	424	
	36	404	608	341	513	292	439	251	378	
	Y-Y Axis	0	2170	3260	1950	2930	1750	2630	1590	2390
		10	2130	3200	1920	2890	1740	2620	1590	2390
		12	2070	3110	1870	2810	1690	2550	1550	2330
		14	2010	3010	1810	2720	1640	2460	1500	2250
		16	1930	2900	1750	2620	1580	2370	1440	2170
		18	1850	2790	1670	2510	1510	2270	1380	2080
		20	1770	2660	1590	2400	1440	2160	1320	1980
		22	1680	2520	1510	2270	1360	2050	1250	1870
		24	1590	2380	1430	2150	1290	1930	1180	1770
		26	1490	2240	1340	2020	1210	1810	1100	1660
		28	1400	2100	1250	1890	1130	1690	1030	1550
30		1300	1950	1170	1750	1050	1570	955	1430	
32		1200	1810	1080	1620	968	1450	882	1320	
34	1110	1670	994	1490	890	1340	810	1220		
36	1020	1530	911	1370	814	1220	740	1110		
Number of Connectors	10	1		1		1		1		
	12	1		1		1		1		
	14	2		2		2		2		
	16	2		2		2		2		
	18	2		2		2		2		
	20	2		2		3		3		
	22	3		3		3		3		
	24	3		3		3		3		
	26	3		3		3		3		
	28	3		3		3		3		
	30	3		3		3		3		
	32	3		3		3		3		
	34	3		3		3		3		
36	3		3		3		3			

"—" indicates that KL/r is greater than 200.

Available Strength in Axial Compression, kips									
Shape			2WT7x88		2WT7x79.5		2WT7x72.5		
Design			P_n/Ω_c ASD	$\phi_c P_n$ LRFD	P_n/Ω_c ASD	$\phi_c P_n$ LRFD	P_n/Ω_c ASD	$\phi_c P_n$ LRFD	
Effective Length, <i>KL</i> (ft), with Respect to Indicated Axis	X-X Axis	0	1430	2150	1270	1920	1140	1720	
		10	1290	1940	1150	1730	1040	1560	
		12	1090	1630	962	1450	862	1300	
		14	1080	1630	954	1430	852	1280	
		16	968	1460	848	1270	753	1130	
		18	781	1170	675	1020	595	894	
		20	743	1120	639	960	560	842	
		22	637	957	541	814	470	707	
		24	495	744	420	631	365	549	
		26	422	634	358	538	311	468	
		28	364	547	309	464	269	404	
		30	317	476	269	404	234	352	
		32	278	419	236	355	206	309	
		34	247	371	209	315	182	274	
		36	220	331	187	281	162	244	
		Y-Y Axis	0	1430	2150	1270	1920	1140	1720
			10	1430	2150	1270	1920	1140	1720
			12	1410	2120	1270	1920	1140	1720
	14		1370	2050	1230	1850	1120	1680	
	16		1310	1970	1180	1780	1080	1620	
	18		1260	1890	1130	1700	1030	1550	
	20		1200	1800	1080	1620	978	1470	
	22		1130	1700	1020	1530	925	1390	
	24		1070	1600	959	1440	870	1310	
	26		999	1500	898	1350	814	1220	
	28		931	1400	836	1260	758	1140	
	30		863	1300	774	1160	702	1060	
	32		796	1200	714	1070	647	972	
	34		731	1100	654	983	592	890	
	36		667	1000	597	897	540	811	
	Number of Connectors		10		1		1		1
			12		1		1		1
			14		2		2		2
		16		2		2		2	
		18		2		2		2	
		20		3		3		3	
22			3		3		3		
24			3		3		3		
26			3		3		3		
28			3		3		3		
30			3		3		3		
32			3		3		3		
34			3		3		3		
36			3		3		3		

"—" indicates that KL/r is greater than 200.

Available Strength in Axial Compression, kips										
Shape		2WT7x66		2WT7x60		2WT7x54.5		2WT7x49.5		
Design		P_n/Ω_c ASD	$\phi_c P_n$ LRFD							
Effective Length, KL (ft), with Respect to Indicated Axis	X-X Axis	0	1040	1560	927	1390	819	1230	725	1090
		10	947	1420	857	1290	765	1150	694	1040
		12	789	1190	709	1070	627	943	567	852
		14	779	1170	699	1050	616	926	556	836
		16	689	1040	615	925	538	809	484	728
		18	546	821	484	727	418	628	374	563
		20	514	772	453	681	389	585	347	522
		22	432	649	379	569	323	485	287	432
		24	336	505	295	443	252	378	225	337
		26	286	431	251	378	215	322	191	288
		28	247	371	217	326	185	278	165	248
		30	215	323	189	284	161	242	144	216
		32	189	284	166	249	142	213	126	190
		34	168	252	147	221	125	189	112	168
	36	149	225	131	197	112	168	—	—	
	Y-Y Axis	0	1040	1560	927	1390	819	1230	725	1090
		10	1040	1560	927	1390	819	1230	725	1090
		12	1040	1560	927	1390	819	1230	725	1090
		14	1000	1510	914	1370	819	1230	725	1090
		16	960	1440	874	1310	790	1190	719	1080
		18	912	1370	830	1250	750	1130	682	1030
		20	862	1300	784	1180	708	1060	644	968
		22	810	1220	736	1110	665	999	604	907
		24	756	1140	686	1030	620	932	563	846
		26	702	1050	636	957	575	864	521	784
		28	648	973	587	882	530	796	480	721
		30	594	893	537	808	485	730	439	660
		32	541	814	489	736	442	664	400	600
		34	491	738	443	666	400	601	361	543
	36	441	663	398	598	359	540	324	487	
	Number of Connectors	10	1		1		1		1	
		12	1		1		1		1	
		14	2		2		2		2	
		16	2		2		2		2	
		18	2		2		2		2	
		20	3		3		3		3	
22		3		3		3		3		
24		3		3		3		3		
26		3		3		3		3		
28		3		3		3		3		
30		3		3		3		3		
32		3		3		3		3		
34		3		3		3		3		
36		3		3		3		N/A		

"—" indicates that KL/r is greater than 200.

Available Strength in Axial Compression, kips										
Shape		2WT7x45		2WT7x41		2WT7x37		2WT7x34		
Design		P_n/Ω_c ASD	$\phi_c P_n$ LRFD							
Effective Length, KL (ft), with Respect to Indicated Axis	X-X Axis	0	634	953	646	970	577	867	519	780
		10	622	935	602	904	540	812	493	742
		12	506	760	556	836	497	747	453	681
		14	494	743	507	762	451	678	410	616
		16	428	644	456	685	402	605	365	549
		18	329	494	404	607	354	532	320	481
		20	303	455	319	479	276	415	276	415
		22	250	376	304	457	262	393	235	353
		24	196	294	258	387	220	331	197	296
		26	167	251	203	305	174	262	156	235
		28	144	216	175	263	150	226	135	202
		30	125	188	153	229	131	197	117	176
		32	110	166	134	202	115	173	103	155
		34	97.6	147	119	179	102	153	91.3	137
	36	—	—	106	159	90.8	137	81.4	122	
	Y-Y Axis	0	634	953	646	970	577	867	519	780
		10	634	953	606	911	550	826	503	757
		12	634	953	562	845	510	766	466	701
		14	634	953	514	773	466	701	426	641
		16	634	953	464	698	421	632	384	577
		18	616	926	414	622	374	563	341	513
		20	581	874	363	546	329	494	299	450
		22	545	819	315	473	285	428	259	389
		24	508	763	269	404	242	364	220	331
		26	470	707	229	344	207	311	187	282
		28	433	651	197	297	178	268	162	243
30		396	595	172	258	155	233	141	212	
32		360	541	151	227	136	205	124	186	
34		325	489	134	201	121	182	110	165	
36	292	438	119	179	108	162	97.8	147		
Number of Connectors	10	1		1		1		1		
	12	1		1		1		1		
	14	2		2		2		2		
	16	2		2		2		2		
	18	2		2		2		2		
	20	3		2		2		3		
	22	3		3		3		3		
	24	3		3		3		3		
	26	3		3		3		3		
	28	3		3		3		3		
	30	3		3		3		3		
	32	3		3		3		3		
	34	3		3		3		3		
	36	N/A		3		3		3		

"—" indicates that KL/r is greater than 200.

Available Strength in Axial Compression, kips										
Shape		2WT7x30.5		2WT7x26.5		2WT7x24		2WT7x21.5		
Design		P_n/Ω_c ASD	$\phi_c P_n$ LRFD							
Effective Length, KL (ft), with Respect to Indicated Axis	X-X Axis	0	440	662	388	584	320	480	248	373
		10	429	645	378	567	318	478	248	373
		12	394	593	351	527	297	446	238	358
		14	357	536	290	436	249	374	203	305
		16	318	478	291	437	249	374	203	305
		18	279	419	259	390	224	336	184	277
		20	217	326	208	312	182	274	153	230
		22	205	307	198	298	157	235	133	201
		24	172	258	169	255	150	226	129	193
		26	136	205	134	201	119	179	103	155
		28	117	176	115	174	103	155	89.2	134
		30	102	154	101	151	89.6	135	77.7	117
		32	89.9	135	88.4	133	78.8	118	68.3	103
	34	79.6	120	78.3	118	69.8	105	60.5	90.9	
	36	71.0	107	69.9	105	62.2	93.5	54.0	81.1	
	Y-Y Axis	0	440	662	388	584	320	480	248	373
		10	439	660	340	511	289	434	233	350
		12	408	612	302	453	258	388	211	316
		14	373	560	262	393	226	340	187	281
		16	337	506	222	334	194	292	163	245
		18	300	451	185	277	163	245	140	210
		20	263	396	150	226	134	202	118	177
		22	228	343	124	187	111	167	97.5	147
		24	195	293	104	157	93.1	140	81.9	123
		26	166	249	88.9	134	79.4	119	69.8	105
		28	143	215	76.7	115	68.4	103	60.2	90.4
30		125	187	66.8	100	59.6	89.6	52.4	78.8	
32		109	165	58.7	88.2	—	—	—	—	
34	97.0	146	—	—	—	—	—	—		
36	86.5	130	—	—	—	—	—	—		
Number of Connectors	10	1		1		1		1		
	12	1		1		1		1		
	14	2		1		1		1		
	16	2		2		2		2		
	18	2		2		2		2		
	20	2		2		2		2		
	22	3		3		2		2		
	24	3		3		3		3		
	26	3		3		3		3		
	28	3		3		3		3		
	30	3		3		3		3		
	32	3		3		N/A		N/A		
	34	3		N/A		N/A		N/A		
36	3		N/A		N/A		N/A			

— indicates that KL/r is greater than 200.

Available Strength in Axial Compression, kips										
Shape			2WT7x19		2WT7x17		2WT7x15		2WT7x13	
Design			P_n/Ω_c ASD	$\phi_c P_n$ LRFD						
Effective Length, KL (ft), with Respect to Indicated Axis	X-X Axis	0	210	315	162	244	125	188	101	152
		10	210	315	162	244	125	188	101	152
		12	197	297	160	240	125	188	98.4	148
		14	204	306	148	222	123	185	99.9	150
		16	178	267	146	219	113	170	93.6	141
		18	162	243	134	201	113	170	91.9	138
		20	162	244	122	183	104	156	85.7	129
		22	137	206	116	174	99.6	150	82.5	124
	24	122	183	105	157	90.9	137	76.4	115	
	Y-Y Axis	0	210	315	162	244	125	188	101	152
		10	181	272	148	222	121	182	75.9	114
		12	156	235	129	194	106	160	61.2	92.0
		14	131	197	110	166	91.5	138	47.4	71.2
		16	107	162	92.0	138	76.9	116	36.3	54.5
		18	85.7	129	74.7	112	63.1	94.8	—	—
		20	69.4	104	60.5	91.0	51.1	76.8	—	—
22		57.4	86.2	50.0	75.2	42.2	63.5	—	—	
24	48.2	72.4	42.0	63.2	35.5	53.3	—	—		
Number of Connectors	10		1		1		1		1	
	12		1		1		1		1	
	14		2		1		1		2	
	16		2		2		1		2	
	18		2		2		2		N/A	
	20		3		2		2		N/A	
	22		3		3		3		N/A	
	24		3		3		3		N/A	

"—" indicates that KL/r is greater than 200.

Available Strength in Axial Compression, kips				
Shape			2WT7x11	
Design			P_n/Ω_c ASD	$\phi_c P_n$ LRFD
Effective Length, KL (ft), with Respect to Indicated Axis	X-X Axis	0	68.1	102
		10	68.1	102
		12	68.1	102
		14	66.6	100
		16	61.4	92.2
	Y-Y Axis	0	68.1	102
		10	56.3	84.6
		12	46.4	69.7
		14	36.9	55.5
		16	28.5	42.9
Number of Connectors	10	1		
	12	1		
	14	1		
	16	1		

"—" indicates that KL/r is greater than 200.

Available Strength in Axial Compression, kips										
Shape		2WT6x168		2WT6x152.5		2WT6x139.5		2WT6x126		
Design		P_n/Ω_c ASD	$\phi_c P_n$ LRFD							
Effective Length, KL (ft), with Respect to Indicated Axis	X-X Axis	0	2910	4380	2630	3950	2400	3610	2170	3260
		10	2670	4010	2390	3590	2170	3260	1940	2910
		12	2550	3830	2270	3410	2050	3080	1820	2740
		14	2420	3630	2140	3210	1920	2890	1700	2550
		16	2270	3410	1990	3000	1780	2680	1570	2350
		18	2110	3180	1840	2770	1640	2460	1430	2140
		20	1780	2680	1530	2310	1350	2030	1290	1930
		22	1790	2690	1530	2300	1340	2020	1150	1720
		24	1620	2440	1380	2070	1200	1800	1010	1520
		26	1460	2200	1120	1680	961	1440	796	1200
		28	1180	1780	1080	1630	922	1390	686	1030
		30	1160	1740	947	1420	803	1210	598	899
		32	1020	1530	774	1160	658	990	526	790
		34	836	1260	686	1030	583	877	465	700
	36	746	1120	612	920	520	782	415	624	
	Y-Y Axis	0	2910	4380	2630	3950	2400	3610	2170	3260
		10	2710	4080	2450	3680	2240	3370	2020	3040
		12	2610	3930	2350	3540	2150	3230	1940	2910
		14	2500	3750	2250	3370	2050	3080	1850	2780
		16	2370	3560	2130	3200	1940	2920	1740	2620
		18	2230	3350	2000	3010	1820	2740	1640	2460
		20	2090	3130	1870	2810	1700	2550	1520	2290
		22	1940	2910	1730	2610	1570	2360	1410	2110
		24	1790	2690	1600	2400	1440	2170	1290	1940
		26	1640	2460	1460	2190	1320	1980	1170	1760
		28	1490	2240	1330	1990	1190	1790	1060	1590
30		1340	2020	1190	1800	1070	1610	950	1430	
32		1210	1810	1070	1610	956	1440	844	1270	
34		1070	1610	948	1420	847	1270	748	1120	
36	955	1440	846	1270	755	1140	667	1000		
Number of Connectors	10	2		2		2		2		
	12	2		2		2		2		
	14	2		2		2		2		
	16	2		2		2		2		
	18	2		2		2		2		
	20	2		2		2		3		
	22	3		3		3		3		
	24	3		3		3		3		
	26	3		3		3		3		
	28	3		4		4		3		
	30	4		4		4		3		
	32	4		4		4		3		
	34	4		4		4		3		
36	4		4		4		3			

"—" indicates that KL/r is greater than 200.

Available Strength in Axial Compression, kips										
Shape		2WT6x115		2WT6x105		2WT6x95		2WT6x85		
Design		P_n/Ω_c ASD	$\phi_c P_n$ LRFD							
Effective Length, KL (ft), with Respect to Indicated Axis	X-X Axis	0	1970	2960	1790	2700	1620	2430	1440	2160
		10	1750	2630	1580	2370	1410	2120	1240	1870
		12	1640	2460	1340	2010	1180	1780	1030	1550
		14	1520	2280	1350	2040	1190	1800	1040	1560
		16	1390	2090	1230	1850	1080	1620	927	1390
		18	1150	1730	1010	1510	867	1300	737	1110
		20	1120	1690	979	1470	840	1260	708	1060
		22	994	1490	857	1290	726	1090	605	910
		24	794	1190	673	1010	562	844	465	700
		26	676	1020	573	861	479	720	397	596
		28	583	877	494	743	413	620	342	514
		30	508	764	430	647	360	540	298	448
		32	447	671	378	569	316	475	262	393
	34	396	595	335	504	280	421	232	349	
	36	353	530	299	449	250	375	207	311	
	Y-Y Axis	0	1970	2960	1790	2700	1620	2430	1440	2160
		10	1840	2760	1680	2520	1520	2280	1350	2030
		12	1760	2650	1610	2410	1450	2180	1290	1940
		14	1680	2520	1530	2300	1380	2070	1230	1840
		16	1580	2380	1440	2160	1300	1950	1150	1730
		18	1480	2230	1350	2020	1210	1820	1080	1620
		20	1380	2070	1250	1880	1120	1690	997	1500
		22	1270	1910	1150	1730	1030	1550	915	1380
		24	1160	1750	1050	1580	943	1420	834	1250
		26	1060	1590	954	1430	853	1280	753	1130
		28	954	1430	858	1290	766	1150	675	1010
30		854	1280	766	1150	682	1030	600	901	
32		756	1140	677	1020	601	904	528	794	
34	670	1010	600	901	533	801	468	703		
36	598	898	535	804	475	714	417	627		
Number of Connectors	10	2		1		1		1		
	12	2		1		1		1		
	14	2		2		2		2		
	16	2		2		2		2		
	18	2		2		2		2		
	20	3		3		3		3		
	22	3		3		3		3		
	24	3		3		3		3		
	26	3		3		3		3		
	28	3		3		3		3		
	30	3		3		3		3		
	32	3		3		3		3		
	34	3		3		3		3		
36	3		3		3		3			

"—" indicates that KL/r is greater than 200.

Available Strength in Axial Compression, kips										
Shape		2WT6x76		2WT6x68		2WT6x60		2WT6x53		
Design		P_n/Ω_c ASD	$\phi_c P_n$ LRFD							
Effective Length, KL (ft), with Respect to Indicated Axis	X-X Axis	0	1280	1920	1130	1690	979	1470	855	1280
		10	1100	1650	966	1450	839	1260	728	1090
		12	1000	1510	879	1320	759	1140	652	981
		14	904	1360	786	1180	674	1010	573	861
		16	801	1200	633	951	537	808	449	675
		18	698	1050	596	896	504	757	417	626
		20	599	901	506	761	423	637	344	517
		22	463	695	387	582	323	485	262	394
		24	389	584	326	489	271	408	220	331
		26	331	498	277	417	231	347	188	282
		28	286	429	239	360	199	299	162	243
		30	249	374	208	313	174	261	141	212
		32	219	329	183	275	153	229	124	186
	34	194	291	162	244	135	203	110	165	
	36	173	260	145	218	—	—	—	—	
	Y-Y Axis	0	1280	1920	1130	1690	979	1470	855	1280
		10	1210	1820	1080	1620	946	1420	838	1260
		12	1150	1740	1030	1550	902	1360	799	1200
		14	1090	1640	973	1460	853	1280	755	1130
		16	1030	1550	913	1370	800	1200	707	1060
		18	958	1440	850	1280	743	1120	657	987
		20	885	1330	784	1180	685	1030	605	909
		22	811	1220	718	1080	626	940	552	829
		24	737	1110	651	979	567	852	499	750
		26	665	999	586	880	509	765	448	673
		28	594	893	522	785	453	681	398	598
30		527	791	462	694	399	600	350	526	
32		463	696	406	610	351	527	308	463	
34	410	616	359	540	311	467	273	410		
36	366	550	321	482	277	416	243	366		
Number of Connectors	10	1		1		1		1		
	12	2		2		2		2		
	14	2		2		2		2		
	16	2		2		2		2		
	18	3		3		3		3		
	20	3		3		3		3		
	22	3		3		3		3		
	24	3		3		3		3		
	26	3		3		3		3		
	28	3		3		3		3		
	30	3		3		3		3		
	32	3		3		3		3		
	34	3		3		3		3		
36	3		3			N/A		N/A		

"—" indicates that KL/r is greater than 200.

Available Strength in Axial Compression, kips										
Shape		2WT6x48		2WT6x43.5		2WT6x39.5		2WT6x36		
Design		P_n/Ω_c ASD	$\phi_c P_n$ LRFD							
Effective Length, KL (ft), with Respect to Indicated Axis	X-X Axis	0	760	1140	676	1020	599	900	533	801
		10	649	976	586	880	482	724	435	654
		12	578	869	520	782	465	699	419	629
		14	504	758	452	680	402	605	360	542
		16	391	588	349	524	308	463	274	412
		18	360	541	321	482	282	423	249	374
		20	295	443	262	393	212	319	187	282
		22	225	339	200	301	175	264	155	233
		24	189	285	168	253	147	221	130	196
		26	161	242	143	215	126	189	111	167
		28	139	209	124	186	108	163	95.6	144
		30	121	182	108	162	94.3	142	83.3	125
	32	106	160	94.6	142	82.9	125	—	—	
	Y-Y Axis	0	760	1140	676	1020	599	900	533	801
		10	756	1140	676	1020	599	900	533	801
		12	721	1080	652	980	590	887	533	801
		14	681	1020	615	924	557	836	507	762
		16	637	958	575	864	520	782	474	712
		18	591	889	533	801	482	724	438	658
		20	544	817	489	735	442	664	402	604
		22	496	745	445	669	402	604	365	548
		24	448	674	401	603	362	544	328	493
		26	401	603	359	539	323	486	293	440
		28	357	536	318	478	286	430	259	389
30		313	471	278	418	251	377	226	340	
32	275	414	245	368	220	331	199	299		
Number of Connectors	10	1		1		1		1		
	12	2		2		2		2		
	14	2		2		2		2		
	16	2		2		2		2		
	18	3		3		3		3		
	20	3		3		3		3		
	22	3		3		3		3		
	24	3		3		3		3		
	26	3		3		3		3		
	28	3		3		3		3		
	30	3		3		3		3		
	32	3		3		3		N/A		

"—" indicates that KL/r is greater than 200.

Available Strength in Axial Compression, kips										
Shape			2WT6x32.5		2WT6x29		2WT6x26.5		2WT6x25	
Design			P_n/Ω_c ASD	$\phi_c P_n$ LRFD						
Effective Length, KL (ft), with Respect to Indicated Axis	X-X Axis	0	464	698	438	659	388	583	383	576
		10	388	582	385	578	351	528	344	517
		12	372	559	340	510	310	466	310	466
		14	319	479	293	441	268	403	274	411
		16	240	361	224	337	205	309	237	356
		18	217	327	204	307	187	281	201	303
		20	164	246	166	249	152	228	168	252
		22	135	203	127	191	116	175	128	193
		24	114	171	107	161	97.9	147	108	162
		26	96.8	145	91.0	137	83.4	125	92.0	138
		28	83.5	125	78.5	118	71.9	108	79.3	119
		30	72.7	109	68.4	103	62.6	94.1	69.1	104
	32	—	—	60.1	90.3	55	82.7	60.7	91.3	
	Y-Y Axis	0	464	698	438	659	388	583	383	576
		10	464	698	431	648	388	583	333	500
		12	464	698	401	602	364	547	295	444
		14	456	685	367	552	333	501	256	385
		16	425	639	332	499	301	452	218	327
		18	393	591	296	445	268	402	181	272
		20	360	542	261	392	235	353	147	221
		22	327	492	227	341	204	306	122	183
		24	294	442	194	291	174	261	102	154
		26	262	394	165	248	148	222	87.1	131
		28	232	348	142	214	128	192	75.1	113
30		202	304	124	187	111	167	65.4	98.3	
32	178	267	109	164	97.7	147	57.5	86.4		
Number of Connectors	10	1	1	1	1	1	1	1	1	
	12	2	2	2	2	2	2	2	2	
	14	2	2	2	2	2	2	2	2	
	16	2	2	2	2	2	2	2	2	
	18	3	3	3	3	3	3	3	3	
	20	3	3	3	3	3	3	3	3	
	22	3	3	3	3	3	3	3	3	
	24	3	3	3	3	3	3	3	3	
	26	3	3	3	3	3	3	3	3	
	28	3	3	3	3	3	3	3	3	
	30	3	3	3	3	3	3	3	3	
32	N/A	3	3	3	3	3	3	3		

"—" indicates that KL/r is greater than 200.

Available Strength in Axial Compression, kips										
Shape		2WT6x22.5		2WT6x20		2WT6x17.5		2WT6x15		
Design		P_n/Ω_c ASD	$\phi_c P_n$ LRFD							
Effective Length, KL (ft), with Respect to Indicated Axis	X-X Axis	0	335	503	262	393	223	335	154	231
		10	306	461	247	371	223	335	154	231
		12	275	413	202	303	187	281	139	209
		14	242	364	198	298	190	285	141	211
		16	191	287	160	240	158	238	121	181
		18	177	265	134	201	138	207	107	161
		20	146	220	125	187	134	202	105	158
		22	112	168	95.9	144	107	161	86.6	130
		24	94.1	141	80.5	121	90.1	135	74.9	113
		26	80.2	121	68.6	103	76.8	115	63.9	96.1
		28	69.1	104	59.2	88.9	66.2	99.5	55.1	82.8
		30	60.2	90.5	51.5	77.5	57.7	86.7	48.0	72.2
	32	52.9	79.6	45.3	68.1	50.7	76.2	42.2	63.4	
	Y-Y Axis	0	335	503	262	393	223	335	154	231
		10	298	447	242	363	181	271	135	203
		12	264	396	217	326	153	230	117	176
		14	228	343	191	286	125	188	99.3	149
		16	194	291	164	247	99.5	150	81.9	123
		18	160	241	139	209	78.6	118	65.7	98.8
		20	130	196	115	173	63.7	95.7	53.2	80.0
		22	108	162	94.9	143	52.6	79.1	44.0	66.1
		24	90.6	136	79.7	120	44.2	66.5	37.0	55.6
		26	77.2	116	67.9	102	—	—	—	—
		28	66.6	100	58.6	88.0	—	—	—	—
30		58.0	87.2	51.0	76.7	—	—	—	—	
32	51.0	76.6	44.9	67.4	—	—	—	—		
Number of Connectors	10	1		1		1		1		
	12	2		1		1		1		
	14	2		2		2		2		
	16	2		2		2		2		
	18	3		2		2		2		
	20	3		3		3		3		
	22	3		3		3		3		
	24	3		3		3		3		
	26	3		3		3		3		
	28	3		3		3		3		
	30	3		3		3		3		
	32	3		3		3		3		

"—" indicates that KL/r is greater than 200.

Available Strength in Axial Compression, kips										
Shape			2WT6x13		2WT6x11		2WT6x9.5		2WT6x8	
Design			P_n/Ω_c ASD	$\phi_c P_n$ LRFD						
Effective Length, KL (ft), with Respect to Indicated Axis	X-X Axis	0	106	159	110	165	76.5	115	52.4	78.7
		10	106	159	102	153	76.5	115	52.4	78.7
		12	102	154	104	156	76.5	115	52.4	78.7
		14	93.8	141	101	152	72.0	108	52.4	78.7
		16	91.0	137	96.3	145	71.0	107	51.1	76.9
		18	82.9	125	87.6	132	68.2	102	51.4	77.3
		20	74.6	112	81.9	123	64.5	96.9	50.0	75.1
	Y-Y Axis	0	106	159	110	165	76.5	115	52.4	78.7
		10	99.5	150	48.6	73.1	39.2	59.0	29.4	44.2
		12	88.7	133	33.8	50.8	27.3	41.0	20.4	30.7
		14	77.3	116	24.8	37.3	—	—	—	—
		16	66.1	99.3	—	—	—	—	—	—
		18	55.2	83.0	—	—	—	—	—	—
		20	45.2	67.9	—	—	—	—	—	—
Number of Connectors	10		1		1		1		1	
	12		1		2		2		1	
	14		1		3		2		2	
	16		2		4		3		2	
	18		2		4		4		3	
	20		2		5		5		4	

"—" indicates that KL/r is greater than 200.

Weld Effective Lengths For Rectangular HSS Overlapped K-Connections

KYLE TOUSIGNANT and JEFFREY A. PACKER

ABSTRACT

One large-scale, 33-ft-span, simply supported Warren truss was tested to assess the performance of welds in rectangular hollow structural section (HSS) overlapped K-connections. Nine overlapped connections, within the truss, were designed to be weld-critical and sequentially failed by producing an axial force distribution with a point load, applied quasi-statically, to strategic panel points. The structural reliability (or safety index) of the existing AISC *Specification for Structural Steel Buildings* formulas for the effective length of welds in rectangular HSS overlapped K-connections, in Table K4.1 of the 2010 AISC *Specification for Structural Steel Buildings*, was determined from the tests. The results indicate that these provisions are conservative; hence, a modification to the current requirements that limits the effective width of the transverse weld elements is proposed. The proposal establishes a more economical and yet still safe weld design method for rectangular HSS overlapped K-connections.

Keywords: hollow structural sections, welded joints, trusses, K-connections, weld effective lengths, fillet welds, flare-bevel-groove welds, flux-cored arc welding.

INTRODUCTION

It is well known that the differences in relative stiffness of rectangular hollow structural section (HSS) walls cause nonuniform load transfer along lines of welds at a branch connection. Historically, international design recommendations have required that these welds be designed to develop the yield strength of the member, such that they may resist any arrangement of loads in the branch. This requirement is almost exclusively based on old recommendations from the International Institute of Welding (IIW, 1989). Designing welds to branches to develop the yield strength of the member is justifiable in situations when there is low confidence in the design forces or if plastic stress redistribution is required in the connection (Packer et al., 2009). This design method is not always merited, and its requirement for large weld sizes is excessively conservative in many situations.

Extensive laboratory tests have been performed at the University of Toronto on welds in both isolated rectangular HSS connections and complete trusses (Frater and Packer, 1992a, 1992b; Packer and Cassidy, 1995; McFadden et al., 2013; McFadden and Packer, 2014), which have led to the development, and international recognition (IIW, 2012;

ISO, 2013), of a more modern design approach based on actual branch member forces to achieve more appropriate and economical weld sizes. This so-called fit-for-purpose approach makes use of effective weld properties to account for the nonuniform loading of the weld perimeter.

In the latest edition of AISC 360, *Specification for Structural Steel Buildings* (AISC, 2010), a detailed design method considering effective weld properties for predominantly statically loaded rectangular HSS-to-HSS connections is given in Section K4: “Welds of Plates and Branches to Rectangular HSS.” Table K4.1, “Effective Weld Properties for Connections to Rectangular HSS,” contains formulas to determine the effective length of welds for axially loaded rectangular HSS connections and the effective elastic section modulus of welds subject to bending.

The design methods in Table K4.1 for welds in axially loaded T-, Y-, X- and gapped K-connections are based on experimental data from full-scale tests on connections in which failure occurred by shear rupture of the weld along a plane through the weld throat, herein called “weld-critical connections” (Frater and Packer 1992a, 1992b; Packer and Cassidy, 1995). However, at the time that AISC 360-10 was published, no such data were available to substantiate the design methods given, in the same document, for welds in unreinforced HSS moment T-connections and axially loaded HSS overlapped K-connections.

In order to evaluate the adequacy of these design methods, AISC initiated a two-phase study at the University of Toronto. The first phase of the study investigated the strength and behavior of welds in unreinforced rectangular HSS moment T-connections. The results of this phase have been published by McFadden and Packer (2014). Phase two of the study is presented herein.

Kyle Tousignant, Ph.D. Candidate in Civil Engineering, University of Toronto, Toronto, Ontario, Canada. E-mail: kyle.tousignant@mail.utoronto.ca

Jeffrey A. Packer, Bahen/Tanenbaum Professor of Civil Engineering, University of Toronto, Toronto, Ontario, Canada (corresponding). E-mail: jeffrey.packer@utoronto.ca

Paper No. 2014-24

EXPERIMENTATION

Scope

An experimental program was developed to test large-scale rectangular HSS overlapped K-connections in order to verify, or adjust, the current weld effective length rules defined by Equations K4-10, K4-11 and K4-12 in Table K4.1 of the *AISC Specification* (AISC, 2010). Nine overlapped, 60-degree K-connections within one large-scale, 33-ft-span, simply supported Warren truss were designed to be weld-critical under the application of tension to the overlapping branch. Key parameters, such as the branch member overlap (O_v), the branch-to-chord width ratio (β -ratio) and the chord wall slenderness (B/t), were investigated and varied within the Limits of Applicability of Section K2.3 of the *Specification*. The nonuniform distribution of normal strain in the branch, near the connection, was measured with strain gages oriented along the longitudinal axis of the member at uniform increments around its perimeter, and the weld strength was obtained directly from strain gages in the constant stress region of the branch. To induce weld rupture, a single point load was applied to various truss panel points in a quasi-static manner. The loading strategy was carefully planned to accentuate the force in the critical web member(s) and resulted in all nine joints failing by shear rupture along a plane through the weld.

Truss Design

General

Connections were welded using a semi-automatic flux-cored-arc-welding (FCAW) process with full CO_2 shielding gas and fabricated from members conforming to CAN/CSA

G40.20/G40.21 Class C (CSA, 2013) and ASTM A1085 (ASTM, 2013). The experimental test designations, and a summary of the key test parameters for each joint (O_v , β and B/t), are given in Table 1.

The amount of overlap was varied, from 30% to 90%, and chord member sections were selected that produced relatively rigid and flexible connections. Connections were made to an HSS7 \times 7 \times 1/2 chord, that were relatively rigid ($\beta = 0.71$ and $B/t = 14.2$) and to an HSS10 \times 10 \times 3/8 chord that were more flexible ($\beta = 0.50$ and $B/t = 27.5$). Web members (HSS5 \times 5 \times 5/16) were specified to minimize the ratio of predicted weld strength to connection resistance and to also allow, by virtue of matched-width web members, either side of the truss connection to be designated as the overlapping (or “test”) branch. The latter detail was intended to support the design of a loading sequence to achieve sequential rupture of welds within the truss (see “Loading Strategy”).

Complete truss testing has been the preferred approach for testing welds in K-connections because it correctly accounts for connection boundary conditions, i.e., member continuity and truss deflection effects (Frater and Packer, 1992a, 1992b, 1992c). The truss layout and its dimensions are shown in Figure 1.

Weld Joint Details

The test welds were those to the overlapping branches, and each was comprised of three distinct weld joint details (see Figure 2): a longitudinal 90-degree fillet-weld detail (side a), a transverse 60-degree fillet-weld detail (sides c and d) and a longitudinal partial-joint-penetration (PJP) flare-bevel-groove-weld detail (side a’). The PJP flare-bevel-groove weld is formed by the butt joint in the matched-width web member connection. In this region, the deposition of sound

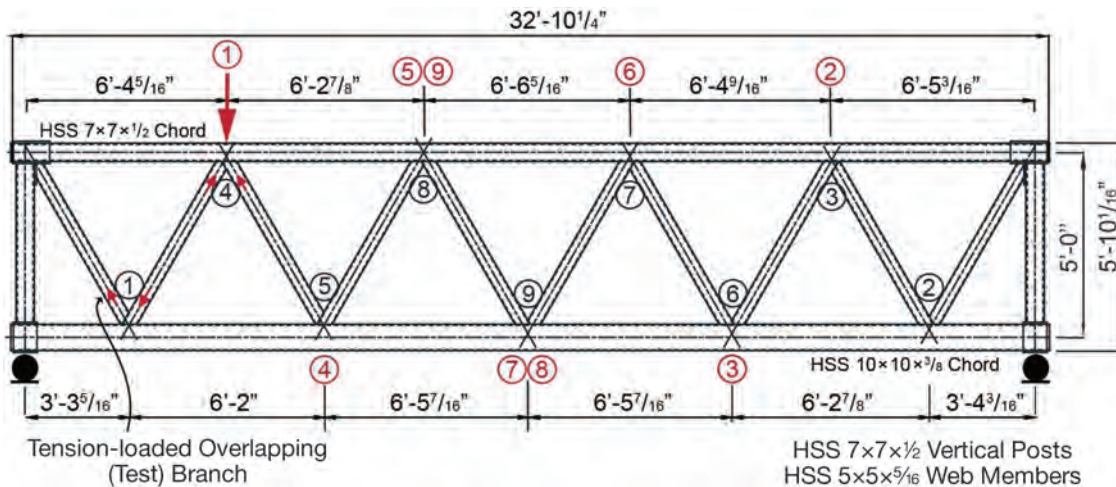


Fig. 1. Elevation of the truss, dimensions and joint designations (load locations for the nine tests shown in red; connection numbers shown in black).

Table 1. Measured Properties of Nine Rectangular HSS Overlapped K- (Test) Connections																										
No.*	Test	HSS Web Member			HSS Chord Member			O_v %	β	B/t																
		$B_b \times H_b \times t_b$ in. x in. x in.	A_b^{**} in. ²	F_{yb}^{***} ksi	$B \times H \times t$ in. x in. x in.	A^* in. ²	F_y^{***} ksi																			
1 5 2 6 9	K-90-0.50a K-90-0.50b K-60-0.50 K-30-0.50a K-30-0.50b	5.00 × 5.00 × 0.306	5.62	59.7	10.02 × 10.02 × 0.364	13.65	56.1	90	0.50	27.5																
3 4 7 8	K-90-0.71 K-60-0.71a K-60-0.71b K-30-0.71							5.00 × 5.00 × 0.306			5.62	59.7	7.03 × 7.03 × 0.494	12.05	55.1	90	0.71	14.2								
— —	T2 Joint 4 [†] T2 Joint 6 [†]															5.03 × 5.03 × 0.465			—	60.3	8.03 × 8.03 × 0.461	—	52.1	50	0.63	17.4

Note: $\theta_i = \theta_j = 60^\circ$; and $B_{bj}/t_{bj} = 16.3$ for connections 1–9.

* Refer to Figure 1.

** Cross-sectional areas determined by cutting a prescribed length of HSS, weighing it, and then using a density of 0.2836 lb/in³ to calculate its cross-sectional area.

*** Yield strength of all HSS determined from tensile coupon tests performed according to ASTM A370 (2009).

† Tests by Frater (1991); failed by a combined mechanism of weld fracture and premature branch yielding.

weld metal to the bottom of the flare can be hindered by bridging the weld puddle between the surfaces of the two branches (Packer and Frater, 2005). Thus, the throat of such welds can be highly variable. It should be noted that correct input for the geometric and mechanical properties of the as-laid welds is requisite to the following analysis; thus, to establish a more reliable (precise) picture of the weld throat in this region, a complete penetration (CP) detail was specified (with a 1/4-in. root gap and backing) and subsequently qualified in accordance with Clause 4.13 of AWS D1.1 (2010). The weld details are shown in Figure 2.

All critical test welds (to the overlapping branches at the connections), with the exception of weld element c, were

performed in the horizontal position. Weld element c was performed in the flat position. Minimum weld sizes, as specified in Table 5.8 and Table 3.4 of AWS D1.1 (2010) and Table J2.4 and Table J2.3 of AISC 360 (2010) for fillet welds and PJP flare-bevel-groove welds, respectively, were used to ensure enough heat input during welding to establish a sound weld. The hidden toe of the overlapped branch was always welded to the chord, and the remainder of the welds in the truss were sized so as to not fail before yielding of the attached branch member. Figure 3 shows the specified weld sizes and the associated welding symbols in a typical connection detail for a joint with $O_v = 30\%$.

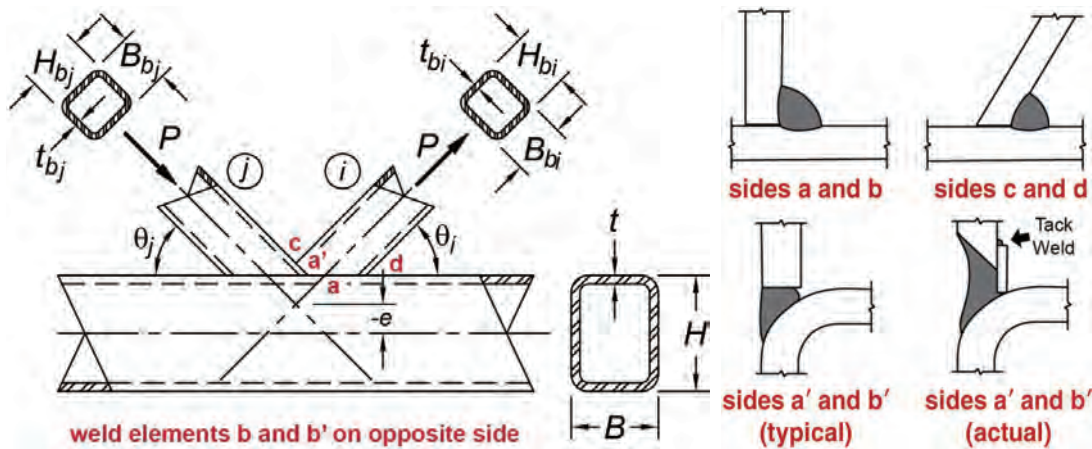


Fig. 2. Terminology for HSS K-connections and weld details (including labeling convention) for test joints.

During fabrication, the backing bar in detail a' of K-60-0.50 was pried about the tack weld (see Figure 2), away from the inside face of the HSS branch. The member itself was the last one to be fitted into the truss and was hammered into place. It is believed that during hammering, the backing bar—which made contact with the chord—was caught, causing it to be pried. This complication was not identified until after welding of the opposite side (details b and b') was complete. The resulting “gap” was filled with weld metal and welding of the test joint proceeded. Based on nondestructive test (NDT) results, this was not a cause for rejection; however, it is speculated that the strength of the joint was nevertheless affected by this defect. The joint is identified in the subsequent analysis (Figures 11 through 16) by a red data point.

All of the test welds were ground (long after welding) to reduce the weld throat dimension to below the minimum sizes specified by AISC and AWS. This was necessary to obtain a weld-fracture failure mode. Because the code provisions are based on achieving the necessary heat input at

the time of welding, and because minimum sizes were at that time provided, the soundness of the welds was likely unaffected.

MATERIAL GEOMETRIC AND MECHANICAL PROPERTIES

The measured geometric and mechanical properties of the HSS members and the nine test connections are shown in Table 1.

For the PJP welds, the throat dimension (t_w) of the PJP flare-bevel-groove welds (side a') was measured according to Equation 1:

$$t_w = t_{bi} - d \quad (1)$$

where d is the greatest perpendicular dimension measured from a line flush to the overlapping branch member surface to the weld surface and t_{bi} is the average measured thickness of the overlapping branch member.

For the fillet welds, t_w was determined by making a negative mold of each fillet weld element at numerous locations along its length. The mold was cut normal to the axis of the weld root, scanned and digitally measured; the effective throat was taken as the minimum distance between the root and face of the diagrammatic weld. Figure 4 shows a cut of the mold and a typical weld throat measurement.

More than 180 weld dimensions were taken for the nine connections (five along each of the four sides of the connection), and the average measured values for the weld throat dimension are shown in Table 2.

Mechanical properties of the as-laid welds were determined by tensile coupon tests (three total) as specified by AWS D1.1 (2010). The results are shown in Table 3. The average yield stress (by 0.2% strain offset) was 81.6 ksi, and the average ultimate strength (F_{EXX}) was 89.8 ksi with 27.5% elongation at rupture. The measured ultimate strength was 28% stronger than the nominal strength of the electrode used (AWS E71T-1C).

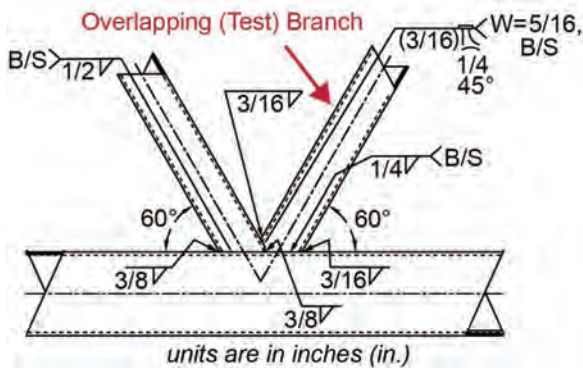


Fig. 3. Typical connection detail drawing (connection K-30-0.50a or K-30-0.50b).

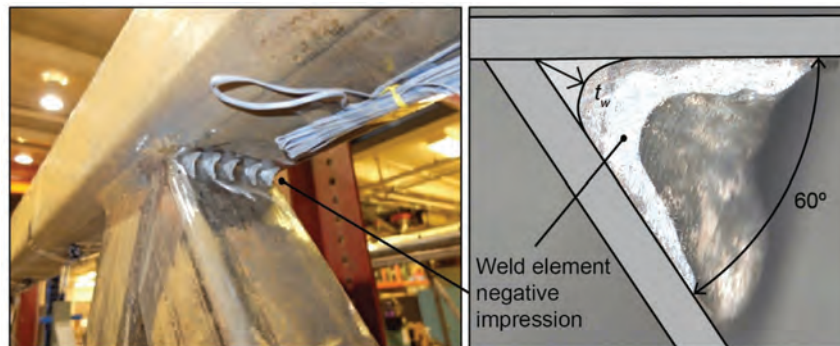


Fig. 4. Typical measurement procedure and mold profile.

Table 2. Average Effective Weld Throat Thickness for Individual Weld Elements

Test	Measured Weld Throat Dimension, in.					
	a	a'	b	b'	c	d
K-90-0.50a	0.136	0.125	0.123	0.141	0.148	0.168
K-90-0.50b	0.181	0.136	0.150	0.144	0.151	0.168
K-60-0.50	0.105	0.150	0.094	0.140	0.152	0.166
K-30-0.50a	0.132	0.181	0.116	0.156	0.171	0.143
K-30-0.50b	0.129	0.169	0.120	0.169	0.158	0.139
K-90-0.71	0.125	0.153	0.125	0.150	0.143	0.151
K-60-0.71a	0.157	0.138	0.152	0.123	0.149	0.152
K-60-0.71b	0.135	0.140	0.127	0.148	0.151	0.156
K-30-0.71	0.180	0.194	0.134	0.188	0.168	0.149
T2 Joint 4 [†]	0.177	0.177	0.173	0.173	0.283	0.264
T2 Joint 6 [†]	0.280	0.280	0.256	0.256	0.358	0.417

Note: b and b' are analogous to a and a' (see Figure 2), but on the opposite side of the overlapping branch.

Table 3. All-Weld-Metal Tensile Coupon Test Results

All-Weld-Metal Coupon Designation	F_y , ksi	$E \times 10^3$ ksi	F_{EXX} , ksi	ϵ_{rup} , %
[i]	81.0	29.3	91.2	27.0
[ii]	81.4	29.0	88.7	26.4
[iii]	82.3	31.8	89.5	29.2
Average	81.6	30.0	89.8	27.5

INSTRUMENTATION AND LOADING STRATEGY

Instrumentation

The actual weld fracture loads (P_a) were obtained from two linear strain gages (SGs) located in-plane and at mid-length (in the constant elastic stress region) of the web members (Mehrota and Govil, 1972). The breaking loads were hence calculated according to Equation 2:

$$P_a = A_b E \epsilon_{avg} \quad (2)$$

where

A_b = cross-sectional area of the branch, determined by weighing the cross-section

E = elastic modulus of the rectangular HSS, determined by tensile coupon tests in accordance with ASTM A370 (ASTM, 2009)

ϵ_{avg} = average strain measured on opposite faces of the rectangular HSS

The nonuniform normal strain distribution around the branch perimeter, adjacent to the weld, was measured using SGs oriented along the longitudinal axis of the member and

1 in. away from the weld toe [in order to avoid the strain concentrations caused by the notch effect (Packer and Cassidy, 1995)]. Because the strain distribution is theoretically symmetric about the y-y axis of the member (for plane-frame behavior), SGs were only installed on half of the member (along H_{bi} and half of B_{bi} on two sides). The SG spacing is shown in Figure 5.

Loading Strategy

The single-point load was applied at a truss panel point by a 600-kip capacity MTS Universal Testing Frame and resulted, by design, in a distribution of member forces that accentuated the load in a particular, predetermined branch member (ergo, the weld to it). Failure was planned to always occur in the test welds, instead of by some connection, member or stability failure mode.

After rupture occurred in the intended test weld, the connection was repaired by overwelding the gap with a new weld designed to develop the yield strength of the member. Hence, the welded connection was no longer critical. The location of the point load was subsequently altered to cause

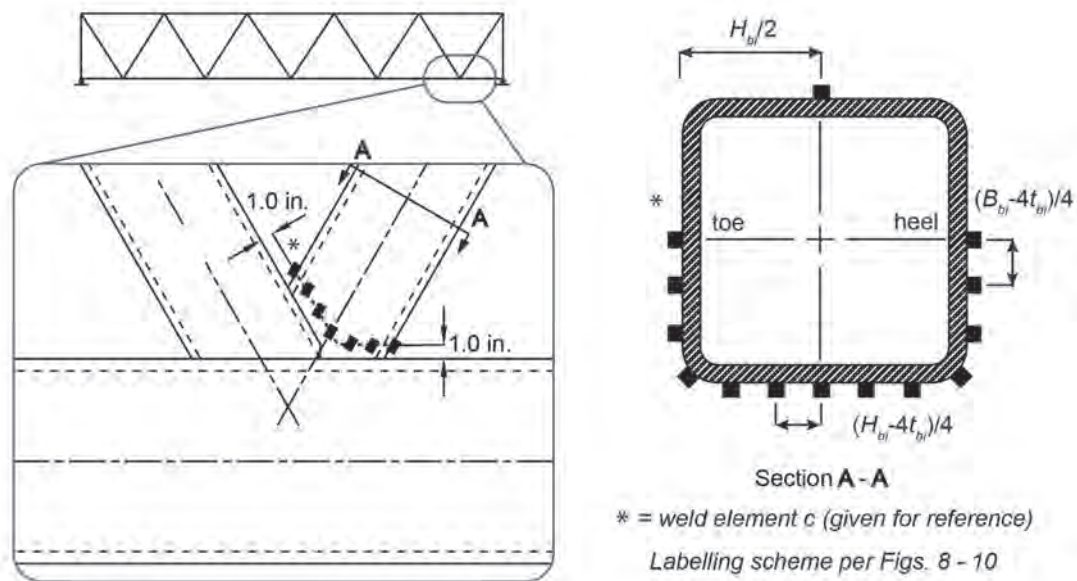


Fig. 5. Spacing of strain gages around the branch footprint adjacent to the welded connection.

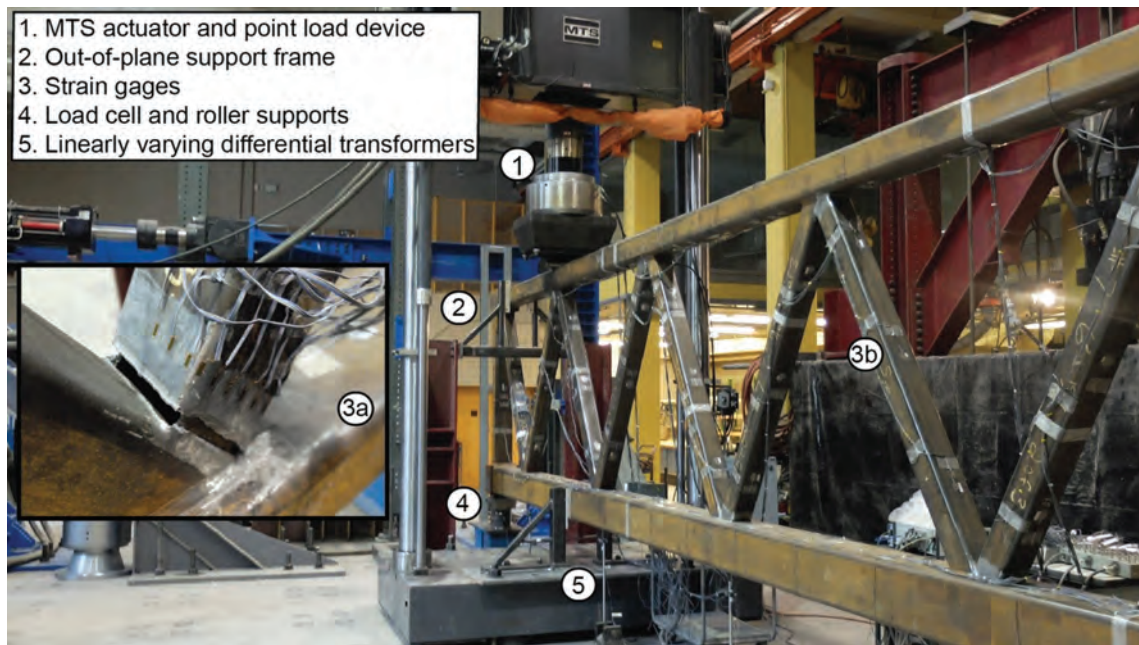


Fig. 6. Laboratory testing arrangement for full-scale HSS overlapped K-connection experiments.

failure at another joint. Because the MTS test frame was fixed to the laboratory floor, the truss itself was either translated, rotated 180 degrees and/or inverted to achieve the new distribution of forces. The roller supports were always located at the ends of the truss, as seen in Figure 1.

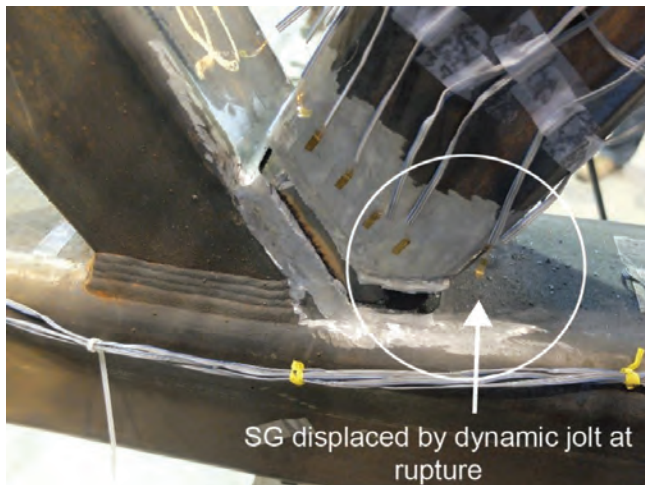
The laboratory testing arrangement and a series of typical weld fractures are shown in Figures 6 and 7, respectively.

RESULTS

All of the test welds failed in a brittle manner by fracture along a plane through the weld, which occurred simultaneously at all locations around the branch perimeter. Failure was sudden and accompanied by a dynamic “jolt” (caused by the release of strain energy) that, in some tests, displaced SGs from the branch member surface (see Figure 7a).

Figure 8 shows the relationship between the applied MTS load and the load in the branch member (measured by SGs in the position shown) for test K-30-0.50a. By virtue of a constant slope (indicating a linear variation in average strain), it can be seen that the member itself remained elastic throughout the entire load range. The branch load at rupture was hence calculated using Equation 2.

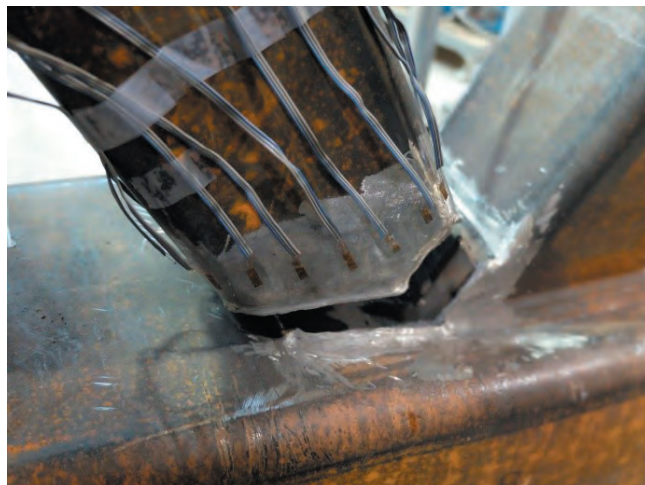
Figures 9, 10 and 11 show the variation in strain measured at 13 different SGs adjacent to the test welds at the initial unloaded stage and at 50%, 80% and 100% of the weld rupture load. For the joints tested, it was found that the magnitude of strain decreased as a function of the distance from the toe of the connection—believed to be caused by differences in the relative stiffness of the chord ($\beta = 0.50$ and $B/t = 27.5$) and the overlapped branch ($\beta = 1.00$ and $B_{bj}/t_{bj} = 16.3$) that results in the latter attracting more load.



(a) Test K-60-0.71a



(b) Test K-30-0.50a



(c) Test K-30-0.50b



(d) Test K-90-0.71

Fig. 7. Typical weld fractures and instrumentation.

As O_v increases, this change becomes less pronounced and is accompanied, generally, by a higher average failure stress in the weld. The magnitude of strain along the branch transverse faces is seen to decrease toward the mid-wall locations (SGs 1 and 13) except for the final stage of stress redistribution (Figures 9 and 11). This variation is expectedly more pronounced when the branch lands on a flexible chord ($\beta = 0.50$, $B/t = 27.5$) and for low values of O_v . The less sudden change in strain approaching the mid-wall along the toe (in Figures 9–11) is due to the more uniform transverse stiffness of the overlapped branch ($\beta = 1.00$ and $B/t = 16.3$).

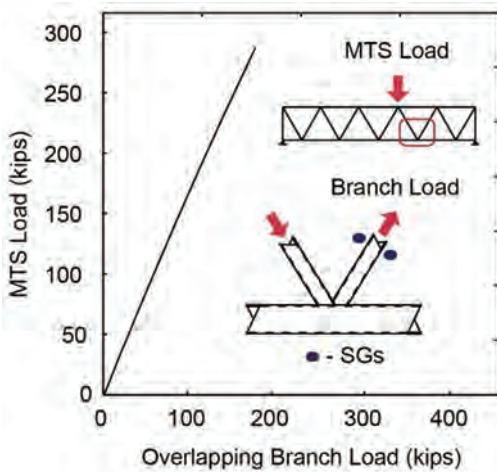


Fig. 8. MTS load versus branch load magnitude relationship (test K-30-0.50a).

In Figure 9, much of the weld to the heel actually remains in compression for the entire load range (branch in tension). The high strain at the toe in Figure 9 may be caused by the proximity of the transverse weld to the hidden toe of the overlapped branch, which was itself welded and thus increased the stiffness of the connection and the weld effective length at this location.

The distributions of strain around the branch members adjacent to the test welds shows that longitudinal welds to overlapped K-connections can be regarded as completely effective at resisting the applied load when $O_v = 60\%$ and 90% . For $O_v = 30\%$ (Figure 9), the strain along the longitudinal weld (SGs 4–10) can be seen to be more nonuniform. The transverse welds are always only partially effective and generally become less effective as the β -ratio decreases, as O_v decreases and as B/t increases. These trends are verified by the actual rupture loads (P_a) given in Table 4. They are generally in accordance with predictions given by the existing AISC Specification (AISC, 2010) formulas (Equations 4–8).

EVALUATION OF AISC 360-10

Existing Provisions for Weld Effective Lengths in Rectangular HSS Overlapped K-Connections

According to the Load and Resistance Factor Design (LRFD) method of AISC 360 (2010), the available strength of welds to axially loaded rectangular HSS branches (P_{nw}) is based on the limit state of shear rupture along the plane of the weld effective throat, according to Equation 3:

$$P_{nw} = F_{nw} t_w l_e \quad (3)$$

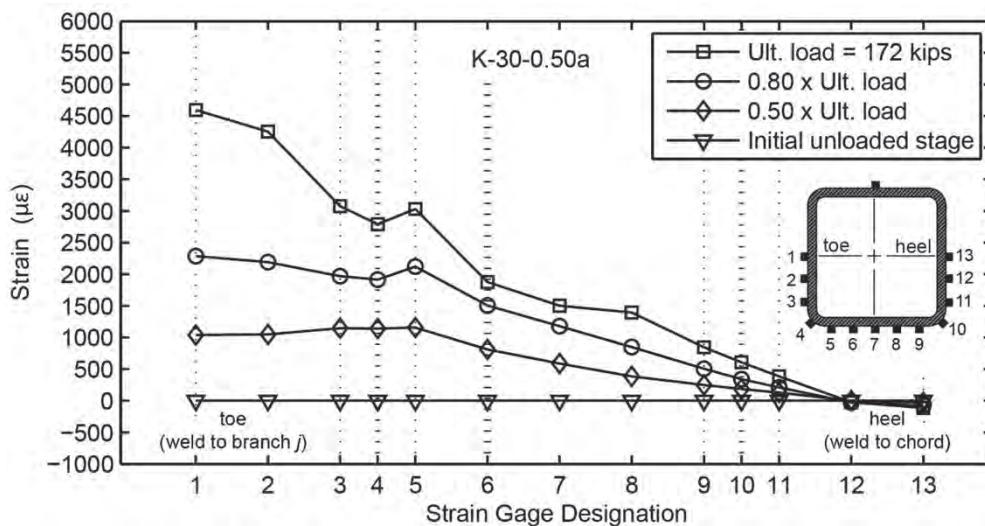


Fig. 9. Typical distribution of normal strain around branch perimeter for specimens with $O_v = 30\%$, $\beta = 0.50$ and $B/t = 27.5$.

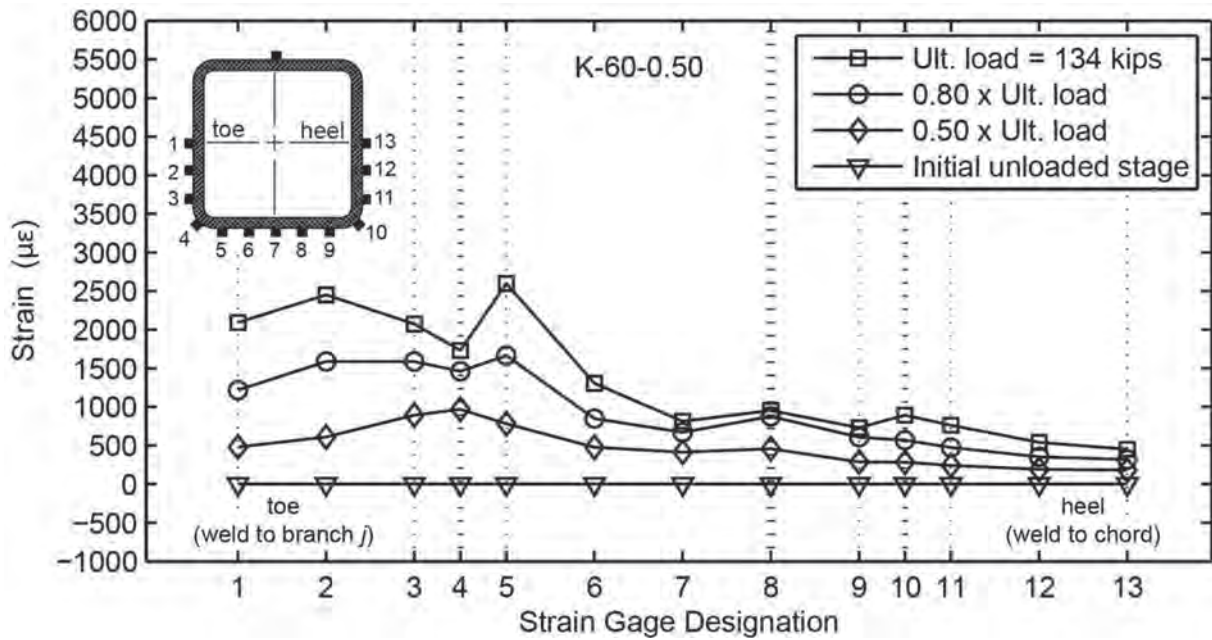


Fig. 10. Typical distribution of normal strain around branch perimeter for specimens with $O_v = 60\%$, $\beta = 0.50$ and $B/t = 27.5$.

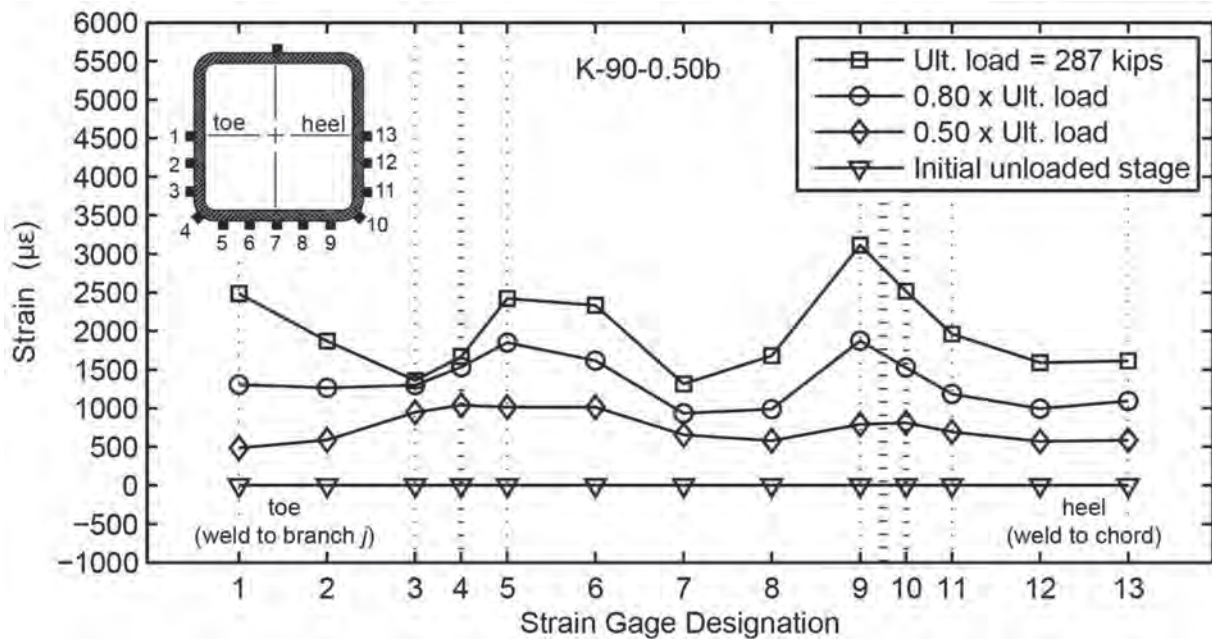


Fig. 11. Typical distribution of normal strain around branch perimeter for specimens with $O_v = 90\%$, $\beta = 0.50$ and $B/t = 27.5$.

Table 4. Actual and Predicted Nominal Weld Strength for Each Test Connection

Test	P_a^{**}	P_{nw}		
	kips	Current AISC 360-10 kips	Modified AISC 360-10 kips	Without Weld Effective Lengths kips
K-90-0.50a	277	187	197	217
K-90-0.50b	287	196	206	227
K-60-0.50*	134	138	<i>154</i>	201
K-30-0.50a	172	86	102	191
K-30-0.50b	166	85	101	187
K-90-0.71	256	199	209	228
K-60-0.71a	219	146	160	201
K-60-0.71b	194	149	163	205
K-30-0.71	237	104	119	213
T2 Joint 4 [†]	379	175	192	257
T2 Joint 6 [†]	375	262	286	378

Note: Italicized values are strength predictions that exceed the measured strength (i.e., nominally unsafe).

* Imperfect weld root detail (see “Weld Joint Details”).

** Force in overlapping web member at weld fracture.

† Tests by Frater (1991); failed by a combined mechanism of weld fracture and premature branch yielding.

where

F_{nw} = nominal strength of weld metal

t_w = weld effective throat around the perimeter of the branch

l_e = effective length of fillet and groove welds.

An LRFD resistance factor, ϕ , equal to 0.75 and 0.80, applies for fillet welds and PJP groove welds, respectively.

In Table J2.5 of AISC 360-10, F_{nw} is specified as $0.60F_{EXX}$ for both fillet and PJP groove welds. In the case of the former, it implies that the failure mode is by shear rupture on the effective throat; however, for PJP groove welds (sides a' and b'), it is an arbitrary reduction factor that has been in effect since the early 1960s to compensate for the notch effect of the unfused area of the joint and does not imply that the tensile failure mode is by shear stress on the effective throat (per AISC 360-10 Commentary to Chapter J). Because a CP detail was provided (see “Weld Joint Details”) in order to establish a high degree of certainty with respect to the fusion area (and the weld throat dimension) in this region, a more suitable term of $1.00F_{EXX}$ has been used herein for F_{nw} for groove welds.

The formulas for l_e are given in Table K4.1 of AISC 360 and are as follows:

- When $25\% \leq O_v < 50\%$:

$$l_{e,i} = \frac{20_v}{50} \left[\left(1 - \frac{O_v}{100} \right) \left(\frac{H_{bi}}{\sin \theta_i} \right) + \frac{O_v}{100} \left(\frac{H_{bi}}{\sin(\theta_i + \theta_j)} \right) \right] + b_{eoi} + b_{eov} \quad (4)$$

- When $50\% \leq O_v < 80\%$:

$$l_{e,i} = 2 \left[\left(1 - \frac{O_v}{100} \right) \left(\frac{H_{bi}}{\sin \theta_i} \right) + \frac{O_v}{100} \left(\frac{H_{bi}}{\sin(\theta_i + \theta_j)} \right) \right] + b_{eoi} + b_{eov} \quad (5)$$

- When $80\% \leq O_v \leq 100\%$:

$$l_{e,i} = 2 \left[\left(1 - \frac{O_v}{100} \right) \left(\frac{H_{bi}}{\sin \theta_i} \right) + \frac{O_v}{100} \left(\frac{H_{bi}}{\sin(\theta_i + \theta_j)} \right) \right] + B_{bi} + b_{eov} \quad (6)$$

where

i = subscript used to refer to the overlapping branch

j = subscript used to refer to the overlapped branch

H_b = overall height of the branch member measured in the plane of the connection

θ = included angle between the branch and the chord = 60° for all test connections

The total weld effective length is shown in Figure 12.

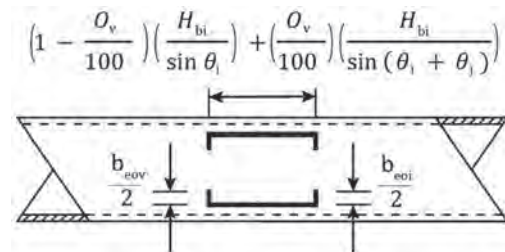


Fig. 12. Weld effective length dimensions.

The terms b_{eoi} and b_{eov} are empirically derived from laboratory tests (Davies and Packer, 1982) and quantify the effective widths of weld to the branch face, normal (transverse) to the plane of the connection:

$$b_{eoi} = \frac{10}{B/t} \left(\frac{F_y t}{F_{ybi} t_{bi}} \right) B_{bi} \leq B_{bi} \quad (7)$$

$$b_{eov} = \frac{10}{B_{bj}/t_{bj}} \left(\frac{F_{ybj} t_{bj}}{F_{ybi} t_{bi}} \right) B_{bi} \leq B_{bi} \quad (8)$$

where

- B = overall width of the chord, normal to the plane of the connection
- B_b = overall width of the branch, normal to the plane of the connection
- t = wall thicknesses of the chord
- t_b = wall thicknesses of the branch
- F_y = yield stress of the chord
- F_{yb} = yield stress of the branch

AISC 360 also currently limits the values of $b_{eoi}/2$ and $b_{eov}/2$ through a notwithstanding clause, which states,

When $B_{bi}/B > 0.85$ or $\theta_i > 50^\circ$, $b_{eoi}/2$ shall not exceed $2t$ and when $B_{bi}/B_{bj} > 0.85$ or $(180^\circ - \theta_i - \theta_j) > 50^\circ$, $b_{eov}/2$ shall not exceed $2t_{bj}$.

Thus, for the HSS overlapped K-connections tested, the upper limits of $b_{eoi} = 4t$ and $b_{eov} = 4t_{bj}$ apply.

Safety Level Implicit in AISC 360

In order to assess whether adequate or excessive safety margins are inherent, one can check to ensure that a minimum safety index ($\beta+$) of 4.0, as currently adopted by AISC 360-10 per Chapter B of the *Specification Commentary* (AISC, 2010), is achieved using a simplified reliability analysis in which ϕ is given by Equation 9 (Fisher et al., 1978; Ravindra and Galambos, 1978):

$$\phi = m_R \cdot \exp(-\alpha\beta^+ COV) \quad (9)$$

where

- m_R = mean of the ratio of actual element strength to predicted nominal element strength
- COV = associated coefficient of variation of the ratio of actual element strength to predicted nominal element strength
- α = coefficient of separation taken to be 0.55 (Ravindra and Galambos, 1978)

In the evaluation that follows, correlation plots are produced using the measured ultimate weld strengths (rupture loads) from the nine tests and the results from two similar

connection tests that were conducted at the University of Toronto, the details of which appear at the bottom of Table 1 (Frater and Packer, 1992a, 1992b).

The implied resistance factor, ϕ , is equal to 0.922 for the existing AISC *Specification* provisions and is larger than the necessary resistance factors for fillet welds and PJP groove welds (0.75 and 0.80, respectively), indicating an excessive level of safety for the current AISC formulas. Figure 13 shows the correlation of the predicted nominal strengths with the experimental results.

RECOMMENDATION

Background

By means of 12 full-scale experiments on isolated T-connections, conducted during phase 1 of the research program, excessive safety was found to exist in the current AISC 360 (2010) formula for the effective elastic section modulus for in-plane bending for rectangular HSS moment T-connections (McFadden and Packer, 2014). The authors proposed a change to the current requirement that restricts the effective widths of welds to the branch face from two times the chord wall thickness ($2t$) to a more reasonable limit of $B_b/4$.

Their proposal increases the effective length of the transverse weld elements in most rectangular HSS connections and was shown to also be applicable to the formulas for the effective length of welds in axially loaded rectangular HSS T- and X- (or cross-) connections.

Proposal

Because the same pattern is observed for rectangular HSS overlapped K-connections, it is proposed that the existing formulas for the effective length of welds be modified in the same manner, by changing the requirement,

When $B_{bi}/B > 0.85$ or $\theta_i > 50^\circ$, $b_{eoi}/2$ shall not exceed $2t$ and when $B_{bi}/B_{bj} > 0.85$ or $(180^\circ - \theta_i - \theta_j) > 50^\circ$, $b_{eov}/2$ shall not exceed $2t_{bj}$.

to

When $B_{bi}/B > 0.85$ or $\theta_i > 50^\circ$, $b_{eoi}/2$ shall not exceed $B_{bi}/4$ and when $B_{bi}/B_{bj} > 0.85$ or $(180^\circ - \theta_i - \theta_j) > 50^\circ$, $b_{eov}/2$ shall not exceed $B_{bi}/4$.

This change produces the correlation with the test data given by Figure 14.

Safety Level Implicit in Recommendation

The implied resistance factor, ϕ , is equal to 0.875 for the recommended modification to the existing AISC *Specification* provisions (AISC, 2010), which is still larger than the necessary resistance factors for fillet welds and PJP groove

welds. More importantly, using these modified AISC provisions for rectangular HSS overlapped K-connections results in consistency for the aggregate recommended design rules for welds in rectangular HSS connections, including axially loaded rectangular HSS T- and X- (or cross-) connections, moment T-connections and overlapped K-connections.

Comments

It is worth noting that if no effective length rules are applied, and if the total weld length is used to determine the strength of the welded joint to the overlapping branch, then the correlation with the test data shown in Figure 15 results. The implied resistance factor, ϕ , is equal to 0.674, which is less than the necessary resistance factors for fillet and PJP welds, illustrating that such an approach provides an insufficient safety margin. If historical tests (Frater, 1991) are omitted from the analysis, a marginal reduction to the inherent safety factors is found; however, the previous discussion still applies, and the recommendation is found to be safe. Correlations to this effect are given in Figures 16, 17 and 18.

If the hidden toe of the overlapped branch was not welded, a smaller effective length may result at the toe of the overlapping branch (b_{eov}) because the restraint to transverse deformation (stiffness) would be less. This would tend to reduce the mean of the actual element strength to predicted nominal element strength (m_R) in Equation 9; however, by virtue of m_R being already higher for connections with $O_v =$

30% relative to the other connections, there would be some counteracting decrease in COV , and thus a minimal effect on the reliability of the proposed changes.

CONCLUSIONS

Based on the results from nine full-scale tests on weld-critical rectangular HSS-to-HSS overlapped K-connections and the measured strength of two overlapped K-connection tests from a previous experimental program (Frater, 1991), it has been found that:

- The distribution of normal strain adjacent to the welded joint in rectangular HSS overlapped K-connections is highly nonuniform.
- As the overlap increases, stiffening the joint, the distribution of normal strain adjacent to the welded joint becomes more uniform.
- Transverse welds are only partially effective and generally become less effective as the β -ratio decreases, as O_v decreases and as B/t (of the landing surface) increases.
- The current effective length rules defined by Equations K4-10, K4-11 and K4-12 and given in Table K4.1 of AISC 360 (2010) for welds in rectangular HSS-to-HSS overlapped K-connections are quite conservative.

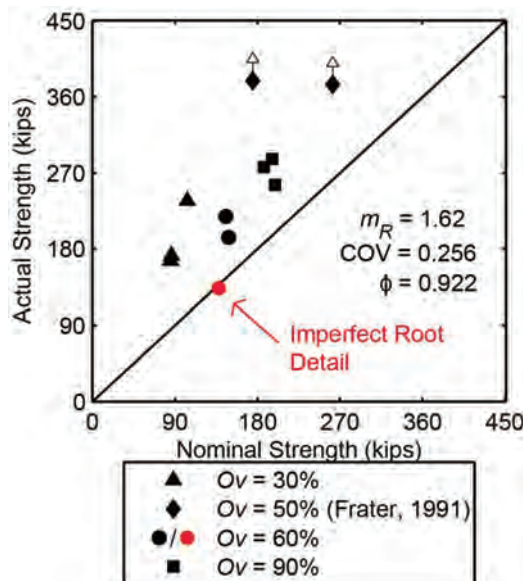


Fig. 13. Correlation with all test results for current AISC 360-10 provisions.

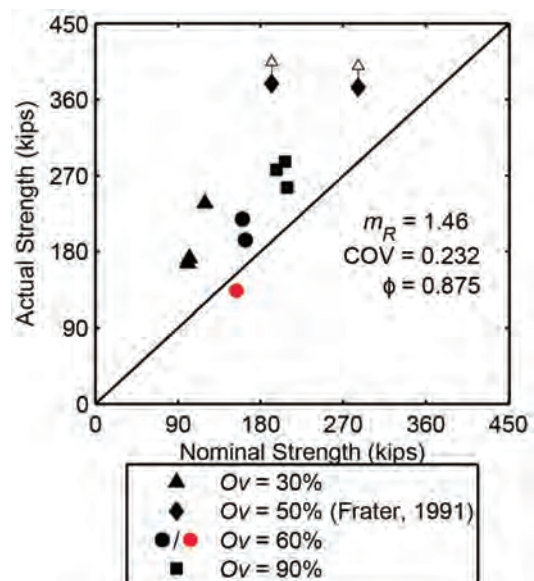


Fig. 14. Correlation with all test results for modified AISC 360-10 provisions.

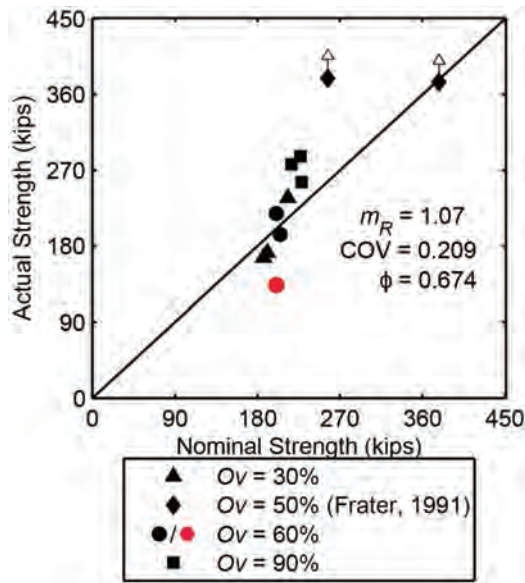


Fig. 15. Correlation with all test results not using effective length rules.

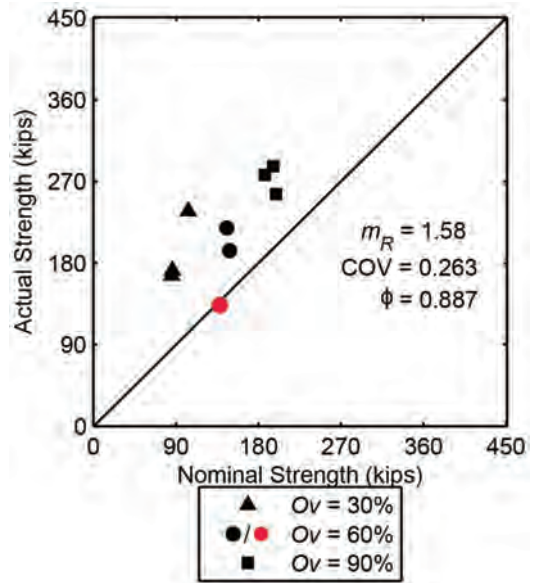


Fig. 16. Correlation with current test results for current AISC 360-10 provisions.

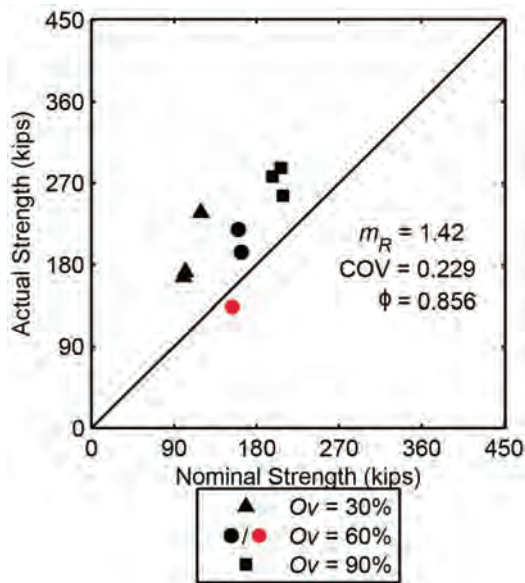


Fig. 17. Correlation with current test results for modified AISC 360-10 provisions.

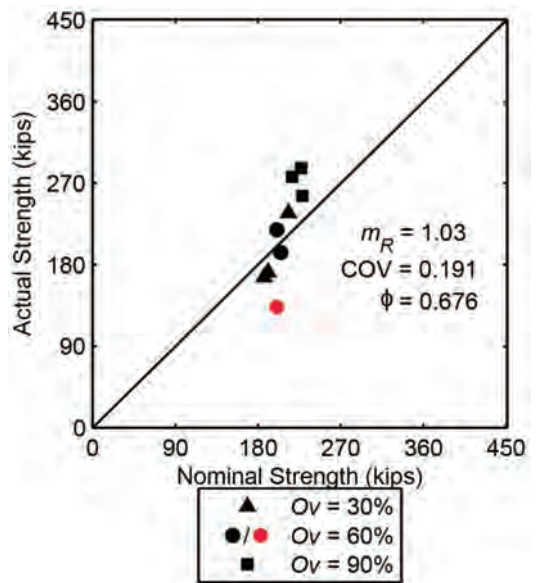


Fig. 18. Correlation with current test results without using weld effective length rules.

RECOMMENDATION

It is recommended to modify the requirement (AISC 360-10)

When $B_{bi}/B > 0.85$ or $\theta_i > 50^\circ$, $b_{eoi}/2$ shall not exceed $2t$ and when $B_{bi}/B_{bj} > 0.85$ or $(180^\circ - \theta_i - \theta_j) > 50^\circ$, $b_{eov}/2$ shall not exceed $2t_{bj}$.

to

When $B_{bi}/B > 0.85$ or $\theta_i > 50^\circ$, $b_{eoi}/2$ shall not exceed $B_{bi}/4$ and when $B_{bi}/B_{bj} > 0.85$ or $(180^\circ - \theta_i - \theta_j) > 50^\circ$, $b_{eov}/2$ shall not exceed $B_{bi}/4$.

to increase the predicted strength of welded joints in rectangular HSS overlapped K-connections. This modification is adopted from McFadden and Packer (2014) and has been shown to still be conservative yet generally provide a more economical design approach for rectangular HSS T-, Y- and X- (or cross-) connections subject to branch axial load or branch bending. Using this recommendation would thus establish consistent rules across AISC 360 for the design of welded truss connections between HSS.

DESIGN EXAMPLE

Given:

A planar roof truss contains the welded HSS 60-degree overlapped K-connection shown in Figure 19. Note that the chord moment is necessary for equilibrium because of the nodding eccentricity. The connection is a balanced K-connection because the vertical component of the compression branch member force is equilibrated (within 20%) by the vertical component of the tension branch member force [see AISC 360-10, Section K2(b)]. The through branch is the wider and thicker branch member. For fabrication, the compression (through) branch is fully welded (overlapped/hidden toe included) to the chord, the diagonal (overlapping) branch is then tacked into place and finally the whole connection is welded together. The loads shown consist of live load and dead load in the ratio of 3:1. Determine the adequacy of the connection under the given loads, and the required weld throat, for each of the branches, using the effective length approach. Assume matched electrodes with a specified ultimate strength of 70 ksi.

From AISC *Manual* Table 2-3 (AISC, 2011), the HSS material properties are as follows:

All members

ASTM A500 Grade B

$$F_y = F_{yb} \\ = 46 \text{ ksi}$$

$$F_u = F_{ub} \\ = 58 \text{ ksi}$$

Weld consumable

$$F_{EXX} = 70 \text{ ksi}$$

From AISC *Manual* Tables 1-11 and 1-12, the HSS geometric properties are as follows:

HSS8×8×½

$$A = 13.5 \text{ in.}^2 \\ B = 8.00 \text{ in.} \\ H = 8.00 \text{ in.} \\ t = 0.465 \text{ in.}$$

HSS6×4×5/16

$$A_{bj} = 5.26 \text{ in.}^2 \\ B_{bj} = 4.00 \text{ in.} \\ H_{bj} = 6.00 \text{ in.} \\ t_{bj} = 0.291 \text{ in.}$$

HSS5×3×¼

$$A_{bi} = 3.37 \text{ in.}^2 \\ B_{bi} = 3.00 \text{ in.} \\ H_{bi} = 5.00 \text{ in.} \\ t_{bi} = 0.233 \text{ in.}$$

Solution:

Limits of Applicability

Check the limits of applicability for rectangular HSS given in AISC *Specification* Section K2.3 (AISC, 2010). Connection nodding eccentricity, $e = -1.00$ in. (negative because the branch centerlines intersect toward the branches, relative to the chord centerline).

q = overlap length measured along the connecting face of the chord beneath the two branches, from geometry

$$= \left(\frac{H_{bj}}{2\sin \theta_{bj}} + \frac{H_{bi}}{2\sin \theta_{bi}} \right) - \left(\frac{e + H/2}{\frac{\sin \theta_{bj} \sin \theta_{bi}}{\sin(\theta_{bj} + \theta_{bi})}} \right)$$

$$= \left(\frac{6.00 \text{ in.}}{2\sin 60^\circ} + \frac{5.00 \text{ in.}}{2\sin 60^\circ} \right) - \left(\frac{-1.00 \text{ in.} + 4.00 \text{ in.}}{\frac{(\sin 60^\circ)^2}{\sin 120^\circ}} \right)$$

$$= 6.35 \text{ in.} - 3.46 \text{ in.}$$

$$= 2.89 \text{ in.}$$

p = projected length of the overlapping branch on the chord

$$= \frac{5.00 \text{ in.}}{\sin 60^\circ}$$

$$= 5.77 \text{ in.}$$

$$O_v = \left(\frac{q}{p} \right) (100\%)$$

$$= \left(\frac{2.89}{5.77} \right) (100\%)$$

$$= 50\%$$

$$-0.55 \leq \frac{e}{H} = -0.125 \leq 0.25 \quad \text{o.k.}$$

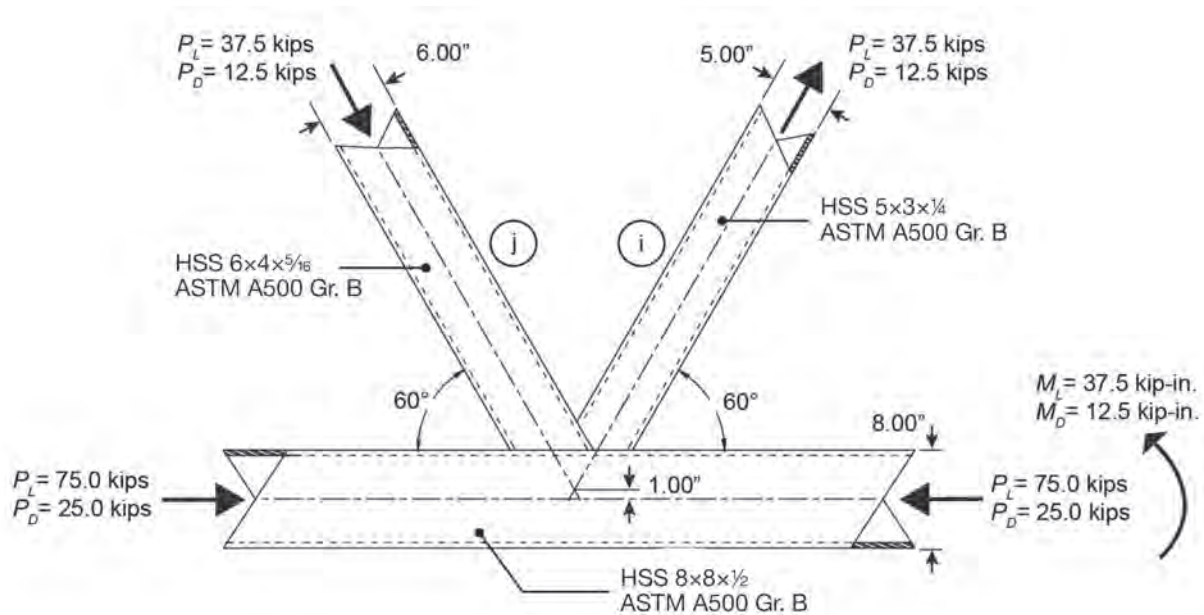


Fig. 19. Welded overlapped K-connection with rectangular HSS.

As the nodding eccentricity satisfied this limit, the resulting total eccentricity moment that it produces [(2(1.00 in.)(50 kips) (cos 60°) = 50 kip-in.] can be neglected with regard to connection design. (However, it would still have an effect on chord member design in general).

$$\begin{aligned}\theta_{bi} &= \theta_{bj} \\ &= 60^\circ \geq 30^\circ \quad \mathbf{o.k.}\end{aligned}$$

$$\begin{aligned}\frac{B}{t} &= \frac{8.00 \text{ in.}}{0.465 \text{ in.}} \\ &= 17.2 \leq 30 \quad \mathbf{o.k.}\end{aligned}$$

$$\begin{aligned}\frac{H}{t} &= \frac{8.00 \text{ in.}}{0.465 \text{ in.}} \\ &= 17.2 \leq 35 \quad \mathbf{o.k.}\end{aligned}$$

For the tension branch:

$$\begin{aligned}\frac{B_{bi}}{t_{bi}} &= \frac{3.00 \text{ in.}}{0.233 \text{ in.}} \\ &= 12.9 \leq 35 \quad \mathbf{o.k.}\end{aligned}$$

$$\begin{aligned}\frac{H_{bi}}{t_{bi}} &= \frac{5.00 \text{ in.}}{0.233 \text{ in.}} \\ &= 21.5 \leq 35 \quad \mathbf{o.k.}\end{aligned}$$

For the compression branch:

$$\begin{aligned}\frac{B_{bj}}{t_{bj}} &= \frac{4.00 \text{ in.}}{0.291 \text{ in.}} \\ &= 13.7 \leq 1.1 \sqrt{\frac{E}{F_{yb}}} = 1.1 \sqrt{\frac{29,000}{46 \text{ ksi}}} = 27.6\end{aligned}$$

$$13.7 \leq 27.6 \quad \mathbf{o.k.}$$

$$\begin{aligned}\frac{H_{bj}}{t_{bj}} &= \frac{6.00 \text{ in.}}{0.291 \text{ in.}} \\ &= 20.6 \leq 1.1 \sqrt{\frac{E}{F_{yb}}}\end{aligned}$$

$$20.6 \leq 27.6 \quad \mathbf{o.k.}$$

For the tension branch:

$$\begin{aligned}\frac{B_{bi}}{B} &= \frac{3.00 \text{ in.}}{8.00 \text{ in.}} \\ &= 0.375 \geq 0.25 \quad \mathbf{o.k.}\end{aligned}$$

$$\begin{aligned}\frac{H_{bi}}{B} &= \frac{5.00 \text{ in.}}{8.00 \text{ in.}} \\ &= 0.625 \geq 0.25 \quad \mathbf{o.k.}\end{aligned}$$

For the compression branch:

$$\frac{B_{bj}}{B} = \frac{4.00 \text{ in.}}{8.00 \text{ in.}}$$
$$= 0.500 \geq 0.25 \quad \mathbf{o.k.}$$

$$\frac{H_{bj}}{B} = \frac{6.00 \text{ in.}}{8.00 \text{ in.}}$$
$$= 0.750 \geq 0.25 \quad \mathbf{o.k.}$$

For the tension branch:

$$0.5 \leq \frac{H_{bi}}{B_{bi}} \leq 2.0$$

$$\frac{H_{bi}}{B_{bi}} = \frac{5.00 \text{ in.}}{3.00 \text{ in.}}$$

$$= 1.67$$

$$0.5 \leq 1.67 \leq 2.0 \quad \mathbf{o.k.}$$

For the compression branch:

$$0.5 \leq \frac{H_{bj}}{B_{bj}} \leq 2.0$$

$$\frac{H_{bj}}{B_{bj}} = \frac{6.00 \text{ in.}}{4.00 \text{ in.}}$$

$$= 1.50$$

$$0.5 \leq 1.50 \leq 2.0 \quad \mathbf{o.k.}$$

For the chord:

$$0.5 \leq \frac{H}{B} = 1.00 \leq 2.00 \quad \mathbf{o.k.}$$

$$25\% \leq O_v = 66.7\% \leq 100\% \quad \mathbf{o.k.}$$

The width of the overlapping branch, B_{bi} , divided by the width of the overlapped branch, B_{bj} , must be greater than or equal to 0.75, where B_{bi} and B_{bj} are the branch widths perpendicular to the longitudinal axis of the chord.

$$\frac{B_{bi}}{B_{bj}} = 0.750 \geq 0.75 \quad \mathbf{o.k.}$$

$$\frac{t_{bi}}{t_{bj}} = 0.801 \leq 1.0 \quad \mathbf{o.k.}$$

$$F_y = F_{yb}$$
$$= 46 \text{ ksi} \leq 52 \text{ ksi} \quad \mathbf{o.k.}$$

$$\frac{F_y}{F_u} = \frac{F_{yb}}{F_{ub}}$$

$$= \frac{46 \text{ ksi}}{58 \text{ ksi}}$$

$$= 0.793 \leq 0.8 \quad \mathbf{o.k.}$$

Required Strength (Expressed as a Force in a Branch)

From Chapter 2 of ASCE/SEI 7-05 (ASCE, 2006), the required strength of the connection, expressed as a force in the tension and compression branches (using the LRFD method) is:

$$\begin{aligned} P_u &= 1.2(12.5 \text{ kips}) + 1.6(37.5 \text{ kips}) \\ &= 75.0 \text{ kips} \end{aligned}$$

Local Yielding of the Branches Due to Uneven Load Distribution

From AISC *Specification* Section K2.3d, the nominal strength of the overlapping branch for the limit state of local yielding due to uneven load distribution is:

$$P_{n,i} = F_{ybi}t_{bi}(2H_{bi} - 4t_{bi} + b_{eov}) \text{ for } 50\% \leq O_v \leq 80\% \quad (\text{Spec. Eq. K2-18})$$

where:

$$\begin{aligned} b_{eoi} &= \frac{10}{B/t} \left(\frac{F_y t}{F_{ybi} t_{bi}} \right) B_{bi} \leq B_{bi} \quad (\text{Spec. Eq. K2-20}) \\ &= \frac{10}{17.2} \left[\frac{46 \text{ ksi} (0.465 \text{ in.})}{46 \text{ ksi} (0.233 \text{ in.})} \right] (3.00 \text{ in.}) \\ &= 3.48 \text{ in.} > B_{bi} = 3.00 \text{ in.} \end{aligned}$$

Therefore, use $b_{eoi} = 3.00 \text{ in.}$

$$\begin{aligned} b_{eov} &= \frac{10}{B_{bj}/t_{bj}} \left(\frac{F_{ybj} t_{bj}}{F_{ybi} t_{bi}} \right) B_{bi} \leq B_{bi} \quad (\text{Spec. Eq. K2-21}) \\ &= \frac{10}{13.7} \left[\frac{46 \text{ ksi} (0.291 \text{ in.})}{46 \text{ ksi} (0.233 \text{ in.})} \right] (3.00 \text{ in.}) \\ &= 2.37 \text{ in.} \leq B_{bi} = 3.00 \text{ in.} \end{aligned}$$

Therefore, $b_{eov} = 2.37 \text{ in.}$

The nominal strength of the overlapping branch is thus:

$$\begin{aligned} P_{n,i} &= 46 \text{ ksi}(0.233 \text{ in.})[2(5.00 \text{ in.}) - 4(0.233 \text{ in.}) + 3.00 \text{ in.} + 2.73 \text{ in.}] \\ &= 159 \text{ kips} \end{aligned}$$

The nominal strength of the overlapped branch is:

$$\begin{aligned} P_{n,j} &= P_{n,i} \left(\frac{F_{ybj} A_{bj}}{F_{ybi} A_{bi}} \right) \quad (\text{Spec. Eq. K2-22}) \\ &= 159 \text{ kips} \left[\frac{5.26 \text{ in.}^2 (46 \text{ ksi})}{3.37 \text{ in.}^2 (46 \text{ ksi})} \right] \\ &= 248 \text{ kips} \end{aligned}$$

The available connection strength, expressed as forces in the tension (overlapping) and compression (overlapped) branches (using the LRFD method), is:

For tension (overlapping) branch:

$$\begin{aligned}\phi P_{n,i} &= 0.95(159 \text{ kips}) \\ &= 151 \text{ kips} \\ 151 \text{ kips} &> 75.0 \text{ kips} \quad \mathbf{o.k.}\end{aligned}$$

For compression (overlapped) branch:

$$\begin{aligned}\phi P_{n,j} &= 0.95(248 \text{ kips}) \\ &= 236 \text{ kips} \\ 236 \text{ kips} &> 75.0 \text{ kips} \quad \mathbf{o.k.}\end{aligned}$$

Determine the Required Weld Throat

Assume a continuous weld effective throat will be provided for each branch, and that both branches will be welded around the entire perimeter (including the hidden toe of the overlapped branch).

From AISC *Specification* Section K4.1, the overlapping member effective weld length is:

$$l_{e,i} = 2 \left[\left(1 - \frac{O_v}{100} \right) \left(\frac{H_{bi}}{\sin \theta_i} \right) + \frac{O_v}{100} \left(\frac{H_{bi}}{\sin (\theta_i + \theta_j)} \right) + b_{eoi} + b_{eov} \right] \quad (\text{Spec. Eq. K4-11})$$

for $50\% \leq O_v \leq 80\%$

where b_{eoi} and b_{eov} are as shown earlier (*Specification* Equations K2-20 and K2-21) for the limit state of local yielding of the overlapping branch due to uneven load distribution. If $b_{eoi} = 3.48 \text{ in.} > B_{bi} = 3.00 \text{ in.}$, then take $b_{eoi} = 3.00 \text{ in.}$ However, the modified requirements proposed in this report state:

When $B_{bi}/B > 0.85$ or $\theta_i > 50^\circ$, $b_{eoi}/2$ shall not exceed $B_{bi}/4$ and when $B_{bi}/B_{bj} > 0.85$ or $(180^\circ - \theta_i - \theta_j) > 50^\circ$, $b_{eov}/2$ shall not exceed $B_{bi}/4$.

Thus, use $b_{eoi} = 2 \left(\frac{B_{bi}}{4} \right) = 1.50 \text{ in.}$

Similarly, when $\frac{b_{eov}}{2} > B_{bi}/4$, use $b_{eov} = 2 \left(\frac{B_{bi}}{4} \right) = 1.50 \text{ in.}$

Therefore, the effective length of the weld to the overlapping branch is:

$$\begin{aligned}l_{e,i} &= 2 \left[\left(1 - \frac{6.67}{100} \right) \left(\frac{5.00 \text{ in.}}{\sin 60^\circ} \right) + \frac{6.67}{100} \left(\frac{5.00 \text{ in.}}{\sin (120^\circ)} \right) \right] + 2(1.50 \text{ in.}) \\ &= 2(1.92 \text{ in.} + 3.85 \text{ in.}) + 2(1.50 \text{ in.}) \\ &= 14.54 \text{ in.}\end{aligned}$$

The effective length of the weld to the overlapped branch, when $B_{bj}/B > 0.85$ or $\theta_j > 50^\circ$, is:

$$\begin{aligned}l_{e,i} &= 2(H_{bj} - 1.2t_{bj})/\sin \theta_j \quad (\text{Spec. Table K4.1}) \\ &= 2[6.00 \text{ in.} - 1.2(0.291 \text{ in.})]/\sin 60^\circ \\ &= 13.0 \text{ in.}\end{aligned}$$

Note: A weld should be provided across the widths of the overlapped branch, B_{bj} , at the toe and the heel (transverse to the chord) even though it is not considered to be at all effective.

The required weld throat, derived from forces in the tension (overlapping) and compression (overlapped) branches, and assuming fillet welds are used, is (using the LRFD method):

For tension (overlapping) branch:

$$\phi P_{nw} = 0.75(F_{nw}t_w l_e)$$

where

$$\begin{aligned} F_{nw} &= 0.60F_{EXX} \\ &= 0.60(70 \text{ ksi}) \\ &= 42 \text{ ksi} \end{aligned}$$

Therefore:

$$\begin{aligned} 0.75(F_{nw}t_w l_e) &\geq 75.0 \text{ kips} \\ t_w &\geq \frac{75 \text{ kips}}{0.75(42 \text{ ksi})(14.54 \text{ in.})} \\ t_w &\geq 0.164 \text{ in.} \end{aligned}$$

For the compression (overlapped) branch:

$$\begin{aligned} t_w &\geq \frac{75 \text{ kips}}{0.75(42 \text{ ksi})(13.0 \text{ in.})} \\ t_w &\geq 0.183 \text{ in.} \end{aligned}$$

Discussion:

If fillet welds were designed to develop the branch member yield strength at all locations around the branch perimeter in accordance with AISC 360-10 (2010), the required weld throat would be as follows:

For the tension (overlapping) branch:

$$\begin{aligned} \phi P_{nw} &\geq \phi P_{n,i} \\ 0.75(F_{nw})(A_{we}) &\geq 0.90(F_{ybi})(t_{bi}) \\ 0.75(42 \text{ ksi})(t_w) &\geq 0.90(46 \text{ ksi})(t_{bi}) \\ t_w &\geq 1.31(t_b) = 0.305 \text{ in.} \end{aligned}$$

For the compression (overlapped) branch:

$$t_w \geq 1.31(t_b) = 0.381 \text{ in.}$$

In the preceding calculations, the branch design wall thickness has been used. The overlapping (tension) branch is loaded to 50% of its factored yield load, and thus the excessively large weld sizes required to develop the branch yield strength are not necessary. As shown previously, the required weld throat calculated using the recommendations of this paper is approximately 50% smaller than the required weld throat to develop the branch yield strength. This is true also for the overlapped (compression) branch, which carries only a fraction of its yield load.

ACKNOWLEDGMENTS

Financial support for this project was provided by the American Institute of Steel Construction, the Natural Sciences and Engineering Research Council of Canada (NSERC), and the Canadian Institute of Steel Construction Education and Research Council. Fabrication was provided, as a gift in-kind, by Walters Inc., Hamilton, Ontario, and the hollow structural sections used were donated by Atlas Tube, Harrow, Ontario.

SYMBOLS AND ABBREVIATIONS

A	Cross-sectional area of the rectangular HSS chord member, in. ²	M_L	Bending moment due to live load, kip-in.
A_b	Cross-sectional area of the rectangular HSS branch member, in. ²	NDT	Nondestructive test
B	Overall width of rectangular HSS chord member, measured normal to the plane of the connection, in.	O_v	Overlap (%) = $(q/p \times 100)$ %
B_b	Overall width of rectangular HSS branch member, measured normal to the plane of the connection, in.	P_D	Axial force due to dead load, kips
B_{bi}	Overall width of the overlapping branch, in.	P_L	Axial force due to live load, kips
B_{bj}	Overall width of the overlapped branch, in.	P_a	Actual weld fracture load, kips
COV	Coefficient of variation	P_n	Predicted weld fracture load, kips
E	Young's modulus of the rectangular HSS, ksi	$P_{n,i}$	Nominal axial strength of the overlapping branch, kips
F_{EXX}	Electrode classification number, ksi	$P_{n,j}$	Nominal axial strength of the overlapped branch, kips
F_{nw}	Nominal strength of the weld metal per unit area, ksi	P_{nw}	Nominal resistance of the weld, kips
F_y	Specified minimum yield stress of rectangular HSS chord, ksi	P_u	Required axial strength in tension or compression, kips
F_{yb}	Specified minimum yield stress of rectangular HSS branch, ksi	SG	Strain gage
F_{ybi}	Specified minimum yield stress of the overlapping branch, ksi	b_{eoi}	Effective width of the branch face welded to the chord, in.; effective length of the weld to the chord, in.
F_{ybj}	Specified minimum yield stress of the overlapped branch, ksi	b_{eov}	Effective width of the branch face welded to the overlapped branch, in.; effective length of the weld to the chord, in.
H	Overall height of rectangular HSS chord member, measured in the plane of the connection, in.	d	Greatest perpendicular dimension measured from a line flush to the base metal surface to the weld surface, in.
H_b	Overall height of rectangular HSS branch member, measured in the plane of the connection, in.	e	Eccentricity in a truss connection, positive being away from the branches, in.
H_{bi}	Overall depth of the overlapping branch, in.	i	Subscript/ term used to identify the overlapping branch member; Subscript/ term used to identify weld elements
H_{bj}	Overall depth of the overlapped branch, in.	j	Subscript/term used to identify the overlapped branch member
$LVDT$	Linearly varying differential transformer	l_e	Effective length of groove and fillet welds for rectangular HSS, in.
M_D	Bending moment due to dead load, kip-in.	m_R	Mean of the ratio (actual element strength/nominal element strength)
		p	Projected length of the overlapping branch on the connecting face of the chord, in.
		q	Overlap length, measured along the connecting face of the chord beneath the region of overlap of the branches, in.
		t	Wall thickness of rectangular HSS chord member, in.

t_b	Wall thickness of rectangular HSS branch member, in.
t_{bi}	Wall thickness of the overlapping branch member, in.
t_{bj}	Wall thickness of the overlapped branch member, in.
t_w	Weld effective throat, in.
α	Coefficient of separation (taken to be 0.55)
β	Width ratio; the ratio of overall branch width to chord width for rectangular HSS
β^+	Safety index
ϵ_{avg}	Average strain, in./in.
ϵ_{rup}	Strain at rupture, in./in.
ϕ	Resistance factor (associated with the load and resistance factor design method)
θ_i	Included angle between the overlapping branch and chord, degrees
θ_j	Included angle between the overlapped branch and chord, degrees

REFERENCES

- AISC (2010), *Specification for Structural Steel Buildings*, ANSI/AISC 360-10, American Institute of Steel Construction, Chicago, IL.
- AISC (2011), *Steel Construction Manual*, 14th ed., American Institute of Steel Construction, Chicago, IL.
- ASCE (2006), *Minimum Design Loads for Buildings and Other Structures*, ASCE/SEI 7-05, American Society of Civil Engineers, Reston, VA.
- ASTM (2009), *Standard Test Methods and Definitions for Mechanical Testing of Steel Products*, ASTM A370-09, American Society for Testing Materials, West Conshohocken, PA.
- ASTM (2013), *Standard Specification for Cold-Formed Welded Carbon Steel Hollow Structural Sections (HSS)*, ASTM A1085-13, West Conshohocken, PA. American Society for Testing Materials.
- AWS (2010), *Structural Welding Code—Steel*, 22, ANSI/AWS D1.1/D1.1M:2010, American Welding Society, Miami, FL.
- CSA (2013), *General Requirements for Rolled or Welded Structural Quality Steel*, G40.20-13/G40.21-13, Canadian Standards Association, Toronto, Canada.
- Davies, G. and Packer, J.A. (1982), “Predicting the Strength of Branch Plate—RHS Connections for Punching Shear,” *Canadian Journal of Civil Engineering*, Vol. 9, No. 3, pp. 458–467.
- Fisher, J.W., Galambos, T.V., Kulak, G.L. and Ravindra, M.K. (1978), “Load and Resistance Factor Design Criteria for Connectors,” *Journal of the Structural Division*, ASCE, Vol. 104, No. 9, pp. 1427–1441.
- Frater, G.S. (1991), “Performance of Welded Rectangular Hollow Structural Section Trusses,” Ph.D. Thesis, University of Toronto, Toronto, Canada.
- Frater, G.S. and Packer, J.A. (1992a), “Weldment Design for RHS Truss Connections, I: Applications,” *Journal of Structural Engineering*, ASCE, Vol. 118, No. 10, pp. 2784–2803.
- Frater, G.S. and Packer, J.A. (1992b), “Weldment Design for RHS Truss Connections, II: Experimentation,” *Journal of Structural Engineering*, ASCE, Vol. 118, No. 10, pp. 2804–2820.
- Frater, G.S. and Packer, J.A. (1992c), “Modelling of Hollow Structural Section Trusses,” *Canadian Journal of Civil Engineering*, Vol. 19, No. 6, pp. 947–959.
- IIW (1989), *Design Recommendations for Hollow Section Joints—Predominantly Statically Loaded*, 2nd ed., Doc. XV-701-89. International Institute of Welding, Paris, France.
- IIW (2012), *Static Design Procedure for Welded Hollow Section Joints—Predominantly Statically Loaded*, 3rd ed., Doc. XV-1402-12, International Institute of Welding, Paris, France.
- ISO (2013), *Static Design Procedure for Welded Hollow-Section Joints—Recommendations*, ISO 14346:2013(E), International Standards Organization, Geneva, Switzerland.
- McFadden, M.R. and Packer, J.A. (2014), “Effective Weld Properties for Hollow Structural Section T-Connections under Branch In-Plane Bending,” *Engineering Journal*, AISC, Vol. 51, No. 4, pp. 247–266.
- McFadden, M.R., Sun, M. and Packer, J.A. (2013), “Weld Design and Fabrication for RHS Connections,” *Steel Construction*, Vol. 6, No. 1, pp. 5–10.
- Mehrotra, B.L. and Govil, A.K. (1972), “Shear Lag Analysis of Rectangular Full-Width Tube Connections,” *Journal of the Structural Division*, ASCE, Vol. 98, No. ST1, pp. 287–305.
- Packer, J.A. and Cassidy, C.E. (1995), “Effective Weld Length for HSS T, Y, and X Connections,” *Journal of Structural Engineering*, ASCE, Vol. 121, No. 10, pp. 1402–1408.

Packer, J.A. and Frater, G.S. (2005), "Recommended Effective Throat Sizes for Flare Groove Welds to HSS," *Engineering Journal*, AISC, Vol. 42, No. 1, pp. 31–44.

Packer, J.A., Wardenier, J., Zhao, X.L., van der Vegte, G.J. and Kurobane, Y. (2009), *Design Guide for Rectangular Hollow Section (RHS) Joints under Predominantly Static Loading*, 2nd ed., CIDECT DG 3, CIDECT, Geneva, Switzerland.

Ravindra, M.K. and Galambos, T.V. (1978), "Load and Resistance Factor Design for Steel," *Journal of the Structural Division*, ASCE, Vol. 104, No. 9, pp. 1337–1353.

System Behavior and Collapse Assessment of Braced Frames

Fourth Quarter 2015

JUDY LIU

INTRODUCTION

Current and recently completed research on system behavior and collapse assessment of braced frames is presented. The research includes work on concentrically braced frames, buckling restrained braced frames, and dual systems with braced frames and secondary moment frames.

Concentrically braced frames (CBFs) are popular for seismic force resisting systems (SFRSs) because of their lateral stiffness and strength. Numerous research investigations into CBF component and system behavior (e.g., Astanteh-Asl et al., 1986; Tremblay 2001, 2002; Uriz and Mahin, 2004) have formed the basis for the AISC *Seismic Provisions* (AISC, 2010). Two studies, highlighted here, build upon contemporary research and further advance the field by examining the dynamic response of chevron CBFs and computational methods for quantifying the collapse capacity of CBFs. The principal investigators for these studies are Professor Dimitrios Lignos, McGill University, and Professor Taichiro Okazaki, Hokkaido University.

Buckling restrained braced frames (BRBFs) have also gained in popularity in recent years, prompting the need for increased knowledge about component and system behavior (Fahnestock et al., 2007a,b). Design guidance on BRBFs has been provided, and researchers have investigated component and system behavior both experimentally and computationally (e.g., Lopez and Sabelli, 2004; Hikino et al., 2013). Further investigation into the connections affecting boundary conditions of the BRBs and BRBF collapse capacity will provide a major step forward in understanding BRBF behavior and design. This research is led by Dr. Luis Ibarra, AISC Milek Fellow and faculty member at The University of Utah.

Rounding out the discussion is a study on a dual-system alternative for seismic design. The secondary frames serve

to improve upon the system behavior of the braced frames. The principal investigator for this study is Professor Paul Richards, Brigham Young University.

DYNAMIC RESPONSE OF CONCENTRICALLY BRACED FRAMES

Large-scale shake table tests of a chevron CBF were conducted to confirm expected component and system behavior. Much of the knowledge base on CBFs is from static loading tests. Specifically, the research program examined the cyclic brace behavior, effects of framing action and frame behavior (Okazaki et al., 2013). The experimental study also incorporated recent design developments for balanced design of gusset plates (Roeder et al., 2011a, 2011b), so as to avoid potential failure of the gusset plate welds as well as for the CBF to withstand large lateral deformations during ground motion shaking.

Test Specimen

Chevron CBFs were chosen for this study because of their architectural advantages and, hence, frequent use. However, the chevron configuration introduces additional considerations for the CBF beams due to the force unbalance from a loaded tension brace and a buckled compression brace. Plastic hinging in the beam may occur, preventing the tension brace from developing its full capacity; inelastic behavior of chevron CBFs with stronger beams is more stable (Tremblay and Robert, 2001). Furthermore, “a large-scale test by Uriz (2005) suggests that, even if the beam is designed for the force unbalance per the ... AISC *Seismic Provisions*, the elastic deflection caused by the force unbalance can be large enough to prevent tensile yielding of the brace” (Okazaki et al., 2013).

The single-story, one-bay CBF test frame represented the bottom story of a three- to five-story steel frame building in Japan. The 70% scale, 13.6-ft (4.15-m) wide, 7.38-ft (2.25-m) tall frame was built with wide-flange beams, HSS columns and square HSS braces (Figure 1). Lateral bracing of the frame was provided at the X's shown in Figure 1. Beam-to-column connections were built as rigid. The column bases

Judy Liu, Ph.D., Research Editor of the AISC Engineering Journal, Professor of Civil and Construction Engineering, Oregon State University, Corvallis, OR. Email: Judy.Liu@oregonstate.edu

were rigidly connected to the shake table through base beams. The 0.177-in. (4.5-mm) gusset plates were designed following the balanced design procedures outlined by Lehman et al. (2008), incorporating an elliptical fold line to accommodate out-of-plane deformations of the brace (Figure 2). The specimen was subjected to six different target amplification levels, ranging from 10% to 70% of the Takatori EW motion (1995 Kobe earthquake). Additional details on the CBF specimen, the test procedure, the instrumentation and loading can be found in Okazaki et al. (2013).

Shake Table Test Results

The shake table tests provided valuable information about chevron CBF behavior. In particular, the final test, at 70% of the Takatori record, demonstrated the effects of unbalanced forces from the braces. Yielding of the beam, near the connections to the columns, began after the specimen obtained a story drift ratio of 0.01 radian. Buckling of the East brace occurred on the brace's first major contraction. After initially recovering its compressive strength, the brace steadily lost its compressive capacity before fracturing near mid-length on its third major extension. Fracture of the West brace was gradual; fracture initiated with failure of the East brace, and the brace saw three more extension cycles before fracturing completely (Figure 3b). Data revealed that the beam deflected down about 0.59 in. (15 mm) due to the force unbalance from the braces but did not develop a plastic hinge as predicted by static pushover analysis. This deformation of the beam affected the brace behavior, causing the

braces to deform more in compression than in tension and to not develop their full tensile strength. The researchers also commented that the “rather limited fatigue life” may have been related to the width–thickness ratios because the braces did not qualify as seismically compact (Okazaki et al., 2013). Meanwhile, the gusset plate connections performed well, developing elliptical yield lines as the braces buckled and deformed out of plane (Figure 3a, Figure 3c). A detailed synthesis of results, including comparisons to numerical simulations, is provided in Okazaki et al. (2013).

COLLAPSE ASSESSMENT OF CONCENTRICALLY BRACED FRAMES

Karamanci and Lignos (2014) proposed a computational approach for collapse assessment of CBFs under seismic loading. The work was motivated by observations of CBF behavior, the resulting challenges in computationally capturing that behavior and challenges in quantifying the collapse capacity for performance-based engineering. Local story mechanisms are common to CBFs. Cyclic deterioration in stiffness and strength of CBFs aggravates P-delta effects and plays a significant role in sideways instability. This cyclic behavior is affected by many geometric and material parameters; researchers have sought to represent this behavior through phenomenological, physical theory, fiber-based and detailed finite element models, as discussed in Karamanci and Lignos (2013). “The main challenge to reliably predict the dynamic behavior of CBFs near collapse is to accurately

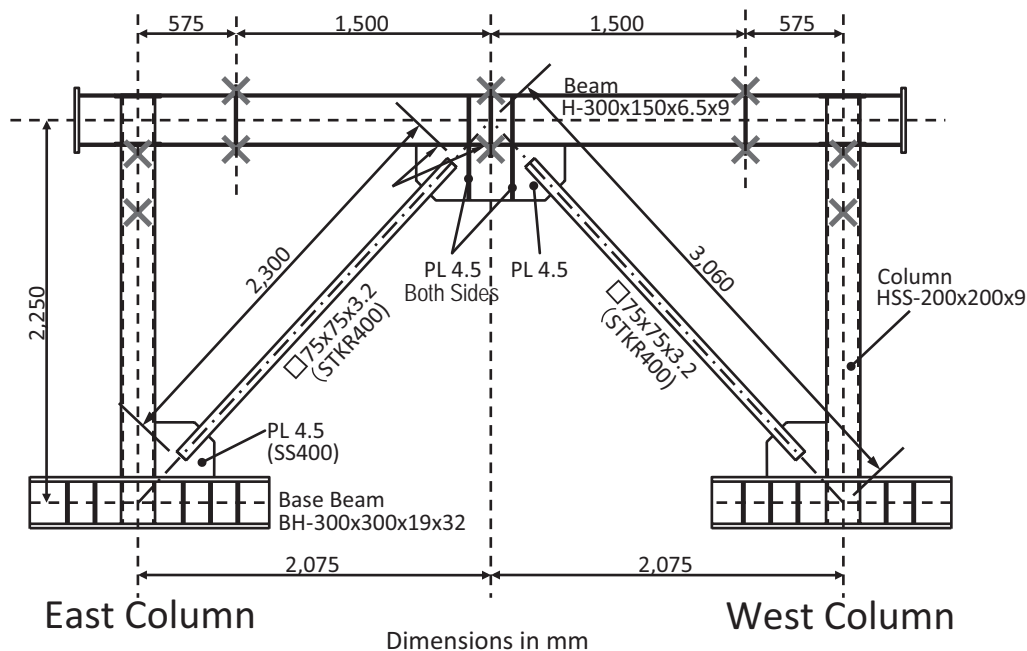


Fig. 1. CBF test specimen (based on Okazaki et al., 2013).

represent the input parameters of the steel brace simulation models that control global/local instabilities and ultimately fracture attributable to low-cycle-fatigue ... Another challenge is to explicitly simulate the strength and stiffness deterioration of steel columns and gusset plate beam-to-column connections under cyclic loading” (Karamanci and Lignos, 2014). Viscous damping has been identified as another important parameter in computational simulations of collapse (e.g., Charney, 2008). Karamanci and Lignos developed a steel brace database and a computational approach

that incorporates consideration of all of these parameters for collapse assessment of CBFs with various types of steel brace shapes.

Modeling of Braces, Connections and Columns

In this computational approach, the model by Uriz (2005) was used to simulate the cyclic behavior of the steel braces. This model captures axial force and second-order bending moment interaction and accounts for large displacements. Fibers represent the brace cross-section in this model, which

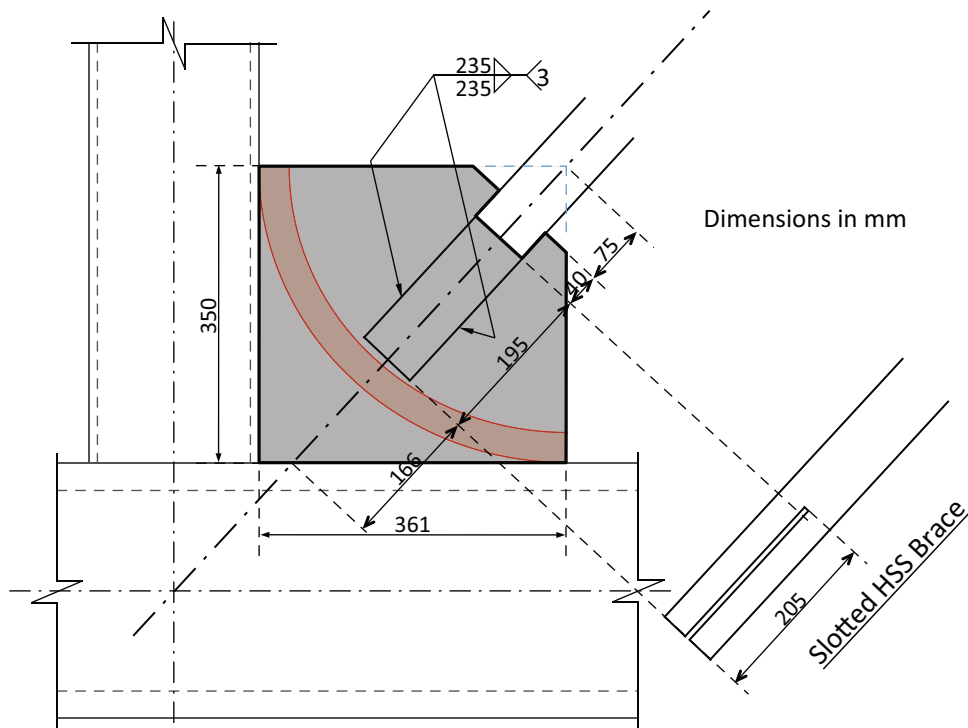


Fig. 2. Gusset plate with elliptical fold line (based on Okazaki et al., 2013).

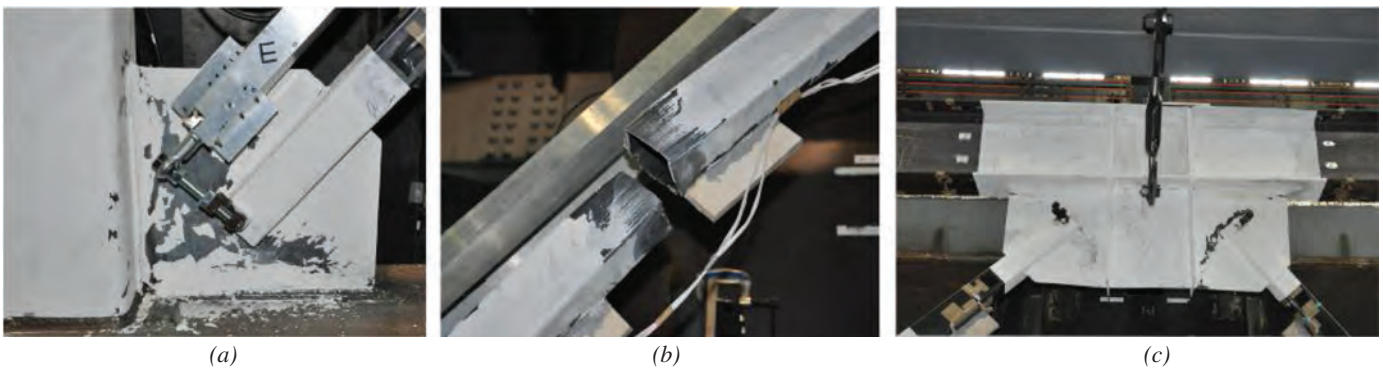


Fig. 3. (a) Gusset plate yielding; (b) steel brace fracture; (c) mid-beam gusset plate yielding.

utilizes the force formulation by Spacone et al. (1996). The use of fibers, following a modified rain-flow counting rule, can simulate gradual or complete fracture through the cross-section. An offset, or initial camber, in the two-element brace component triggers flexural buckling. In this modeling approach, slender cross-sections may behave in a manner that does not correspond well to the plane-sections-remain-plane assumption; therefore, Karamanci and Lignos (2014) recommend detailed finite element approaches (e.g., Fell et al., 2009; Huang and Mahin, 2010) for slender sections. Meanwhile, the models of the gusset plates capture out-of-plane flexural strength and stiffness, based on Hsiao et al. (2012).

An important product from the research was a database of steel braces for use in modeling post-buckling behavior. Databases had existed (e.g., Hsiao et al., 2013; Tremblay, 2002; Lee and Bruneau, 2005), but the work by Karamanci and Lignos (2014) brought together more data and for more types of cross-sections that are commonly used in practice. Information for 317 steel braces was collected; the inventory included 158 rectangular or square HSS braces, 55 round HSS braces, 65 W-shape braces, 37 angle braces and 2 stitched angle braces. The data pulled from 24 experimental programs was for steel braces that failed due to low-cycle fatigue following local buckling. Model input parameters—in particular, those that control the fatigue life of the brace—were related to the brace properties. Measured geometric and material properties, when available, were used in the calibration of the fiber-based model. Expected material properties, following AISC 341-10 (AISC, 2010), were used as needed. Parameters such as initial camber (to trigger global buckling), number of elements or segments for the brace model, and number of fibers to represent the cross-section were optimized. Detailed information on the calibration procedure can be found in Karamanci and Lignos (2013, 2014); the steel brace database, with searchable

interface, will be provided at <http://dimitrios-lignos.research.mcgill.ca/databases/>. The result is excellent correspondence between simulation results and experimental data, as shown in Figure 4 for HSS brace tests by Uriz and Mahin (2008) and Fell et al. (2009).

Modeling recommendations for inelastic buckling and fracture of steel HSS, round HSS and wide-flange braces are summarized in Karamanci and Lignos (2014). Meanwhile, a number of observations of HSS, W-shape and angle brace behavior can be made. Karamanci and Lignos (2014) comment that “fracture life of the three steel brace shapes is primarily affected by the individual local slenderness parameters of the cross sections. However, as the kL/r slenderness increases, global (elastic) buckling of a steel brace is triggered (prebuckling behavior).” Fracture potential also increases with higher yield stress and kL/r values. However, the effect of yield stress is not as pronounced for slender steel braces. Severe local buckling and “crimping” at the corners of rectangular and square HSS braces increase their susceptibility to fracture.

The computational approach for collapse assessment of CBFs also includes modeling of the cyclic deterioration of the steel columns and the beam-to-column connections at the gusset plates. Model development for the connections was based on work by Stoakes and Fahnstock (2011) and Liu and Astaneh-Asl (2000, 2004). Model development for the cyclic deterioration of the steel columns was based on work by Nam and Kasai (2011), Scott and Ryan (2013), and others. The contribution of the connections and columns is on the order of 40% of story shear forces once braces have fractured (Karamanci and Lignos, 2014).

Sideway Collapse and Viscous Damping

Karamanci and Lignos (2014) define dynamic, or sideway, collapse of a CBF as “the point in which an individual story (or a series of stories) displaces sufficiently so that the

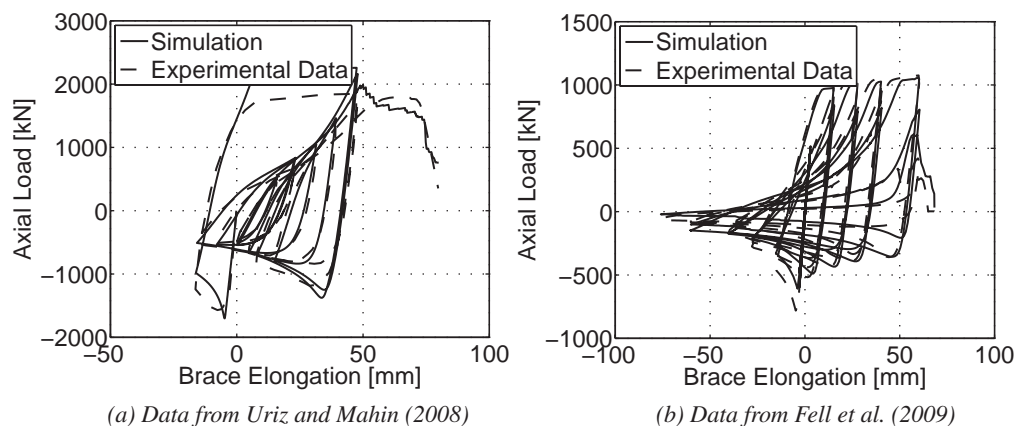


Fig. 4. Comparisons of simulation results to experimental data [Simulation results adapted from Karamanci and Lignos (2014)].

second order P-delta effects accelerated by component deterioration fully offset the first order story shear resistance of the CBF. At this point, the CBF loses its gravity load resistance.” This definition highlights the need for incorporating cyclic deterioration of the various frame components in the computational approach. The definition also correlates well to shake table collapse tests of steel moment resisting frames and CBF frames (e.g., Suita et al., 2008; Lignos et al., 2011; Okazaki et al., 2013), as well as quasi-static tests of CBF frames (e.g., Uriz, 2005). Base shear and story drift responses (Figure 5) illustrate sideways collapse of a two-story CBF modeled using the computational approach described previously. The story drift histories indicate a first story collapse mechanism following brace fracture and the onset of column strength deterioration.

The role of viscous damping was investigated through collapse assessment of a 12-story steel CBF building. Details of the building, modeling and evaluation can be found in Karamanci and Lignos (2014). The researchers found that use of initial stiffness of CBF braces for formation of the Rayleigh damping matrix can significantly overestimate collapse capacity. Buckling and fracture of the braces cause large stiffness changes in the numerical model, in turn creating large artificial damping forces. For more realistic CBF behavior, the researchers recommended that tangent stiffness values be used for modeling of components that behave nonlinearly, excluding their geometric stiffness component to avoid a negative stiffness component of effective damping.

Summary and Future Work

The modeling approach captures important characteristics of the steel CBF components and behavior. Cyclic strength

and stiffness deterioration, fracture, P-delta effects and viscous damping are addressed through this comprehensive, computational approach. A valuable new database for modeling of post-buckling behavior of steel braces has been created, and a rigorous definition of sideways collapse has been developed. The work has been validated against results from quasi-static cyclic and shake table tests. However, the researchers call for further validation against shake table collapse experiments (Karamanci and Lignos, 2014). The proposed approach is currently being utilized to (1) quantify the effect of gravity-framing on the collapse resistance of archetype steel frame buildings with CBFs, (2) quantify the earthquake-induced economic losses in steel frame buildings with CBFs (Hwang et al., 2015), and (3) develop recommendations for the expected post-buckling resistance loads for the seismic design of bracing connections and other members (Cerri et al., 2015).

BEHAVIOR AND COLLAPSE CAPACITY OF BUCKLING RESTRAINED BRACED FRAMES

Similar research on system behavior and collapse capacity, but of buckling restrained braced frames (BRBFs), is in progress. The 2013 Milek Fellowship research, “Effects of BRB Boundary Conditions on Seismic Resilience of BRBFs,” is considering effects of gusset plates and beam-column-gusset connections. BRBFs meet serviceability and collapse capacity objectives under the design basis earthquake (DBE), but some performance issues require more study. For example, Ariyaratana and Fahnestock (2011) indicated that BRBFs may exhibit relatively large residual interstory drifts at DBE seismic level, whereas Sabelli et al. (2003) reported residual

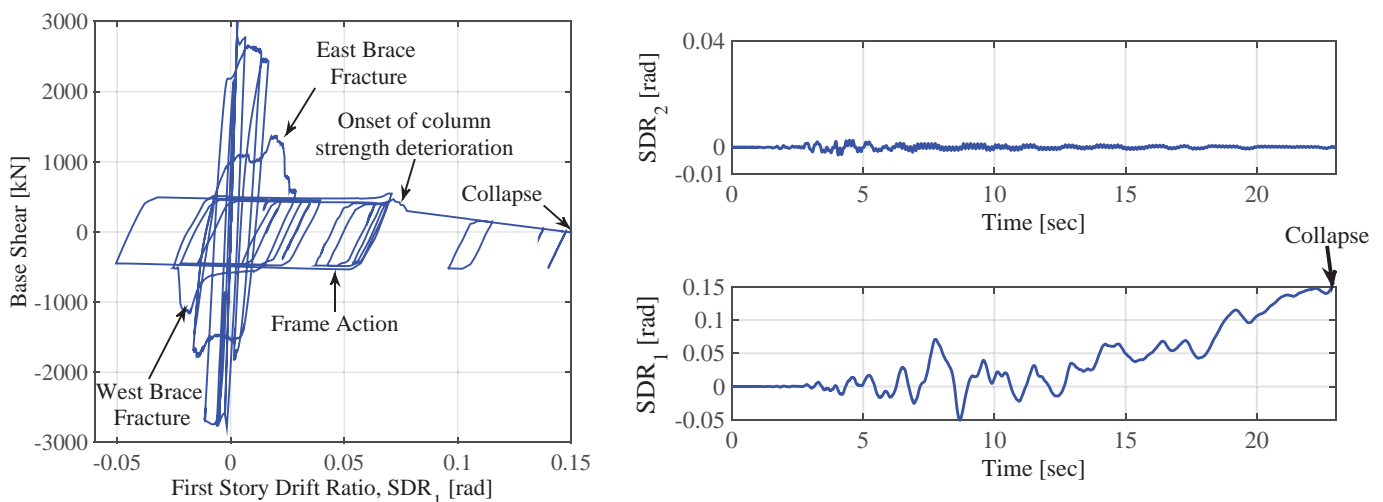


Fig. 5. Base shear–drift ratio and story drift histories for a two-story CBF [simulation results adapted from Karamanci and Lignos (2014)].

story drifts that were on average 40 to 60% of the maximum drifts. In addition, BRB qualification tests show that most braces present stable hysteretic loops under axial loading up to drifts of 2.5 to 3.5%. At these drift levels, the BRB may fail due to core plate fracture, post-buckling behavior, local case buckling and brace plate failure, among other factors. However, these tests usually include oversized gusset plates that guarantee failure will take place in the BRB, preventing failure modes on gusset plates and beam-column-gusset connections. Therefore, this fellowship research includes experimental tests and numerical simulations to evaluate the effect of BRB boundary conditions on the collapse capacity of BRBFs. Some simulation results will be presented, and the planned experimental tests will be introduced.

BRB Boundary Conditions

Some studies have investigated effects of BRB boundary conditions (BCs) on BRBF behavior. Tsai and Hsiao (2008) designed single gusset plates adopting Whitmore's approach, where the gusset plate buckling strength, P_{cr} , was required to be greater than the BRB maximum compressive capacity force, P_{maxC} :

$$P_{cr} = \frac{\pi^2 E}{(kL_c/r)^2} b_e t \geq P_{maxC}$$

L_c is the critical unbraced length, and k is the effective length factor and was taken as 0.65. Tsai and Hsiao found that the gusset plates buckled out of plane at a brace force significantly lower than the calculated gusset buckling strength, P_{cr} . They then designed gusset stiffeners to address the

buckling failure. Similar conclusions were reached by Chou et al. (2012) when evaluating BRBFs with single and dual gusset connections. Also, Takeuchi et al. (2014) performed cyclic experiments on six BRBs set to an out-of-plane story drift of 1/100 using different core-confinement clearance, encasement, embedment ratios and, in some cases, free-edge stiffeners on gusset plates. Finite element modeling (FEM) work performed by Sheng et al. (2002) and Naghipour et al. (2013) showed that a gusset under compression will displace minutely in the out-of-plane dimension elastically until the gusset buckles. Once buckling occurs, the gusset will continue to carry some axial load but with large out-of-plane displacements.

Regarding beam-column-gusset connections, Fahnestock et al. (2007a) and Prinz (2007) performed numerical simulations of BRBFs using hinged, or spliced, beams (i.e., non-moment resisting connection, as shown in Figure 6) and continuous beams. They showed that beam splices reduce stresses in the beam-column-gusset connection region by more than 50%. The experimental results also indicate that the potential for gusset plate failure may be reduced if non-moment resisting connections are considered (Fahnestock et al., 2007b). However, use of these connections may increase residual story drifts (Wigle and Fahnestock, 2010), which is one of the concerns in terms of BRBF seismic resilience. Such behaviors are being investigated through the Milek Fellowship research.

Numerical Study

The numerical investigation has addressed effects of hinged beams and gusset plate out-of-plane behavior on collapse capacity of BRBFs. The prototype structure used in the numerical study is a four-story, single diagonal braced bay structure modified from the AISC *Seismic Manual* (2012) BRBF example (Figure 7). The BRBF has a bay width of 19.33 ft, a 14-ft-tall first story and 12.5-ft-tall upper stories. The structure's beams, columns and gussets are designed with a 50-ksi yield strength, and the BRB core cross-sectional area (A_{sc}) are sized based on a yield stress (F_y) of 42 ksi. The brace overstrength factors for tension (ω) and compression (β) are assumed as 1.36 and 1.1, respectively.

The prototype BRBF seismic performance was evaluated for two gusset plate designs with different average buckling lengths. These lengths represent the range of extremes of possible unbraced lengths while still qualifying as "compact," according to Dowswell (2006). The first gusset plate design (Gusset-1) has an average unbraced length of about 5.0 in. (Figure 8a) and meets Dowswell's (2006) and Thornton's (1984) design criteria. Dowswell checks a gusset's geometry for stability based upon a collection of experimental results, while Thornton checks a gusset's stability using column-buckling design. For the numerical model, Gusset-1 is given a strength that is equal to the AISC (2012) prescribed

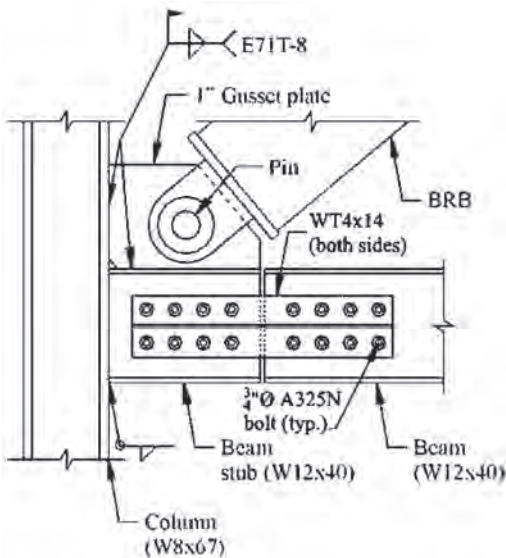


Fig. 6. Hinged beam at gusset plate connection [AISC, 2010; from Fahnestock et al., (2006)].

$P_{cr} = 1.1\beta\omega A_{sc}F_y$. For the future physical experimentation, Gusset-1 will have an average unbraced length of about 5.0 in. (Figure 8a) to reach a strength that similarly just meets code requirements. In Gusset-1, the elliptical fold zone is the elliptical line that crosses virtually through the last bolt closest to the beam, giving the zone a width roughly equal to the gusset's thickness (t_g). The second gusset plate design (Gusset-2) (Figure 8b) will have a longer average unbraced length that meets Dowswell's criterion, but it does not have the required buckling strength when designed per the Thornton method with an effective length factor of 0.65. Gusset-2, as modeled, is now susceptible to premature buckling. For the future physical experimentation, Gusset-2 will have an average unbraced length of about 12.6 in. (Figure 8b). Gusset-2 has an elliptical fold zone width of approximately $16t_g$.

Two numerical models have been developed in PERFORM 3D (CSI, 2011) and OpenSees (McKenna, 2014) software. The model in OpenSees will be used to explicitly consider out-of-plane displacement of the gusset plates, but it is not in the scope of this research update. The PERFORM

3D model will be used to validate the results of the most complex OpenSees model and includes an element with a trilinear backbone curve that accounts for the isotropic and kinematic behavior observed in BRB hysteretic responses. Also, the model can capture the plastic rotational deformations of beam-column elements. For the numerical analyses, the BRBs were assigned an ultimate strain capacity of 4%. Experimental tests commonly report BRB ultimate strain levels between 2.5 and 3.5% (Xu, 2015; CoreBrace, 2015). The use of a larger maximum strain level implies that the BRBs would withstand larger ground motions, increasing the likelihood of gusset plate buckling failure.

For the gusset plate, the tensile stress-strain response was assumed to be elastic-perfectly-plastic with an ultimate allowable tensile strain of 0.2. For compressive loading, the gusset buckling capacity was approximated in PERFORM 3D with inelastic buckling elements, representing the gusset's unbraced length and located at each end of the BRB. The buckling is controlled by the member's axial deformation. Strain limitations for the PERFORM 3D model were

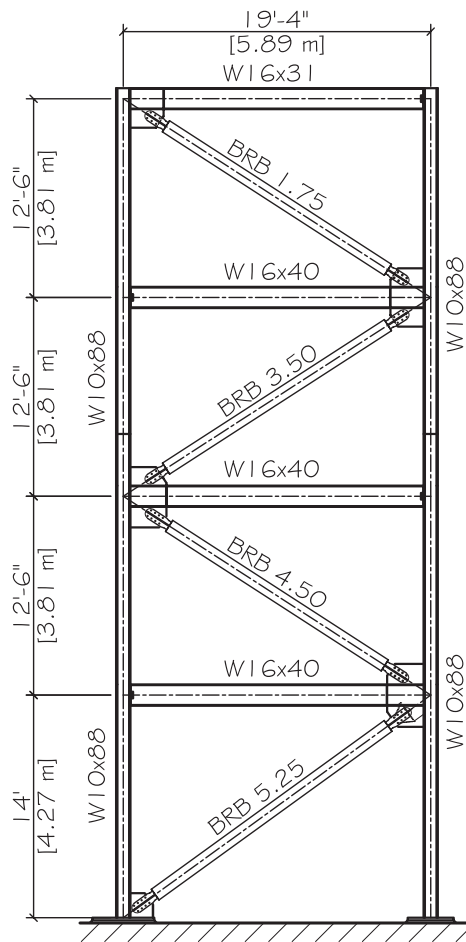


Fig. 7. Full-scale prototype structure.

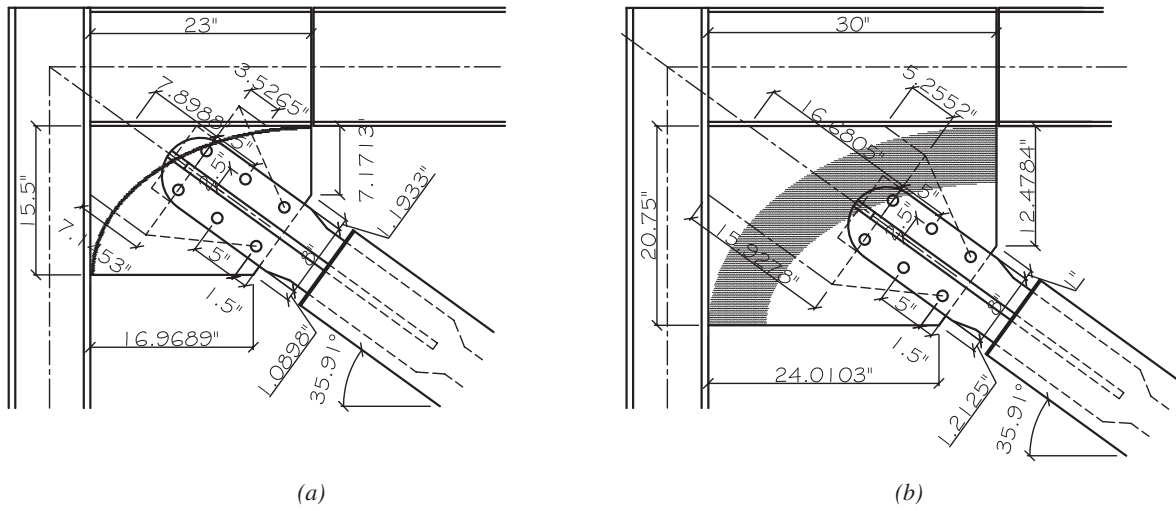


Fig. 8. (a) Gusset-1 configuration, (b) Gusset-2 configuration.

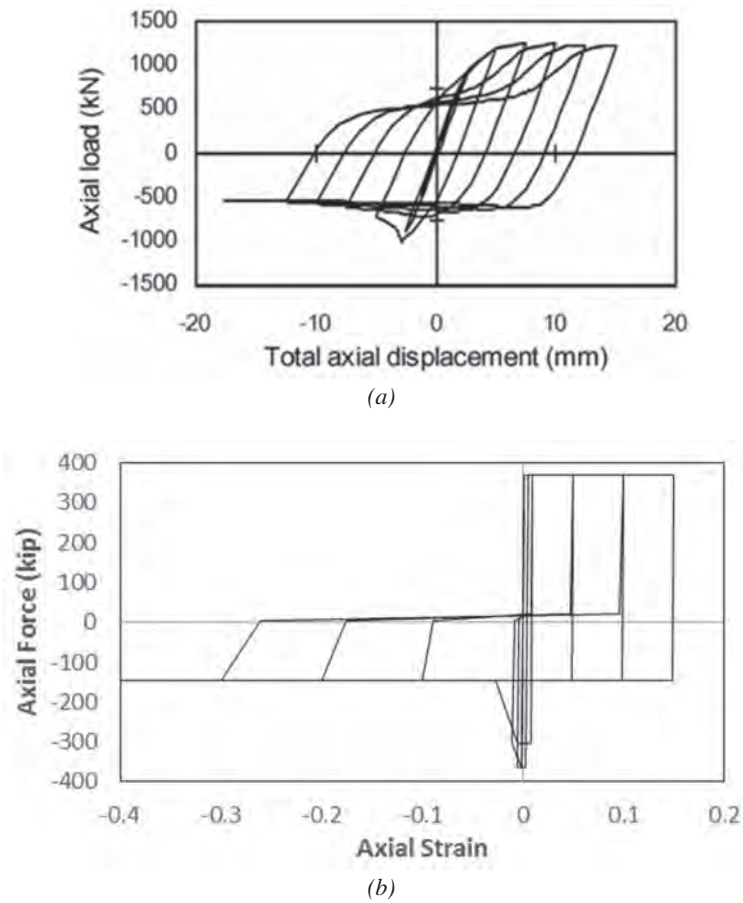


Fig. 9. (a) Cyclic response of a gusset plate (Walbridge et al., 2005); (b) numerical simulation.

estimated using results primarily from Walbridge et al. (2005) and Sheng et al. (2002). By curve fitting the Sheng et al. data, the buckling strain was estimated to be 0.015 mm/mm, and the ultimate strain limit was assumed as 0.50 mm/mm; a best case scenario that allows for the level of gusset nonlinearity observed in the testing of Walbridge et al. Figure 9 shows the hysteretic response of one of the gusset plates evaluated by Walbridge et al. under quasi-static loading, along with the response obtained from a time-history analysis in PERFORM 3D.

The seismic performance to collapse of the prototype BRBF was computed using incremental dynamic analyses (IDAs) for both types of gussets. The frames were also evaluated assuming splices at the end of the gusset that created beam-hinges capable of releasing stresses from the gusset

plates. To perform IDAs, a set of 13 records was selected from FEMA P-695 (2009) far-field ground motions. The spectral accelerations were scaled in incremental steps of 0.2 g, until collapse occurred. The collapse capacity was computed within a tolerance of 0.02 g. Figure 10 shows the median IDAs for the evaluated four-story BRBFs. The frames with Gusset-1 exhibited a larger collapse capacity because, in most cases, failure was caused by BRB ultimate drift capacity. BRBFs with Gusset-2 exhibited gusset plate buckling failure in about half of the simulations, resulting in a loss of collapse capacity of more than 20%. The inclusion of splices to create beam-hinges did not have a large effect for drifts of 2% or less. The collapse fragility curves presented in Figure 10 corroborate the small effect of beam splices on the frame performance.

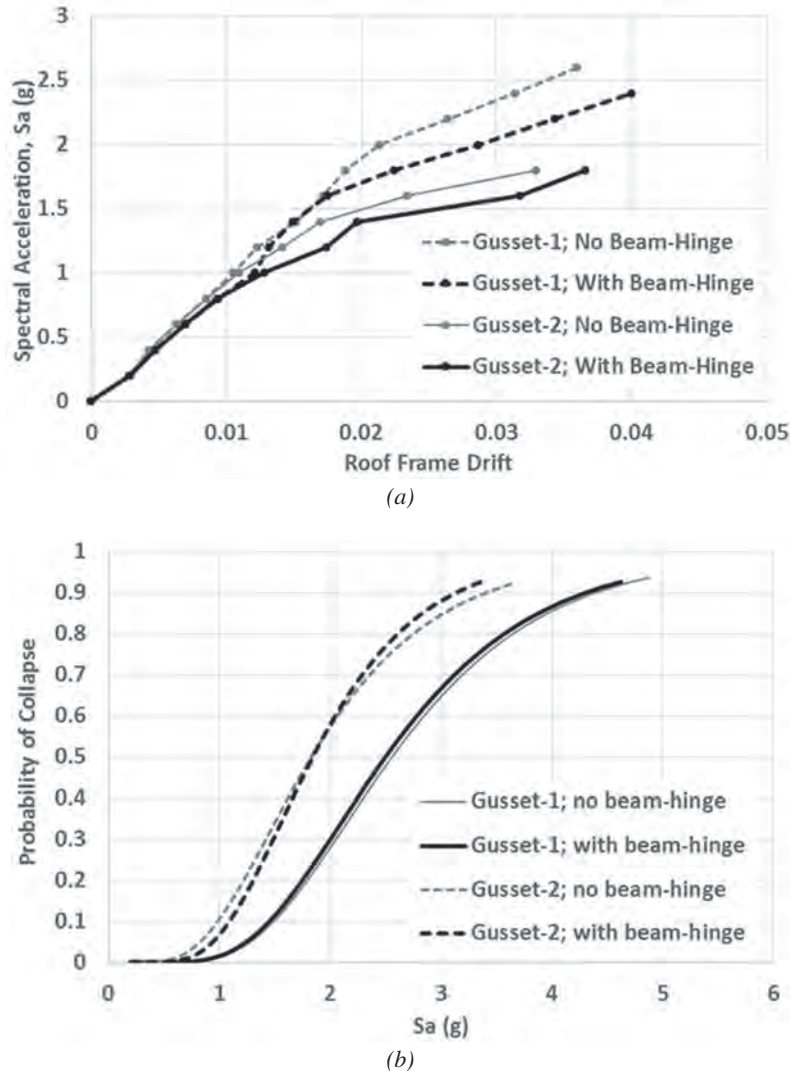


Fig. 10. (a) IDAs for four-story BRBFs; (b) fragility curves for collapse limit state.

Planned Experimental Tests and Expected Outcomes

For the experimental tests, a 75% scale, one-story portal frame will be built. The loading protocol will be based on the AISC *Seismic Provisions* (2010) for cyclic testing of BRBs. Alternative loading protocols are permitted by AISC and will be considered in the numerical simulation. Figure 11 shows the prototype that it is expected to be tested in the next phase of the project. It is anticipated that the frames will be first tested with beam splices until plate yielding starts, at which point the beam splice will be bolted at the flanges, creating a continuous beam. Then, the frames will be retested until significant frame or connection damage is detected. This approach will provide information about the BRBFs' maximum displacements, gusset stresses and buckling capacity, as well as the effect of BRB boundary conditions on frame collapse capacity. The experimental tests will also be used to calibrate the numerical models; a parametric study, based on time-history analyses, will be performed.

DUAL SYSTEMS

Recent, complementary research demonstrates how the performance of braced frames can be improved upon in dual systems through the use of secondary moment frames. Secondary moment frames can prevent concentrated story drifts and reduce residual drifts in braced frames (e.g., Pettinga et al., 2007). Furthermore, designing the frames for positive stiffness throughout a seismic event is beneficial for mitigation of residual drift. This positive stiffness can be achieved through high-yield-drift (HYD) moment frames with elastic

response up to 4% drift. A possible HYD moment frame uses a theoretically pinned connection at one end of the beam and a rigid connection at the other. Another possible HYD configuration may use this one-end, rigidly connected beam at alternate stories within the frame.

Miller and Richards (2015) investigated and provided recommendations for dual systems with HYD moment frames; they used buckling-restrained braced frames for their study but commented on the ability to use HYD frames for dual systems with other types of braced frames. They conducted non-linear time-history analyses of 4- to 20-story dual systems, with both HYD frames and with conventional, secondary moment frames. Design basis earthquake (DBE) and maximum considered earthquake (MCE) demands were considered. The researchers concluded that the HYD configuration with the one-end, rigidly connected beams at alternate stories had the highest connection efficiency of the HYD frames studied, with half of the rigid connections required for a comparable conventional frame. Maximum and residual drift levels in the dual-HYD systems were lower than those for the conventional system. Additional details of the study and synthesis of results are provided in Miller and Richards (2015).

SUMMARY

Several unique but related studies on seismic behavior and collapse capacity of braced frames have been presented. Some recently completed work on the dynamic response of chevron CBFs has been highlighted, along with

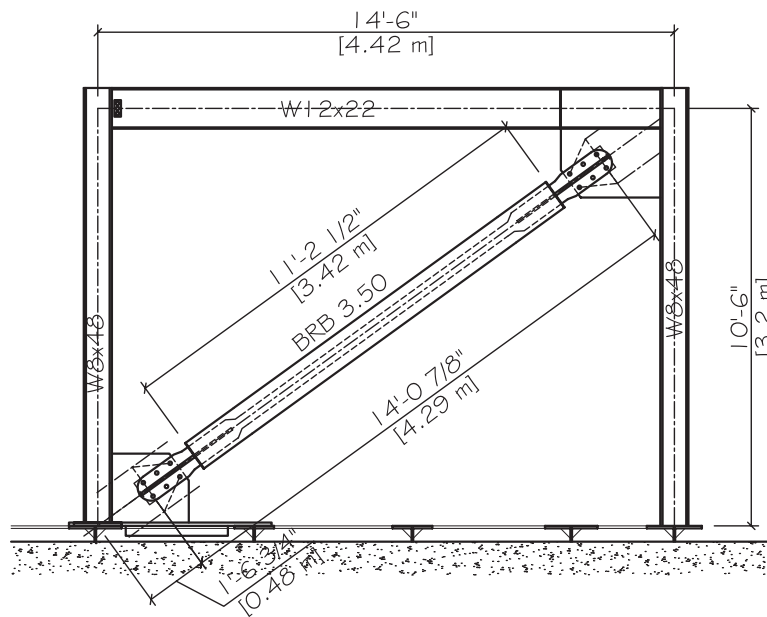


Fig. 11. Portal frame to test gusset plate out-of-plane behavior.

investigations into computational collapse assessment of CBFs. Similar themes, including the significance of out-of-plane gusset plate behavior, are found in research on effects of BRB boundary conditions on the seismic behavior of BRBFs. Meanwhile, a slightly different approach to seismic resilience is found in an investigation of high-yield-drift moment frames in dual systems with braced frames.

ACKNOWLEDGMENTS

Special thanks to Luis Ibarra, Dimitrios Lignos and Paul Richards for their contributions to this article. Financial support for the research on the dynamic behavior of chevron CBFs was provided by National Research Institute for Earth Science and Disaster Prevention of Japan; technical support was provided by the Hyogo Earthquake Engineering Research Center (E-Defense). The research on collapse assessment of CBFs was supported by the National Science and Engineering Research Council of Canada (NSERC) under the Discovery Grant Program. Partial support for the development of the steel brace database was through the McGill University Summer Undergraduate Research in Engineering (SURE) program. The BRB boundary condition and BRBF collapse capacity work has support from the American Institute of Steel Construction, with additional support from the Department of Civil and Environmental Engineering at the University of Utah. The dual systems with high-yield-drift secondary moment frames were studied with support from Brigham Young University.

REFERENCES

- AISC (2010), *Seismic Provisions for Structural Steel Buildings*, ANSI/AISC 341-10, American Institute of Steel Construction, Chicago, IL.
- AISC (2012), *Seismic Design Manual*, 2nd ed., American Institute of Steel Construction, Chicago, IL.
- Ariyaratana C., and Fahnestock, L.A. (2011), "Evaluation of Buckling-Restrained Brace Frame Seismic Performance Considering Reserve Strength," *Engineering Structures*, Vol. 33, pp. 77–89.
- Astaneh-Asl, A., Goel, S.C. and Hanson, R.D. (1986), "Earthquake-Resistant Design of Double Angle Bracing," *Engineering Journal*, Vol. 23, No. 4, pp. 133–147.
- Cerri, S., Moir, H. and Lignos, D.G. (2015), "Development of R_y , R_t Factors and Probable Brace Resistance Axial Loads for the Seismic Design of Bracing Connections and Other Members," *Proc., 8th International Conference on Behavior of Steel Structures in Seismic Regions*, Shanghai, China, July 1–3, 2015, Paper 207.
- Charney, F. (2008), "Unintended Consequences of Modeling Damping in Structures," *Journal of Structural Engineering*, 10.1061/(ASCE)0733-9445(2008)134:4(581), pp. 581–592.
- Chou, C.C., Liu, J.H. and Pham, D.-H. (2012), "Steel Buckling-Restrained Braced Frames with Single and Dual Corner Gusset Connections: Seismic Tests and Analyses," *Earthquake Engineering and Structural Dynamics*, Vol. 41, pp. 1137–1156.
- CSI (2011), *PERFORM-3D: Nonlinear Analysis and Performance Assessment for 3-D Structures*, Computers and Structures, Inc., Berkeley, California.
- CoreBrace (2015), "CoreBrace, Testing." <http://www.corebrace.com/testing.html>.
- Dowswell, B. (2006), "Effective Length Factors for Gusset Plate Buckling," *Engineering Journal*, Second Quarter, pp. 91–101.
- Fahnestock, L. A. Ricles, J.M. and Sause, R. (2006), "Experimental Study of a Large-Scale Buckling Restrained Using the Pseudo-Dynamic Testing Method," *Proc. 8th National Conference on Earthquake Engineering*, San Francisco, CA, April.
- Fahnestock, L., Sause, R. and Ricles, J. (2007a) "Seismic Response and Performance of Buckling-Restrained Braced Frames." *Journal of Structural Engineering*, Vol. 133, No. 9, pp. 1195–1204.
- Fahnestock, L., Ricles, J. and Sause, R. (2007b) "Experimental Evaluation of a Large-Scale Buckling-Restrained Braced Frame." *Journal of Structural Engineering*, Vol. 133, No. 9, pp. 1205–1214.
- Fell, B.V., Kanvinde, A.M., Deierlein, G.G. and Myers, A.T. (2009), "Experimental Investigation of Inelastic Cyclic Buckling and Fracture of Steel Braces," *Journal of Structural Engineering*, 10.1061/(ASCE)0733-9445(2009)135:1(19), 19–32.
- FEMA P-695 (2009), "Quantification of Building Seismic Performance Factors," Federal Emergency Management Agency, Washington, DC.
- Hikino, T., Okazaki, T., Kajiwara, K. and Nakashima, M. (2013), "Out-of-Plane Stability of Buckling-Restrained Braces Placed in Chevron Arrangement," *Journal of Structural Engineering*, Vol. 139, No. 11, pp. 1812–1822.
- Hsiao, P.C., Lehman, D.E. and Roeder, C.W. (2012), "Improved Analytical Model for Special Concentrically Braced Frames," *Journal of Constructional Steel Research*, Vol. 73, No. 3, pp. 80–84.
- Hsiao, P.C., Lehman, D.E. and Roeder, C.W. (2013), "A Model to Simulate Special Concentrically Braced Frames Beyond Fracture," *Earthquake Engineering & Structural Dynamics*, Vol. 42, No. 2, pp. 183–200.

- Huang, Y. and Mahin, S.A. (2010) "Simulating the Inelastic Seismic Behavior of Steel Braced Frames Including the Effects of Low-Cycle Fatigue," Report No. PEER 2010/104, Pacific Earthquake Engineering Research Center, University of California at Berkeley, CA.
- Hwang, S-H, Elkady, A., Al-Bardaweel, S. and Lignos, D.G. (2015), "Earthquake Loss Assessment of Steel Frame Buildings Designed in Highly Seismic Regions," *Proc. 5th ECCOMAS Thematic Conference on Computational Methods in Structural Dynamics and Earthquake Engineering*, Crete Island, Greece, May 25–27, 2015 (M. Papadrakakis, V. Papadopoulos, V. Plevris, Eds.).
- Okazaki, T., Lignos, D., Hikino, T. and Kajiwara, K. (2013), "Dynamic Response of a Chevron Concentrically Braced Frame," *Journal of Structural Engineering*, Vol. 139, No. 4, pp. 515–525. [http://dx.doi.org/10.1061/\(ASCE\)ST.1943-541X.0000679](http://dx.doi.org/10.1061/(ASCE)ST.1943-541X.0000679)
- Karamanci, E. and Lignos, D.G. (2013), "Collapse Assessment and Performance-Based Evaluation Techniques for Concentrically Braced Frames Designed in Seismic Regions," M.S. Thesis, Department of Civil Engineering and Applied Mechanics, McGill University, Montreal, Quebec, Canada.
- Karamanci, E. and Lignos, D. (2014), "Computational Approach for Collapse Assessment of Concentrically Braced Frames in Seismic Regions," *Journal of Structural Engineering*, Vol. 140, Special Issue: Computational Simulation in Structural Engineering, A4014019. [http://dx.doi.org/10.1061/\(ASCE\)ST.1943-541X.0001011](http://dx.doi.org/10.1061/(ASCE)ST.1943-541X.0001011)
- Lee, K. and Bruneau, M. (2005), "Energy Dissipation of Compression Members in Concentrically Braced Frames: Review of Experimental Data," *Journal of Structural Engineering*, 10.1061/(ASCE)0733-9445(2005)131:4(552), pp. 552–559.
- Lignos, D.G., Krawinkler, H. and Whittaker, A.S. (2011), "Prediction and Validation of Sidesway Collapse of Two Scale Models of a 4-Story Steel Moment Frame," *Earthquake Engineering Structural Dynamics*, Vol. 40, No. 7, pp. 1215–1228.
- Liu, J. and Astaneh-Asl, A. (2000), "Cyclic Testing of Simple Connections Including Effects of Slab," *Journal of Structural Engineering*, 10.1061/(ASCE)0733-9445(2000)126:1(32), pp. 32–39.
- Liu, J. and Astaneh-Asl, A. (2004), "Moment-Rotation Parameters for Composite Shear Tab Connections," *Journal of Structural Engineering*, 10.1061/(ASCE)0733-9445(2004)130:9(1371), pp. 1371–1380.
- Lehman, D.E., Roeder, C. W., Herman, D., Johnson, S. and Kotulka, B. (2008), "Improved Seismic Performance of Gusset Plate Connections," *Journal of Structural Engineering*, Vol. 134, No. 6, pp. 890–901.
- Lopez, W. and Sabelli, R. (2004), "Seismic Design of Buckling-Restrained Braced Frames," Structural Steel Educational Council, Steel Tips, July 2004.
- McKenna, F. (2014), "Open System for Earthquake Engineering Simulation (OpenSees)," Berkeley, CA.
- Miller, D.J. and Richards, P.W. (2015), "High-Yield-Drift Steel Moment Frames for Dual Systems," *Journal of Constructional Steel Research*, in review.
- Naghypour, M., Abdollahzadeh, G. and Shokri, M. (2013), "Analysis and Design Procedure of Corner Gusset Plate Connection in BRBFs," *Iranica Journal of Energy & Environment*, Vol. 4, No. 3, pp. 271–282.
- Nam, T.T. and Kasai, K. (2011), "Dynamic Analysis of a Full-Scale Four-Story Steel Building Experimented to Collapse by Strong Ground Motions," *Proc. 8CUEE Conference*, Center for Urban Earthquake Engineering (CUEE), Tokyo, Japan.
- Okazaki, T., Lignos, D., Hikino, T. and Kajiwara, K. (2013), "Dynamic Response of a Chevron Concentrically Braced Frame," *Journal of Structural Engineering*, Vol. 139, No. 4, pp. 515–525.
- Pettinga, D., Christopoulos, C., Pampanin, S. and Priestley, N. (2007), "Effectiveness of Simple Approaches in Mitigating Residual Deformations in Buildings," *Earthquake Engineering & Structural Dynamics*, Vol. 36, pp. 1763–1783.
- Prinz, G.S. (2007), "Effect of Beam Splicing on Seismic Response of Buckling Restrained Braced Frames," M.S. Thesis, Brigham Young University, Provo, UT.
- Roeder, C.W. et al. (2011a), "Influence of Gusset Plate Connections and Braces on the Seismic Performance of X-Braced Frames," *Earthquake Engineering & Structural Dynamics*, Vol. 40, No. 4, pp. 355–374.
- Roeder, C.W., Lumpkin, E.J. and Lehman, D.E. (2011b), "A Balanced Design Procedure for Special Concentrically Braced Frame Connections," *Journal of Constructional Steel Research*, Vol. 67, No. 11, pp. 1760–1772.
- Sabelli R., Mahin S. and Chang C. (2003), "Seismic Demands on Steel Braced Frame Buildings with Buckling-Restrained Braces," *Engineering Structures*, Vol. 25, pp. 655–666.
- Scott, M.H. and Ryan, K.L. (2013), "Moment-Rotation Behavior of Force Based Plastic Hinge Elements," *Earthquake Spectra*, Vol. 29, No. 2, pp. 597–607.
- Sheng, N., Yam, C.H. and Iu, V.P. (2002), "Analytical Investigation and the Design of the Compressive Strength of Steel Gusset Plate Connections," *Journal of Constructional Steel Research*, Vol. 58, pp. 1473–1493.

- Spacone, E., Filippou, F.C. and Taucer, F.F. (1996), "Fiber Beam-Column Model for Nonlinear Analysis of R/C Frames, Part I: Formulation," *Earthquake Engineering & Structural Dynamics*, Vol. 25, No. 7, pp. 711–725.
- Stoakes, C.D. and Fahnestock, L. A. (2011), "Cyclic Flexural Testing of Concentrically Braced Frame Beam-Column Connections." *Journal of Structural Engineering*, 10.1061/(ASCE)ST.1943-541X.0000326, pp. 739–747.
- Suita, K., Yamada, S., Tada, M., Kasai, K., Matsuoka, Y. and Shimada, Y. (2008), "Collapse Experiment on 4-Story Steel Moment Frame: Part 2 Detail of Collapse Behaviour," *Proc. 14th World Conference on Earthquake Engineering (14WCEE)*, China Earthquake Administration, Ministry of Housing and Urban-Rural Development, Beijing, China.
- Takeuchi T., Ozaki, H., Matsui, R. and Sutcu, F. (2014), "Out-of-Plane Stability of Buckling-Restrained Braces Including Moment Transfer Capacity," *Earthquake Engineering & Structural Dynamics*, Vol. 43, No. 6, pp. 851–869.
- Thornton, W.A. (1984), "Bracing Connections for Heavy Construction," *Engineering Journal*, Vol. 21, No. 3, pp. 139–148.
- Tremblay, R. (2001), "Seismic Behavior and Design of Concentrically Braced Steel Frames," *Engineering Journal*, Vol. 38, No. 3, pp. 148–166.
- Tremblay, R. (2002), "Inelastic Seismic Response of Steel Bracing Members." *Journal of Constructional Steel Research*, Vol. 58, No. 5–8, pp. 665–701.
- Tremblay, R. and Robert, N. (2001), "Seismic Performance of Low- and Medium-Rise Chevron Braced Steel Frames," *Canadian Journal of Civil Engineering*, Vol. 28, No. 4, pp. 699–714.
- Tsai K.-C. and Hsiao, P.-C. (2008), "Pseudo-Dynamic Test of a Full-Scale CFT/BRB Frame—Part II: Seismic Performance of Buckling-Restrained Braces and Connections," *Earthquake Engineering & Structural Dynamics*, Vol. 37, pp. 1099–1115.
- Uriz, P. (2005), "Towards Earthquake Resistant Design of Concentrically Braced Steel Structures," Ph.D. Dissertation, Department of Civil and Environmental Engineering, University of California, Berkeley, CA.
- Uriz, P. and Mahin, S.A. (2004), "Seismic Performance Assessment of Concentrically Braced Steel Frames," *Proc. 13th World Conference on Earthquake Engineering*, Vancouver, BC, August 1–6, 2004, Paper No. 1639.
- Uriz, P. and Mahin, S.A. (2008), "Toward Earthquake-Resistant Design of Concentrically Braced Steel-Frame Structures," PEER 2008/08, Pacific Earthquake Engineering Research Center, Berkeley, CA.
- Walbridge, S., Grondin, G. and Cheng, J.J. (2005), "Gusset Plate Connections under Monotonic and Cyclic Loading," *Canadian Journal of Civil Engineering*, Vol. 32, No. 5, pp. 981–995.
- Wigle V.R. and Fahnestock, L.A. (2010), "Buckling-Restrained Braced Frame Connection Performance," *Journal of Constructional Steel Research*, Vol. 66, No. 1, pp. 65–74.
- Xu, W.J. (2015), "Buckling Performance of Buckling-Restrained Brace (BRB) and Connection Assembly (In preparation)," Ph.D. Dissertation, University of Utah.

GUIDE FOR AUTHORS

SCOPE: The ENGINEERING JOURNAL is dedicated to the improvement and advancement of steel construction. Its pages are open to all who wish to report on new developments or techniques in steel design, research, the design and/or construction of new projects, steel fabrication methods, or new products of significance to the uses of steel in construction. Only original papers should be submitted.

GENERAL: Papers intended for publication may be submitted by mail to the Editor, Margaret A. Matthew, ENGINEERING JOURNAL, AMERICAN INSTITUTE OF STEEL CONSTRUCTION, One East Wacker Drive, Suite 700, Chicago, IL, 60601, or by email to matthew@aisc.org.

The articles published in the *Engineering Journal* undergo peer review before publication for (1) originality of contribution; (2) technical value to the steel construction community; (3) proper credit to others working in the same area; (4) prior publication of the material; and (5) justification of the conclusion based on the report.

All papers within the scope outlined above will be reviewed by engineers selected from among AISC, industry, design firms, and universities. The standard review process includes outside review by an average of three reviewers, who are experts in their respective technical area, and volunteers in the program. Papers not accepted will not be returned to the author. Published papers become the property of the American Institute of Steel Construction and are protected by appropriate copyrights. No proofs will be sent to authors. Each author receives three copies of the issue in which his contribution appears.

MANUSCRIPT PREPARATION: Manuscripts must be provided in Microsoft Word format. Include a PDF with your submittal. View our complete author guidelines at www.aisc.org/ej.



There's always a solution in steel.

ENGINEERING JOURNAL
American Institute of Steel Construction
One East Wacker Drive, Suite 700
Chicago, IL 60601

312.670.2400

www.aisc.org